COMPARISON OF LIMIT EQUILIBRIUM AND 2-D, 3-D FINITE ELEMENT
SLOPE STABILITY MODELS: A CASE STUDY ON THE SLOPE IN AKPINAR
DISTRICT, IN ANKARA

A THESIS SUBMITTED TO
THE GRADUATE SCHOOL OF NATURAL AND APPLIED SCIENCES
OF
MIDDLE EAST TECHNICAL UNIVERSITY

BY

MEHMET CAN ETİZ

IN PARTIAL FULFILLMENT OF THE REQUIREMENTS
FOR
THE DEGREE OF MASTER OF SCIENCE
IN
CIVIL ENGINEERING

DECEMBER 2019

Approval of the thesis:

**COMPARISON OF LIMIT EQUILIBRIUM AND 2-D, 3-D FINITE
ELEMENT SLOPE STABILITY MODELS: A CASE STUDY ON THE
SLOPE IN AKPINAR DISTRICT, IN ANKARA**

submitted by **MEHMET CAN ETİZ** in partial fulfillment of the requirements for the
degree of **Master of Science in Civil Engineering Department, Middle East
Technical University** by,

Prof. Dr. Halil Kalıpçılar
Dean, Graduate School of **Natural and Applied Sciences** _____

Prof. Dr. Ahmet Türer
Head of Department, **Civil Engineering** _____

Prof. Dr. Bahadır Sadık Bakır
Supervisor, **Civil Engineering, METU** _____

Examining Committee Members:

Prof. Dr. Erdal Çokça
Civil Engineering, METU _____

Prof. Dr. Bahadır Sadık Bakır
Civil Engineering, METU _____

Assoc. Prof. Dr. Nejan Huvaj Sarıhan
Civil Engineering, METU _____

Assoc. Prof. Dr. Mustafa Abdullah Sandıkkaya
Civil Engineering, Hacettepe University _____

Assist. Prof. Dr. Onur Pekcan
Civil Engineering, METU _____

Date: 03.12.2019

I hereby declare that all information in this document has been obtained and presented in accordance with academic rules and ethical conduct. I also declare that, as required by these rules and conduct, I have fully cited and referenced all material and results that are not original to this work.

Name, Surname: Mehmet Can Etiz

Signature:

ABSTRACT

**COMPARISON OF LIMIT EQUILIBRIUM AND 2-D, 3-D FINITE
ELEMENT SLOPE STABILITY MODELS: A CASE STUDY ON THE
SLOPE IN AKPINAR DISTRICT, IN ANKARA**

Etiz, Mehmet Can
Master of Science, Civil Engineering
Supervisor: Prof. Dr. Bahadır Sadık Bakır

December 2019, 152 pages

This study presents comparisons of Two-Dimensional (2D) Limit Equilibrium Method (LEM), Finite Element Method (FEM), and Three-Dimensional (3D) FEM slope stability models for the slope in Akpınar District in Ankara. A landslide has occurred on the aforementioned slope following heavy rain in June 2011. One of the buildings on the slope has overturned about 3 to 5 degrees and some other buildings in the area have suffered substantial damages. Following the landslide, several field investigations and subsequent studies have been conducted by geotechnical experts and academicians. In this research, previous studies have been summarized, velocity-time plots have been constructed from the site inclinometer data and the performance of the slope has been studied by different methods on a comparative basis as a case. In the first part of the study, namely static analyses, back-analyses have been conducted to obtain equilibrium strength parameters. Also, the possible effects of the foundation excavation which existed on the toe of the landslide have been investigated. The impact of heavy rain on the slope has been modeled with 2D-LEM and 2D-FEM while the equilibrium condition has been modeled with 3D-FEM. For the seismic stability assessment of the slope, the effects of possible earthquake scenarios have been modeled. Both short term and long-term parameters have been

used in the analyses. Pseudo-static coefficients for 2D-LEM, pseudo-static coefficients, and time-history analysis methods for 2D-FEM have been utilized for dynamic calculations. Consequently, it has been shown that deep and shallow sliding surfaces were triggered on the slope as a result of the heavy rain and that the existence of foundation excavation had an unfavorable effect on the initiation of the deep slide surface. Besides, almost in every case for the slope, FEM has provided approximately 10% lower safety factors compared to those offered by LEM. Also, for pseudo-static approach short term parameters and for time-history analyses, long term parameters have provided safer results.

Keywords: Landslide Velocity, Flood Condition, Earthquake Time-History Analysis, Limit Equilibrium and Finite Element Methods, Slope Stability

ÖZ

LİMİT DENGE, 2 BOYUTLU VE 3 BOYUTLU SONLU ELEMANLAR MODELLERİ İLE ŞEV DURAYLILIĞI KARŞILAŞTIRMASI: ANKARA AKPINAR MAHALLESİNDEKİ BİR ŞEVDE ÖRNEK VAKA İNCELEMESİ

Etiz, Mehmet Can
Yüksek Lisans, İnşaat Mühendisliği
Tez Danışmanı: Prof. Dr. Bahadır Sadık Bakır

Aralık 2019, 152 sayfa

Bu çalışma Ankara- Akpınar Mahallesinde heyelan belirtileri görülen bir şevin Limit Denge Yöntemi (LDY), 2 Boyutlu (2B) ve 3 Boyutlu (3B) Sonlu Elemanlar Yöntemi (SEY) ile modellendirilmelerini karşılaştırmaktadır. Söz konusu şevde, 2011 yılı Haziran ayında meydana gelen yağışlardan deplasmanlar görülmüş ve bir bina 3-5 derece civarında eğilmiş, bölgedeki diğer binalarda da belirgin hasarlar gözlenmiştir. Vakayı araştırmak için geoteknik uzmanları ve akademisyenler tarafından bazı çalışmalar yapılmıştır. Bu araştırmada şimdiye kadar yapılan çalışmalar özetlenmiş, sahadaki inklinometre verilerinden hız-zaman grafikleri oluşturulmuş ve söz konusu şev tekrar modellenmiştir. Çalışmanın ilk kısmı olan statik analizlerde geri analiz yöntemiyle denge parametreleri araştırılmıştır. Ayrıca şevin topuğunda yer alan bir temel kazısının heyelan stabilitesine olan etkileri incelenmiş, yağışların şev üzerindeki etkisi 2B-LDY ve 2B-SEY ile; heyelanın denge durumu ise 3B-SEY ile modellenmiştir. Sahada meydana gelebilecek olası sismik hareketlerin şev üstündeki etkileri olası deprem senaryoları üzerinden incelenmiştir. Ayrıca analizlerde uzun dönem ve kısa dönem parametreleri ayrı ayrı kullanılmıştır. 2B-LDY 'de yarı-statik katsayılar, 2B-SEY' de yarı-statik katsayılar ve Zaman Tanım Alanında Hesap Yöntemi kullanılmıştır. Sonuç olarak sığ ve derin heyelan yüzeylerinin civardaki söz

konusu ağır yağışlar sonucunda tetiklendiği, söz konusu temel kazısının derin heyelanın ortaya çıkışında önemli bir rol oynadığı sonucuna varılmıştır. Diğer taraftan, karşılaştırma yapılan hemen hemen her durumda sonlu elemanlar yöntemi yaklaşık %10 civarında daha düşük güvenlik katsayıları vermiştir. Ek olarak yarı-statik deprem analizinde kısa dönem parametreleri, Zaman Tanım Alanında Hesap Yöntemi ile yapılan deprem analizlerinde uzun dönem parametreleri daha güvenli sonuçlar vermiştir.

Anahtar Kelimeler: Heyelan Hızı, Sel Durumu, Zaman Tanım Alanında Deprem Hesap Yöntemi, Limit Denge ve Sonlu Elemanlar Yöntemleri, Şev Stabilitesi

To the immortal memory of my well-beloved father.

"Use your mind, always"

ACKNOWLEDGEMENTS

TABLE OF CONTENTS

LIST OF TABLES

LIST OF FIGURES

FIGURES

LIST OF ABBREVIATIONS

2D	Two-Dimensional
3D	Three-Dimensional
AFAD	Directorate of Disaster and Emergency Management, Republic of Turkey Ministry of Interior
ASCE	American Society of Civil Engineers
BH	Borehole
CCE	Chamber of Civil Engineers
CE	Civil Engineering
CGE	Chamber of Geological Engineers
DOF	Degree of Freedom
FE	Finite Element
FEM	Finite Element Method
FS	Factor of Safety
GPS	Generalized Procedure of Slices
GWT	Ground Water Table
LE	Limit Equilibrium
LEM	Limit Equilibrium Method
METU	Middle East Technical University
PGA	Peak Ground Acceleration
PI	Plasticity Index
PLAXIS	Finite Element Software for Geotechnical Problems (Plaxis bv)
PWP	Pore Water Pressure
RQD	Rock Quality Designation
RS2	2D-Finite Element Software for Soil and Rock Application (Rocscience)
RS3	3D-Finite Element Software for Soil and Rock Application (Rocscience)
SC	Clayey-Sand according to the Unified Soil Classification System.spt
SK	Borehole (Turkish)
SLIDE	Limit Equilibrium Software for Slope Stability Analysis (Rocscience)
SPT	Standard Penetration Test
SRF	Strength Reduction Factor
SSR	Shear Strength Reduction
UCTEA	The Union of Chambers of Turkish Engineers and Architects

USACE   United States Army Corps of Civil Engineers
USGS   United States Geological Survey, United States Department of Interior
UU   Unconsolidated-Undrained

CHAPTER 1

INTRODUCTION

1.1. Research Goals

In this research, the landslide which was triggered following the heavy rainfall which occurred in June 2011 in the Akpınar District of Ankara has been investigated as the case study. The slope has been modeled using two-dimensional (2D) Limit Equilibrium Method (LEM) as well as with two and three-dimensional (3D) Finite Element Method (FEM) under static loading conditions to investigate the predictive capabilities of the methods mentioned above. Besides, the effect of a supported vertical cut due to a foundation excavation at the toe of the slope has been investigated. Potential effects due to probable seismic events on the slope were searched by the two-dimensional models (LEM and FEM) through pseudo-static and time history analyses.

1.2. Scope of the Study

The theoretical background of slope stability, in general, has been introduced in Chapter 2 regarding the methods utilized in this study. In Chapter 3, the limit equilibrium and finite element software which have been used to conduct the stability analyses are presented. Later in Chapter 4, the description of geotechnical circumstances and stability problems observed on the slope have been provided and the findings from previous studies are presented. In addition, the velocity-time plots from the borehole inclinometer data have been constructed. Chapter 5 consists of static analyses of the slope under various circumstances, including the influence of heavy rain and foundation excavation at the toe of the slope. Possible effects of the seismic activity on the slope which are likely to influence the area are searched in Chapter 6 through pseudo-static and time history analyses. The results and discussion are

presented in Chapter 7. Finally, the case study has been completed by stating of the overall conclusions and recommendations in Chapter 8.

CHAPTER 2

LITERATURE REVIEW

Limit equilibrium (LE) solutions and finite element (FE) modeling of the slopes are reviewed on a comparative basis and the methods available for the assessment of the seismic response of slopes are discussed.

2.1. Definition of the Landslide

According to USGS[1] , a landslide is the movement of earth, debris, or a mass of rock in the downslope direction. Displacement in a slope occurs when driving forces that act downslope exceed the shear strength of earth material composing the slope. Causes of the landslide movements can be categorized in two groups in general:

1. Factors that increase the driving forces.

2. Factors that decrease the shearing strength of the slope material.

Landslides can be initiated by rainfall, snowmelt, groundwater table (GWT) level change, volcanic eruptions, earthquakes and construction activities such as cuts in the toe of the potential landslide area. Typical components of a landslide are shown in Figure 2.1.

---

[1] United States Geological Survey
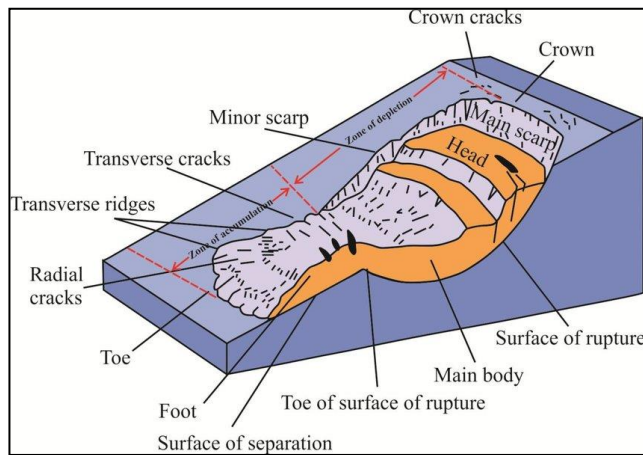
Figure 2.1. Components of a landslide (USGS, 2019).

Recent practices classify landslides on the basis of movement rate. Cruden and Varnes (1996) have categorized the landslides according to movement velocity ranging from 15 mm per year to 5 m per second (Figure 2.2).

Velocity Class	Description	Velocity (mm/sec)	Typical Velocity	Probable Destructive Significance
7	Extremely Rapid			Catastrophe of major violence; buildings destroyed by impact of displaced material; many deaths; escape unlikely
		5×10^3	5 m/sec	
6	Very Rapid			Some lives lost; velocity too great to permit all persons to escape
		5×10^1	3 m/min	
5	Rapid			Escape evacuation possible; structures; possessions, and equipment destroyed
		5×10^{-1}	1.8 m/hr	
4	Moderate			Some temporary and insensitive structures can be temporarily maintained
		5×10^{-3}	13 m/month	
3	Slow			Remedial construction can be undertaken during movement; insensitive structures can be maintained with frequent maintenance work if total movement is not large during a particular acceleration phase
		5×10^{-5}	1.6 m/year	
2	Very Slow			Some permanent structures undamaged by movement
		5×10^{-7}	15 mm/year	
	Extremely SLOW			Imperceptible without instruments; construction POSSIBLE WITH PRECAUTIONS

Figure 2.2. Velocity classification of landslides (Cruden and Varnes,1996).

Cruden and Varnes (1996) have also classified landslides from the kinematics viewpoint (i.e., how movements are characterized throughout the displaced mass) as follows:

1. Flow.
2. Fall.
3. Spread.
4. Slide.
5. Topple.

2.2. Shear Strength for Slope Stability

The stability of a slope can be assessed either in terms of effective or total stress parameters. For the case of cohesionless soils forming the slope material, since drainage occurs rapidly following loading (or unloading) of the slope, disregarding exceptional circumstances, only the effective stress analyses will be meaningful. Whereas for clay type soils, which are typical of low permeability, pore pressures, and hence the stability of the slope are subject to variation in time. An example of such is schematically illustrated in Figure 2.3 for a cut slope in saturated clay.

If the pore water pressures (PWP) can be estimated reasonably closely, the analysis can be carried out using effective stress principles with drained shear strength parameters. The total stress type of analysis may have to be employed if the pore water pressures are unknown or cannot be determined reliably. In practice, by and large, the total stress analysis is used for short-term stability problems and the effective stress approach is used to assess the long-term stability, presuming any excess pore pressure generated during loading will be fully dissipated. The undrained strength parameter c_u ($\Phi_u=0$) is used for total stress analysis based on the assumption that the soil behaves in an exclusively "cohesive" manner. For effective stress analyses, c' and Φ', along

with the pore pressure, u, are required to calculate the factor of safety (FS) (Abramson et al., 2001).
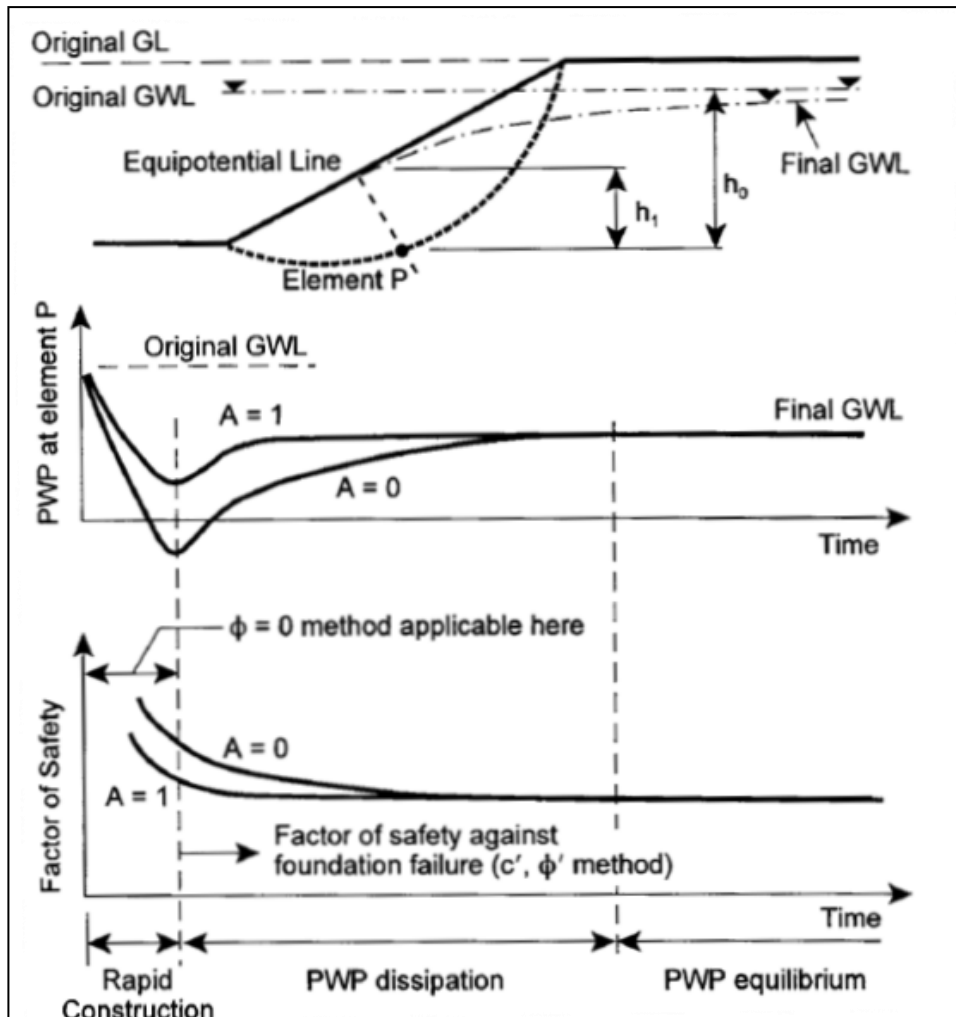
Figure 2.3. Dependence of FS on PWP in time in a cut slope (Abramson et al., 2001).

2.3. Static Slope Stability

2.3.1. Limit Equilibrium Method

The limit equilibrium method is the traditional slope stability assessment approach, which considers force or moment equilibria of the soil mass remaining above a

probable failure surface. In this method, the soil mass above the slip surface is assumed to be rigid, and at the time of failure, the available shear strength is presumed to be mobilized at the same rate at all points of the slip surface. Hence, the FS is constant throughout the failure surface. Accordingly, the stability is represented by a factor of safety, which is expressed as the proportion of available shear strength to the existing shear stress on the potential slide surface.

The method of slices approach is widely used in the limit equilibrium method in which the sliding mass is vertically divided into a number of slices and the equilibrium of each slice is considered individually. Slicing for different subsurface circumstances is shown in Figure 2.4.
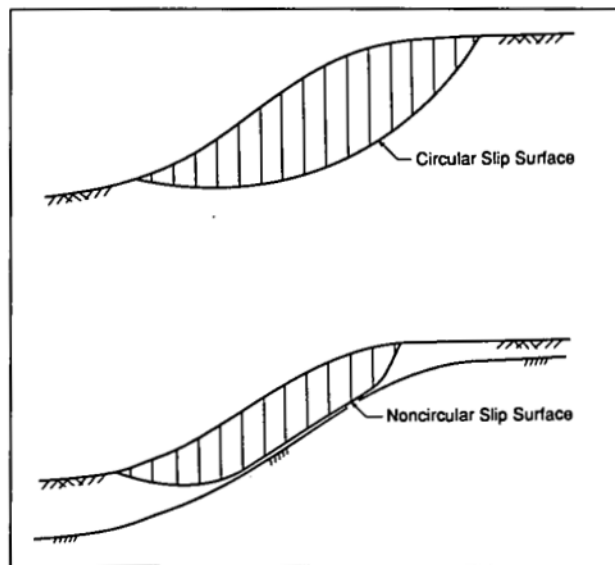
Figure 2.4. Division of sliding masses into slices (Duncan,1996).

If the equilibrium condition is satisfied for each slice, the equilibrium of the entire mass is also satisfied. The forces acting on an individual slice is shown in Figure 2.5.
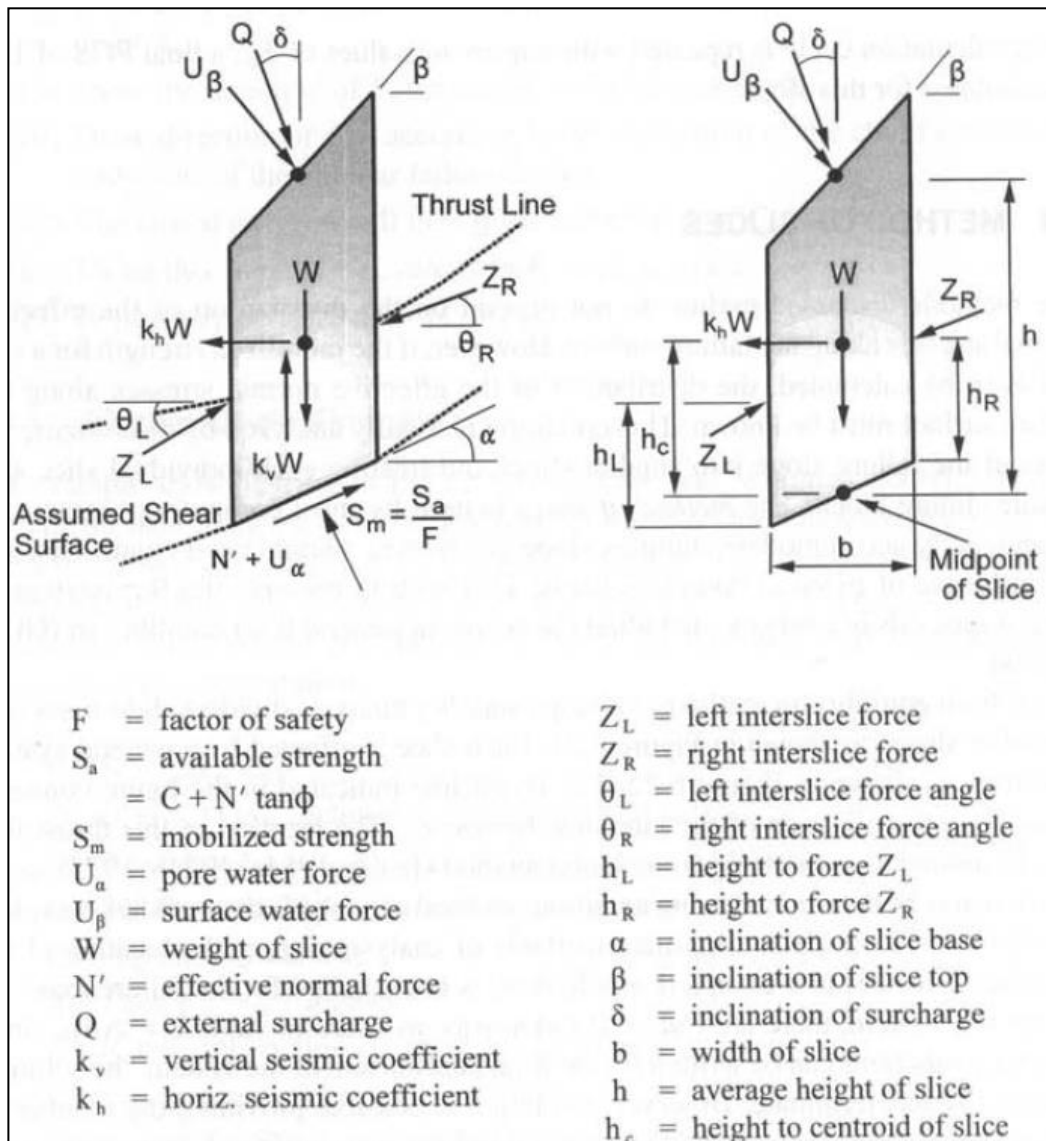
Figure 2.5. Forces which act on a typical slice (Abramson et al., 2001).

The thrust line, which is shown in Figure 2.5 indicates the junction of the application points of the interslice forces. The location of the thrust line is assumed in the rigorous Janbu method (1954a, 1954b, 1973), which satisfies all of the equilibrium conditions. Whereas the simplified methods neglect the consideration of thrust line and

equilibrium is only partly satisfied. For the system of slices, there are 6n-2 unknowns which are listed in Table 2.1.

Table 2.1. *Unknowns and available equations related to the method of slices (reproduced from Abramson et al., 2001).*

Equations	Condition
n	Moment equilibrium for each slice
2n	Force equilibrium in two directions (for each slice)
n	Mohr-Coulomb relationship between shear strength and normal effective stress
4n	**Total Number of Equations**
Unknowns	Variable
1	Factor of safety
n	Normal force at the base of each slice N'
n	Location of normal force, N'
n	Shear force at the base each slice, S_m
n-1	Interslice force, Z
n-1	Inclination of interslice force, θ
n-1	Location of interslice force (line of thrust)
6n-2	**Total Number of Unknowns**

On the other hand, force and moment equilibria and Mohr-Coulomb relationship provide 4n equations. Thus, the system is statically indeterminate. It is generally assumed that the normal force on the base of the slice acts at the midpoint; therefore, the total number of unknowns is reduced to 5n-2. However, there are still additional n-2 equations needed to solve the system. Several researchers have proposed certain assumptions to overcome this problem of indeterminacy. These assumptions, which categorize and constitute the differences in existing solution techniques from each other, are presented in Table 2.2.

Table 2.2. *Properties of the common methods of limit equilibrium approach for slope stability (Reproduced from Abramson et al. [2001] and [Duncan,1996]).*

Method	Force Equilibrium		Moment Equilibrium	Additional Information
	1st Direction * (e.g., Vertical)	2nd Direction * (e.g., Horizontal)		
The ordinary method of slices (Fellenius 1927)	Yes	No	Yes	Neglects interslice shear forces and does not satisfy force equilibrium both for the entire slide mass and individual slices.
Bishop's simplified method (Bishop 1955)	Yes	No	Yes	All interslice forces are assumed to be zero, which reduces the number of unknowns by (n-1). Remaining (4n-1) unknowns, overdetermined solution as horizontal force equilibrium not satisfied for a slice.
Janbu's simplified method (Janbu 1968)	Yes	Yes	No	Assuming no interslice shear forces, remaining (4n — 1) unknowns, overdetermined

Method	Force Equilibrium 1st Direction * (e.g., Vertical)	2nd Direction * (e.g., Horizontal)	Moment Equilibrium	Additional Information
				solution as moment equilibrium conditions not completely satisfied. Janbu proposes a correction factor, f_0, to overcome this situation.
Modified Swedish method (U.S. Army Corps of Engineers [USACE] 1970)	Yes	Yes	No	The interslice forces' inclination is either parallel to the ground surface or equal to the average sloping angle between the horizontal endpoints of the failure surface.
Lowe and Karafiath's method (Lowe and Karafiath 1960)	Yes	Yes	No	Assuming inclination of the interslice forces is the average of the slope surface angle and slice base angles, leaving ($4n$ — 1) unknowns which does not satisfy moment equilibrium.

Method	Force Equilibrium 1st Direction * (e.g., Vertical)	2nd Direction * (e.g., Horizontal)	Moment Equilibrium	Additional Information
Janbu's generalized procedure of slices (Janbu 1968)	Yes	Yes	**	The location of the thrust line is assumed (the actual location is also an unknown), equilibrium satisfied if the location of the mentioned line is chosen correctly.
Bishop's rigorous method (Bishop 1955)	Yes	Yes	Yes	$(n - 1)$ Interslice shear forces are assumed, remaining $(4n - 1)$ unknowns, moment equilibrium is not satisfied for all slices. Bishop suggests an additional unknown saying there is a particular distribution of the resultant interslice force, which will satisfy the conditions of equilibrium.
Spencer's method (Spencer 1967)	Yes	Yes	Yes	Resultant interslice forces have a

Method	Force Equilibrium 1st Direction * (e.g., Vertical)	2nd Direction * (e.g., Horizontal)	Moment Equilibrium	Additional Information
				constant, but unknown, inclination. Consequently, 4n equations are required.
Sarma's method (Sarma 1973)	Yes	Yes	Yes	Assuming mobilization of the shear strength on the sides of all slices. There is a variation in the inclination of the slice interfaces to obtain critical conditions.
Morgenstern and Price's method (Morgenstern and Price 1965)	Yes	Yes	Yes	Similar to that of Spencer's approach, except that the inclination of the resultant interslice forces is found by an arbitrary function and this satisfies the equilibrium conditions.
* Any of two orthogonal directions can be selected for the summation of forces **** Moment equilibrium is used to calculate interslice shear forces.**				

As can be seen from Table 2.2, each method has its distinct assumption to provide a sufficient number of equations required to solve for the unknowns. Also, some other

methods like Fellenius Method (1927) and Bishop's simplified method (Bishop,1955) do not match all the conditions of equilibrium or even the conditions of the force equilibrium.

It has been shown in the computational accuracy studies that if the selected analysis method satisfies all the equilibrium conditions, then the FS will be accurate in the range of ±6%. Because the FS values calculated using methods (satisfying all equilibrium conditions) differ maximum by 12% from each other or ±6 % from a central value if the assumptions of these methods are reasonable. The methods that satisfy all the equilibrium conditions and have reasonable assumptions are (Duncan, 1996):

1. The generalized procedure of slices (GPS) (Janbu 1968).

2. Spencer (1967).

3. Morgenstern and Price (1965).

4. Sarma (1973).

It has been shown in the studies that FS values calculated by the methods mentioned above differ a maximum of 6% from FS values that have been calculated with the FEM or the log-spiral method. However, Bishop's method, which applies to circular surfaces only, is an exception; although it does not satisfy all the equilibrium conditions, it is as accurate as of the methods listed above.

2.3.2. Finite Element Method

The finite element method (FEM) bypasses the limitations of the limit equilibrium method. In FEM, the soil continuum is divided into discrete units called "finite elements," an example of which is shown in Figure 2.6.

The finite elements are interconnected at nodal points and the prescribed boundaries of the mass continuum. In typical geotechnical applications, the displacement method of formulation of the FEM is utilized to calculate displacements, stresses, and strains at the nodal points.
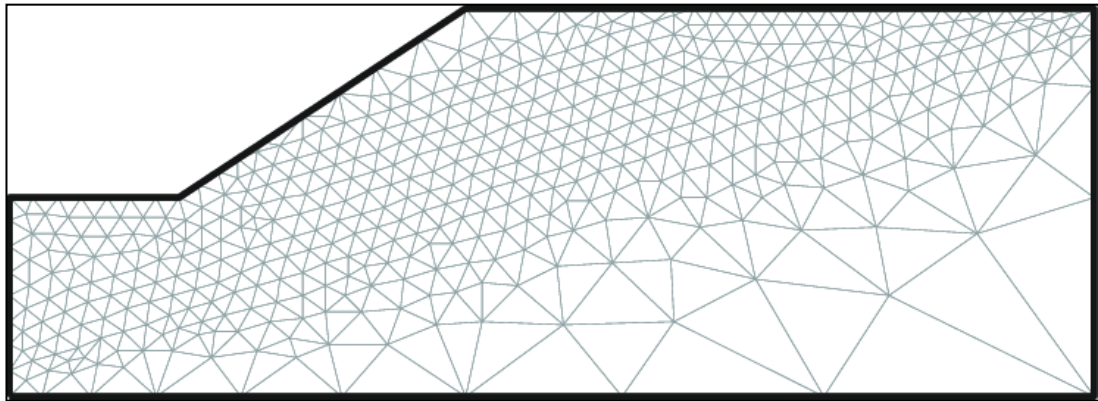
Figure 2.6. Graded meshing example of a slope soil continuum (Liu and Zhao, 2013).

For using finite element slope stability program, one should need the following data:

1. An appropriate constitutive model.
2. Availability of different types of meshes.
3. Relevant material properties based on field and laboratory test data.

The following failure criteria can be utilized in finite element slope stability solutions:

1. Bulging of slope line (Snitbhan and Chen, 1978).

2. Limit shear (Duncan and Dunlop, 1969).

3. Nonconvergence of the solution (Zienkiewicz, 1971).

Bulging of slope line (Snitbhan and Chen, 1978): This criterion is described by the horizontal displacements of the surface of a slope and is established by specifying a maximum tolerable limit for these horizontal displacements.

Limit shear (Duncan and Dunlop, 1969): In this case, the calculated FEM stresses along a probable failure surface are computed to estimate an FS. This FS equals to the ratio of available strength along the failure surface to the computed stresses.

Nonconvergence of the solution (Zienkiewicz, 1971): This may be indicative of the collapse of the elements under the imposed loading conditions. With this approach, the shear strength parameters are reduced until non-convergence or numerical instabilities occur. The FS is then represented as the ratio of the available strength to the lowest strength that produced a viable solution.

2.3.3. Finite Element Method versus Limit Equilibrium Method

Akbaş (2015) summarized the comparison of FEM and LEM approaches in slope stability calculations, stating that although comparative studies exist in the literature, they do not signify well-accepted conclusions. In most of the studies, similar safety factors (FS, or SRF [Strength Reduction Factor]) have been obtained within 5%-10% differences. However, under which circumstance FEM or LEM gives safer results is not explicit (Akbaş, 2015).

2.4. Seismic Slope Stability

One of the main triggering factors of slope instabilities is earthquakes. When designing/analyzing a slope, an engineer should consider the seismic stability to model the dynamic stresses/strains/displacements which occur due to earthquake shaking.

Slope instabilities by seismic effects may be divided into two groups:

1. Inertial instabilities.
2. Weakening instabilities.

Inertial instabilities are explained as temporary exceedance of the shear strength, which results in slope deformations caused by earthquake-induced stresses. Whereas weakening instabilities are defined as the weakening of the soil strength due to earthquake shaking such that the slope becomes unstable.

Cyclic mobility and flow liquefaction are the most common causes of weakening instability. In this case study, an analysis of the inertial instability will be emphasized and adopted to examine the effects of possible earthquake scenarios on the slope.

Earthquake motions may induce shear stresses strong enough to initiate a slope failure. Various techniques have been proposed to analyze the inertial slope instabilities. These approaches are mainly divided into four categories (Kramer, 1996):

1. Pseudo-static analysis.
2. Newmark sliding block analysis.
3. Makdisi-Seed analysis.
4. Stress-deformation analysis.

2.4.1. Pseudo-Static Analysis

Seismic stability analyses of earth structures by pseudo-static approach were used starting from 1920s, and specific applications have been attributed to Terzaghi (1950) (Kramer, 1996). In this method, earthquake effects are represented by constant accelerations, which produce inertial forces acting on the centroid of failure mass, as shown in Figure 2.7.
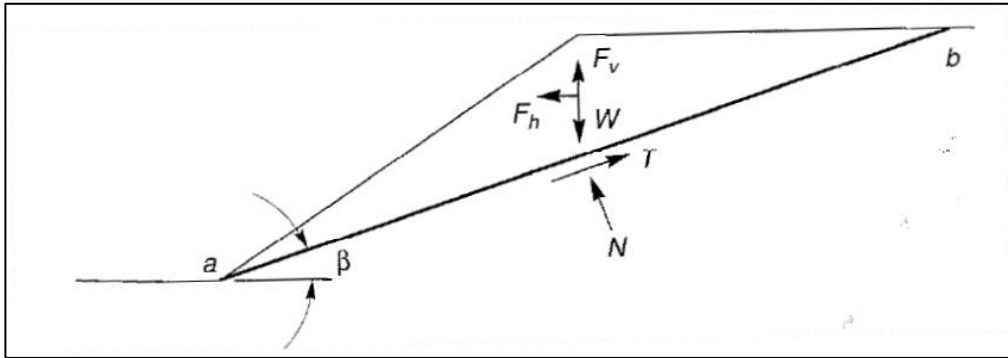
Figure 2.7. Forces that act on a triangular wedge of soil above a potential failure surface
(Kramer,1996)

The pseudo-static forces are expressed as follows:

$$F_h = \frac{a_h * W}{g} = k_h * W \tag{2.1}$$

$$F_v = \frac{a_v * W}{g} = k_v * W \tag{2.2}$$

Where a_k and a_v are horizontal and vertical accelerations, k_h and k_v are dimensionless coefficients representing the severity of the earthquakes in horizontal and vertical directions, respectively, and W is the weight of the failure mass.

A factor of safety is defined as the ratio of resisting forces to driving forces, which follows as:

$$FS = \frac{Resisting\ force}{Driving\ force} = \frac{c*l_{ab}+[(W-F_v)*cos\beta-F_h*sin\beta]*tan\phi}{(W-F_v)*sin\beta+F_h*cos\beta} \tag{2.3}$$

where,

c=cohesion,

ϕ=internal friction angle,

l_{ab} = length of the failure plane.

From Figure 2.7 and Equation 2.3, it can be inferred that with an increase in F_h the driving forces increase and the FS decreases. F_v has relatively less influence on the FS since it increases or decreases both the resisting and driving forces. Therefore, the vertical component of the earthquake-induced forces is frequently neglected in the pseudo-static analyses.

The selection of pseudo-static coefficient is an essential aspect since it directly defines the pseudo-static force on the failure mass, and this force should somehow be related to the amplitude of the inertial force in the potentially unstable soil mass. The inertial force would reach its maximum value when the horizontal acceleration reaches its maximum. In practice, since the actual slope is not rigid and maximum horizontal acceleration (a_{max}) exists for a substantially short time duration, pseudo-static acceleration coefficients are chosen below a_{max}.

Terzaghi (1950) first suggested $k_h=0.1$ for "severe" earthquakes (Rossi-Forel Scale X) and $k_h=0.5$ for catastrophic earthquakes. Seed (1979) presented design criteria based on a data set of 14 dams from 10 countries (seismically active) requiring 12 minimum FS from 1.0 to 1.5 with pseudo-static coefficients of 0.10 to 0.12.

Marcuson (1981) proposed 1/3 to 1/2 of the maximum acceleration as a pseudo-static coefficient for dams, including amplification and deamplification effects. The reader may refer to Kramer (1996) for further details.

Seed and Martin (1966), Dakoulas and Gazetas (1986) used shear beam model showing that the inertial force on a potentially unstable slope in an earth dam is related to the response of the dam. When the pseudo-static coefficients for a deep-seated

19

failure and surface failure is compared, deep-seated failure requires a substantially smaller pseudo-static coefficient.

Seed (1979) have also demonstrated that for earth dams of ductile soils (which are defined as those do not generate high PWPs or show more than 15% strength loss upon cyclic loading) with crest accelerations less than 0.75g, $k_h = 0.10$ (M = 6.5) or $k_h = 0.15$ (M = 8.25) acceptable deformations would result in a factor of safety of at least 0.75. This criterion allows the use of pseudo-static acceleration as small as 13% to 20% of peak crest accelerations.

Later Hynes-Griffin and Franklin (1984) applied Newmark sliding block analysis (which will be explained in the following section) to over 350 accelerograms and found that earth dams with pseudo-static FS greater than 1.0 using $k_h = 0.5 \cdot a_{max}/g$ will not experience hazardous deformations. In addition to engineering judgment, Hynes-Griffin and Franklin (1984) may be treated as a rule of thumb for most slopes.

Shortcomings of the pseudo-static approach may be summarized as:

1. It cannot simulate complex dynamic inertial forces with a time dependence.
2. It gives no deformation information caused by earthquake shaking.
3. It is not reliable for ductile soils. There are some examples in which the pseudo-static analyses produced ample FS (i.e., well above 1) for several dams later failed during earthquakes (Kramer, 1996).

Despite the limitations mentioned, the pseudo-static approach has certain advantages: firstly, computations are easy to recognize and perform; and secondly, the method produces quantitative means of stability.

2.4.2. Newmark Sliding Block Analysis

Newmark (1965) proposed a sliding block analogy to computing the displacements under cyclic loading if the material is not subjected to liquefaction. The background idea of this approach is based upon a rigid block sliding on a plane which is shown in Figure 2.8.
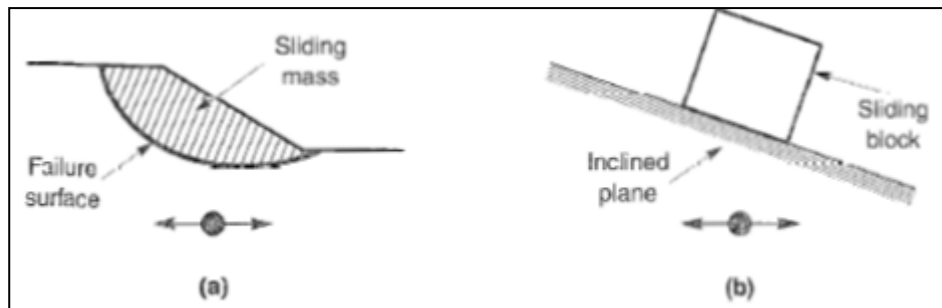
Figure 2.8. The analogy between (a) potential landslide and (b) block resting on an inclined plane (Kramer,1996).

If the inertial forces on a potential slide mass are large enough to overcome the yield resistance, the slope failure initiates and movements start. Therefore, considering the point at which the inertial forces sufficiently high to cause the yielding to start in Figure 2.9, the corresponding acceleration (yield acceleration as a function of time) can be integrated to find velocities and permanent displacements of the sliding mass. (Figure 2.10) (Seed, 1979)
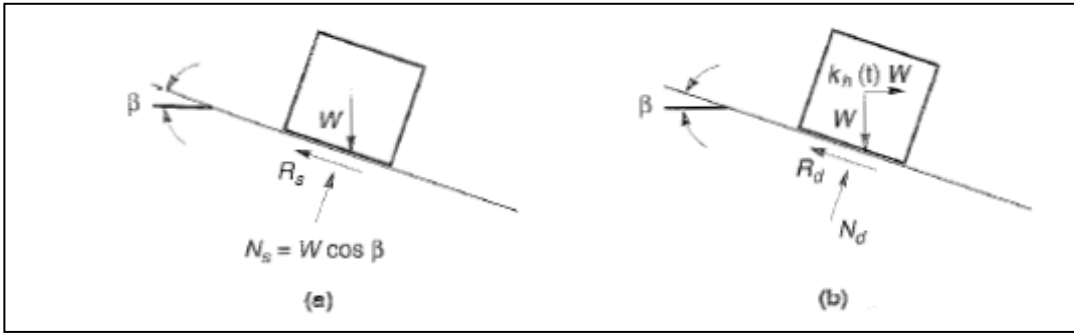
Figure 2.9. Forces that act on a block resting on an inclined plane: (a) static conditions;(b) dynamic
conditions (Kramer,1996).
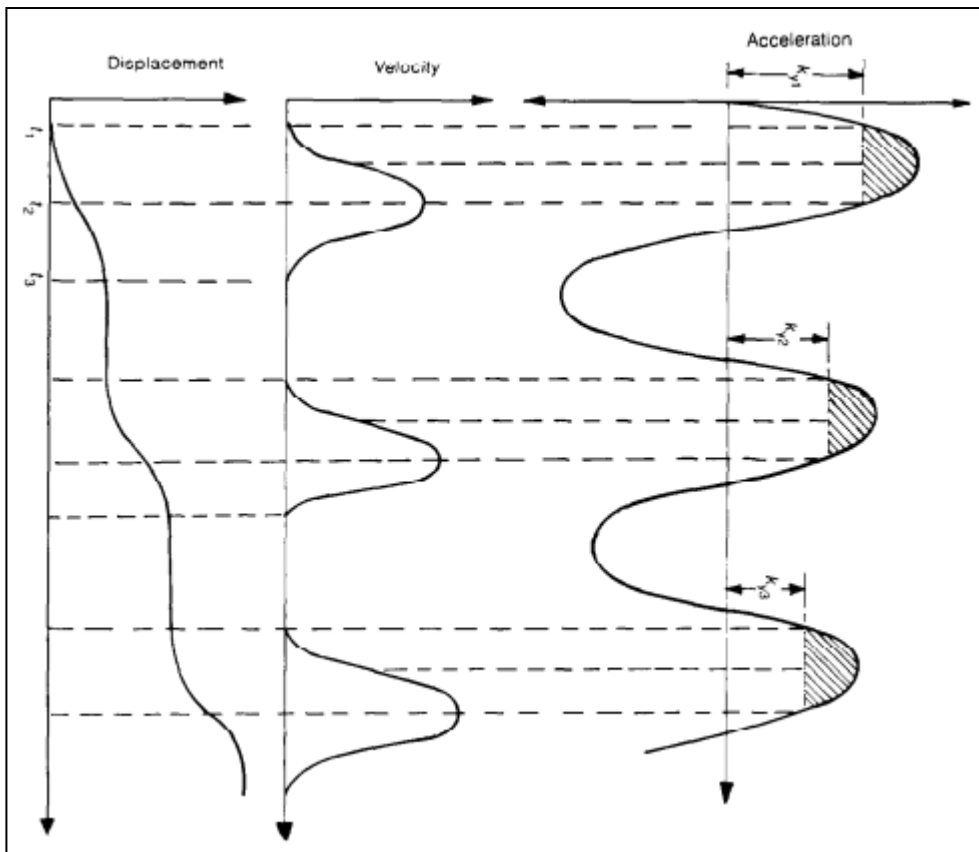
Figure 2.10. Integration of effective acceleration time-history to determine velocities and
displacements (Seed,1979).

Two parameters are required to calculate the permanent deformations:

22

A. Yield acceleration (k_y: the pseudo-static inertial coefficient which results in a factor of safety of 1.0 for the potential sliding mass).

B. Base acceleration time history.

Newmark's assumptions for the construction of this method are (Akış (Keklikoğlu), 2002) :

1. The soil shows rigid-perfectly plastic behavior.
2. Displacements take place along a single, particular slip surface.
3. The soil does not lose any strength after shaking.

Jibson (1993) prepared simplified design charts that predict sliding block displacement based on yield acceleration and Arias intensity by using eleven earthquake time histories. Sarma (1975) accounted for the generation of pore pressure along the shear surface when developing his simplified design charts. Houston et al. (1987) modified the procedure of Newmark to extend for strain-softening soils.

2.4.3. Makdisi-Seed Analysis

Makdisi and Seed (1978) utilized average accelerations calculated by the Chopra (1966) procedure and Newmark Sliding Block Analysis to calculate earthquake-induced permanent deformations of embankments and earth dams. A simplified procedure was constructed with the help of some simplifying assumptions about the results of dynamic FEM and shear beam analyses. The summary of this procedure is that yield acceleration for a probable surface is calculated using dynamic yield strength (80% of the undrained strength). The dynamic response of the dam/embankment explained by an acceleration ratio, which varies with the depth of the potential surface relative to the height of the dam/embankment. (Figure 2.11)
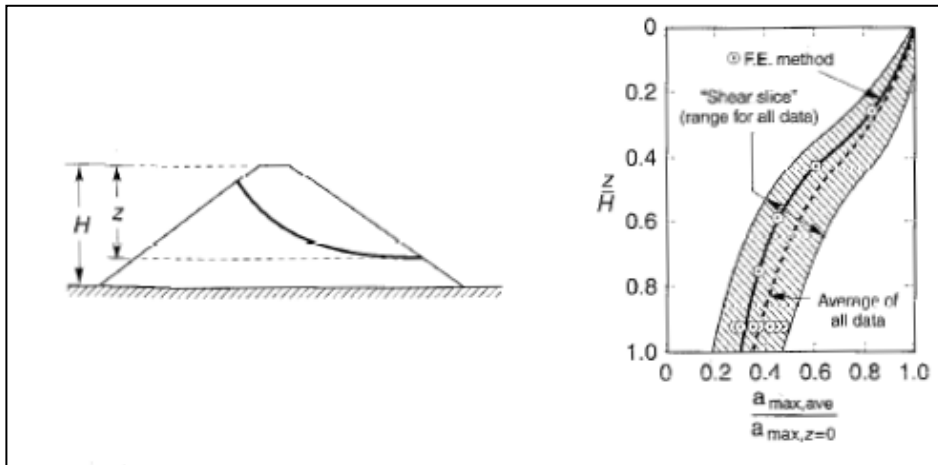
Figure 2.11. Variation of average maximum acceleration with a depth of potential failure surface for dams and embankments. (After Makdisi and Seed [1978]).

Makdisi and Seed calculated the variation of permanent displacement with a_y/a_{max} and magnitude by using real and hypothetical dams as well as actual and synthetic earthquakes. Prediction of permanent displacements can be performed with the charts shown in Figure 2.12.
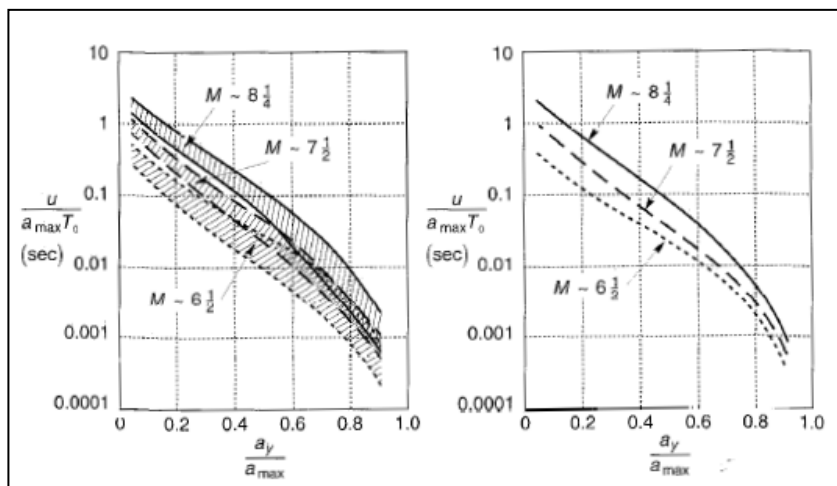
Figure 2.12. Variation of normalized permanent displacement with yield acceleration for earthquakes of different magnitudes: (a) summary for several earthquakes and dams/embankments; (b) average values. (After Makdisi and Seed [1978]).

2.4.4. Stress-Deformation Analysis

Seismic slope stability with stress deformation analysis can be carried out utilizing numerical approaches such as the finite element method. In such analyses, the earthquake-induced permanent strains in each element of the FE mesh can be integrated to compute permanent displacements using several methods. These are (Kramer, 1996):

- Strain potential approach.

- Stiffness reduction approach.

- Nonlinear analysis approach.

The stiffness reduction and strain potential approaches estimate permanent strains from laboratory test results to determine the stiffness of the soil subjected to cyclic earthquake loading. The nonlinear analysis approach uses the nonlinear inelastic stress-strain behavior of the soil to find the development of permanent strains during an earthquake. It is essential to remind that the accuracy of this model depends principally on the accuracy of the constitutive or stress-strain model on which the material behavior is based.

2.4.5. Finite Element Method Accuracy for Wave Propagation Problems

Lysmer and Kuhlemeyer (1973) show that for the accurate representation of wave transmission through a model, the spatial element size should be:

$$Element\ size \ \leq \ \frac{\lambda}{10}$$

Where λ is the wavelength associated with the highest frequency component that contains considerable energy. To satisfy this criterion for a velocity input with a high

peak and short rise time, a rather fine mesh may be necessary, which in turn requires an excessive amount of computing time. Fortunately, for most of the earthquakes, the more significant part of the input velocity (or acceleration) is contained in the lower-frequency components. By filtering the input velocity and removing high-frequency components, mesh size can be increased without affecting the results considerably (Rocscience, Rocscience RS2 Online Help, 2019).

2.4.6. Rayleigh Damping

Differential equation of a dynamic system:

$$[M]\left(\frac{d^2x}{dt^2}\right) + [C]\left(\frac{dx}{dt}\right) + [K]\big(x(t)\big) = F_{stat.} + F_{dyn.} \tag{2.4}$$

$x(t)$ =displacement function with respect to time

[M]= mass matrix

[C]= damping matrix

[K]= stiffness matrix

In Rayleigh damping, the damping matrix [C] is expressed as:

$$[C] = (\propto_M) * [M] + (\beta_K) * [K] \tag{2.5}$$

where α_M and β_K are constants that have units of s^{-1} and s, respectively. [K] refers to the linear stiffness matrix of the structure, which is constructed with initial tangential stiffness. Thus, [C] has a stiffness-proportional term and a mass-proportional term. In this way, the damping becomes proportional to the mass and stiffness of the system.

The procedure to determine α_M and β_K involves choosing proper values of damping to the modes of a linear system. Damping of mode, i is expressed by the damping ratio, ξ_i, the ratio of the mode's damping to the critical value. Hence, if α_M and β_K are known, ξ_i can be computed from:

$$\xi_i = \frac{1}{2\omega_i}\alpha_M + \frac{\omega_i}{2} * \beta_K \qquad (2.6)$$

where ω_i is the natural frequency (rad/s) of mode i. This procedure results in a nearly constant damping value for modes with a frequency range from $\hat{\omega} - R\hat{\omega}$ where R>1.

The multiple degree of freedom (DOF) model systems have many natural frequencies. However, a constant level of damping for all frequencies is not possible. In Rayleigh damping, it is allowed to define the damping ratio for two frequencies and the rest of the frequencies are defined by a curve, an example of which is given in Figure 2.13. In general, the frequencies in between the mentioned two frequencies have a damping ratio lower than the specified damping ratios, and the outside frequencies are damped more heavily (Rocscience, Rocscience RS2 Online Help, 2019).
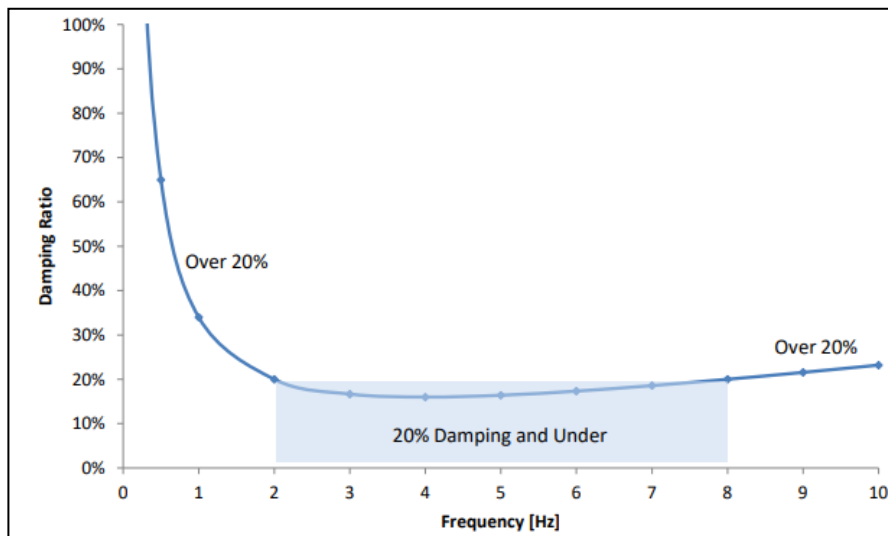
Figure 2.13. Damping ratio plot, 20% damping at 2 and 8 Hz (Rocscience,2019).

The soil stiffness decays with the increasing strain level induced by the cyclic loading, and the sequence of loading and unloading paths produces a hysteretic loop with the dissipation of energy and consequent damping. Some of the traditional constitutive models, for example, Mohr-Coulomb, cannot describe the hysteretic damping. Instead, the total amount of damping is presented through the frequency-dependent Rayleigh formulation defined using viscous damping, which should be consistent with the strain level caused by the earthquake (Laera, 2015).

To model the soil with the Mohr-Coulomb approach in dynamic calculations, the proper selection of the stiffness parameters is essential to predict the wave velocities correctly in the soil, requiring a much larger small strain stiffness rather than a stiffness at engineering strain levels. The Mohr-Coulomb soil model can generate plastic strains in the cyclic loading if stress points reach the failure criterion, which leads to damping. However, stress cycles under failure envelope will only create elastic strains and no (hysteretic) damping, nor strain accumulation or PWP, and no liquefaction. Rayleigh

damping may be used in dynamic soil modeling to simulate damping characteristics of the soil in cyclic loading (Plaxis, 2019).

CHAPTER 3

SOFTWARE USED IN THE CASE STUDY

This chapter presents slope stability software programs that have been used for the case study. For the two-dimensional limit equilibrium analyses, Rocscience SLIDE, for two and three-dimensional FE analyses Rocscience RS2 and Rocscience RS3 have been utilized, respectively.

3.1. Limit Equilibrium Analysis with SLIDE

SLIDE can be utilized to analyze both circular and non-circular slip surfaces of soil and rock slopes using a vertical slice or non-vertical slice limit equilibrium methods (e.g., Sarma, Spencer, Janbu, Bishop, etc.). It also has an FE groundwater seepage analysis option for transient and steady-state conditions. The program has the following three modules: SLIDE Model, SLIDE Compute, and SLIDE Interpret (Rocscience, Rocscience SLIDE Online Help, 2019).

Model is the program for pre-processing, which consists of entering and editing the model boundaries, loads, material properties, slip surface definition, groundwater conditions and saving the input file. Model, Compute and Interpret modules work as separate standalone programs and they interact with each other in a way that:

1. Compute and Interpret can both be started from within the Model.
2. Compute must be run on a file before results can be analyzed with Interpret (red arrow).
3. The model can be started from Interpret.

A new file may be created, or an existing model file may be opened (i.e., importing SLIDE, SLOPE/W and XSTABL) in the modeling module. After creating or opening a file, the module will offer three different analysis (modeling) modes: Slope Stability Mode, Steady State Groundwater Mode, and Transient Groundwater Mode.

The program offers users two options when defining the critical failure surfaces, which are manual critical slip surface and grid search options. Groundwater surfaces may also be defined as piezometric lines. After finishing the modeling, one should conduct computation in the modeling module. A window (Compute Module) is opened, which shows the computation stage. Later the results of the analysis are obtained from the Interpret Module. Results include FS, probability of failure, reliability index, and critical failure surfaces. The Interpret Module is useful to organize the desired data such as filtering and exporting data, creating contours, etc.

3.2. Two-Dimensional Finite Element Analysis with RS2

RS2 is a program which conducts two-dimensional finite element analyses of geotechnical structures for civil and mining applications. The program was previously named as "Phase 2". RS2 is a general-purpose geotechnical finite element program, and the fields of application are slope stability, tunnel and support design, consolidation, dynamic analysis of foundations, embankments, groundwater seepage and more. As in SLIDE, RS2 has the same three modules: RS2 Model, RS2 Compute and RS2 Interpret (Rocscience, Rocscience RS2 Online Help, 2019).

RS2 creates finite element meshes in the modeling module. The program interface is similar to SLIDE. The user should first start with defining the external boundaries after that material and groundwater boundaries have to be specified. Later, the material type and properties of the materials should be defined and assigned between the

boundaries. The meshing stage can be completed afterward. External loads may be assigned to the element nodes of the external boundary, while restraints and supports may also be defined element nodes inside of the model. Upon completion of the model, the user should run the software to calculate the stresses and displacements at the nodal points of the model mesh.

It is possible in the shear strength reduction (SSR) method to automatically perform FE slope stability analyses and calculate a critical strength reduction factor (SRF) for the model. This factor is equivalent to the FS of the slope. The basic concept behind the shear strength reduction method may be summarized as follows:

1. The strength parameters of a slope are reduced by a specific factor (SRF), and FE stress analysis is computed.
2. This process is repeated for increasing values of SRF until the model becomes unstable (i.e., the analysis results do not converge)
3. The critical SRF or safety factor of the slope is determined.

If a user carries out SSR analysis in RS2, the program considers the stability of the entire model by default, meaning that the critical failure zone may occur anywhere in the model. Alternatively, the user may wish to focus on particular potential failure zones in the model. Focusing can be done by the SSR search area option, which allows the user to apply the SSR analysis to any region of a model. Materials outside the area are assumed to behave elastically.

It is possible in RS2 to conduct dynamic analyses of geotechnical structures due to earthquake loading or other dynamical applied loading. To begin dynamic modeling, one has to select the Dynamic Analysis option from the project settings and enter the number of stages. Hence, the time history data can be uploaded, and dynamic loads

can be defined and assigned to the model. Once the computation is finished, the resulting SRF, displacement contours, stress distribution, etc. can all be seen from the Interpret Module.

3.3. Three-Dimensional Finite Element Analysis with RS3

RS3 is the three-dimensional modeling and analyzing finite element program version of RS2, and it has the same areas of applications. Aside from two-dimensional applications, the use of RS3 needs some additional terminology to ensure the available resources are apparent. An entity is a common term used to describe any item that is added to the model. Entities may include geometry, loads, groundwater, support, etc. Every operation adds entities to the model to build up the features of the three-dimensional simulation. Geometry entity examples are lines, surfaces, and volumes, which can generate the model shape. Boundary refers to vertices, edges, or faces of a geometry entity to apply loads, restraints and other boundary conditions. There are also project summary page, side panels, and workflows as in RS2 and SLIDE. The viewports are the four major modeling and result viewing screens in RS3. Three viewports show the model in XY, ZX, and YZ perspective while the fourth viewport is for the three-dimensional view (Rocscience, Rocscience RS3 Online Help, 2019).

Geometry entities and existing RS3 models can be imported from the related menu buttons. Resulting three-dimensional entity shapes may be defined as different layers. Therefore, material types and groundwater can be assigned to those layers. For each layer, one material type can be specified. The borehole manager helps users to layer the existing geometry entity.

The loading option of the program includes the application of field stress to represent initial stress conditions. A pseudo-static seismic load can be applied to the model as a

seismic loading. The Add Load option allows users to add various distributed or concentrated loads to boundaries on surfaces, edges or points.

Restraints on the geometry of the model can be defined from the Restraints Menu. Upon completion of the model, the analysis is initiated by the Compute button, a new computation module is opened as in SLIDE and RS2 results can be seen from the Interpret the Results tab, which is located inside the program, unlike SLIDE and RS2 interpreters, which are standalone. Analysis results displayed in the viewports include surface contours, contours on any user-defined plane, iso-surfaces, line queries, yielded elements and deformation vectors.

All in all, the reader should review the online help documents and the project settings of each program carefully to gain insight.

CHAPTER 4

DESCRIPTION OF THE CASE SLOPE AND PREVIOUS INVESTIGATIONS

The case slope is located in the Akpınar District, which is in Dikmen/Çankaya municipality region in Ankara. Figure 4.1 shows its location and a satellite view of the area; Figure 4.2 and Figure 4.3 are views from the case site. Surface topography of the site consists of a 20° inclination on the average, rising towards east. Due to the intense and rapid urbanization in the recent decade, several new multistory residential buildings have been constructed within the area, including the slope under consideration. During this transformation, excavated soil from foundation pits were in part dumped over the slopes, which aggravates the slope stability problems in the area.
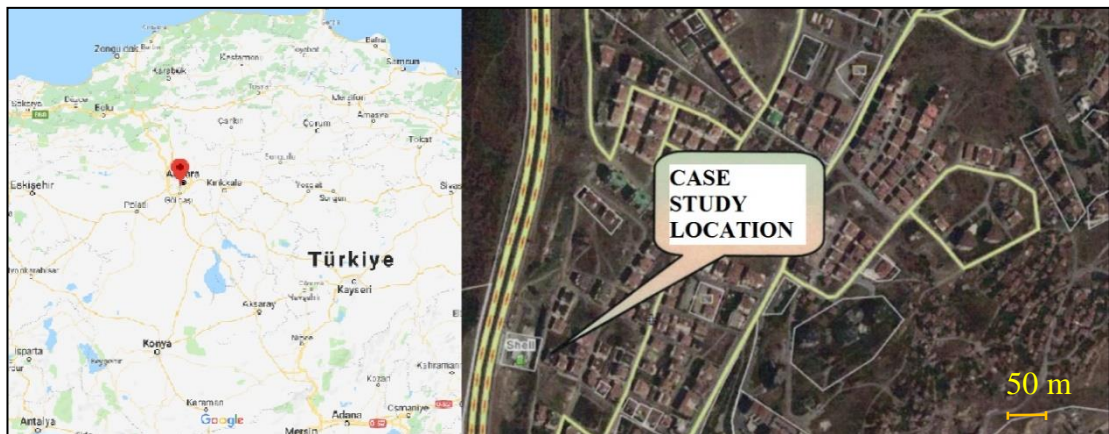
Figure 4.1. Location and satellite view of the case slope.

Figure 4.2. A view of the slope towards north (July 2019).

Figure 4.3. A view from the toe of the slope towards crest (July 2019).

4.1. Case Study Definition

On 16 June 2011, a heavy rainfall occurred in Ankara, causing local flash floods and various forms of damage to residential units and transportation systems in the city. Regarding the building structures on the case slope, damage was inflicted over several multi-story residential buildings. The pattern of the damage was in the form of cracks in structural elements and infill walls. These damages, which occurred within days following the heavy rainfall, were understood to be originating from ground deformations apparently due to saturation of the foundation soils. One of such buildings (Güneş Apartment) located on the case slope (Figure 4.4 - enclosed with a yellow box), was leaned at its foundation in the slope direction by 4 to 5 degrees and had to be demolished later[2]. In addition, formation of tension cracks and limited downward movements were observed at a few locations on the slope surface.

Foundation excavation was ongoing for the construction of a business center on the toe of the slope at the time of the aforementioned heavy rain. The excavation, which was 18 m high and 44 m wide in the direction normal to slope inclination, was retained by an anchored reinforced concrete wall. Following the heavy rainfall, cracks started to form on the wall surface. There exists a gas station which is retained by a wall with permanent ground anchors adjacent to the business center construction. Figure 4.5 shows the locations of the Güneş Apartment (small yellow box) and the business center construction site (big yellow box). Güneş Apartment does not appear in this rather recent picture since it had already been demolished.

---

[2] Figure 4.4 was taken in 2011, before the demolition of the Güneş Apartment.

Figure 4.4 A view of Güneş Apartment from the downhill (Çokca et al., 2011).

Figure 4.5. Locations of Güneş Apartment and the business center construction site (Yandex,2019).

Subsequently, triggering off a slope instability was suspected in the area due to the heavy rain and detailed investigations were deemed necessary. Accordingly, the Directorate of Disaster and Emergency Management and Çankaya Municipality initiated a comprehensive investigation campaign and hired several companies for this purpose and required consultancy services from METU (Middle East Technical University) Civil Engineering Department. Subsurface investigations at the site included drilling of boreholes, installation of several inclinometers in the area as well as relevant field and laboratory tests.

4.2. Summary of the Previous Studies

Several reports delineating the geotechnical site conditions in the area and searching into the characteristics and extent of slope instability were issued by several sources previous to the present study. A list of these reports is given in Table 4.1 in the chronological order and briefly summarized in the following.

Table 4.1. *Relevant reports issued on Akpınar landslide in the chronological order.*

Name	Date
İller Bankası (İlbank) Geological Investigation Report	May 1987
Site Investigation Report of Business Center	July 2010
Chamber of Civil Engineers Report	July 2011
Chamber of Geological Engineers Report	July 2011
Dr. B. S. Bakır (Middle East Technical University [METU]) Report-1	July 2011
Directorate of Disaster and Emergency Management (AFAD) Report	August 2011
Dr. B. Kiper (Bülent Kiper Engineering Co.) Report[3]	September 2011
METU Geotechnical Division Report[4]	December 2011
Dr. B. S. Bakır (METU) Report-2	January 2012

---

[3] The report will be briefly named as "Kiper Report" and the company as "Kiper Co." in the succeding sections.
[4] Will be briefly named as ''METU Report'' in the succeding sections.

Name	Date
Kilci Engineering Co. Report[5]	July 2012
Dr. B. S. Bakır (METU) Report-3	September 2012

4.2.1. İller Bankası (İlbank) Geological Investigation Report

İlbank issued a geological investigation report regarding the broader area of the case slope as early as 1987. It was stated in the report that the area in question had a potential for slope instability and hence was not suitable for settlement. Further studies regarding the slope and appropriate precautions were recommended for foundations in case the settlement would be allowed in the region (Tanverdi and Ekici, 1987).

4.2.2. Site Investigation Report of Business Center

A detailed site investigation report was prepared for the business center area previous to its construction. Four boreholes (BH) having depths of 17 m to 25 m were drilled within the footprint of the building. Starting from the surface, residual soils and greywacke layers were reported to be encountered in the borehole logs. No static water table was observed within the borehole depths. In the report, allowable bearing capacity and settlement calculations were provided for the business center building and suggestions were made for the proper retaining of the sides of foundation excavation (Saygı, 2010).

4.2.3. Chamber of Civil Engineers Report

Residents of the Güneş apartment appealed to the Chamber of Civil Engineers (CCE) for an investigation of damages in the building. However, there were no cracks yet in the structural load-bearing system when the report was prepared. Cracks existed only in the stairs at the entrance of the building besides those in the infill walls. Accordingly, minor repairs and construction of new retaining structures supported by

---

[5] The report will be briefly named as "Kilci Report" and the company as "Kilci Co." in the succeding sections.

short piles were recommended in the report. Also, the situation was recommended to be monitored for a sufficient period of time (Kocaman and Doğan, 2011).

4.2.4. Chamber of Geological Engineers Report

Chamber of Geological Engineers (CGE) prepared an investigation report in July 2011 upon request of Güneş Apartment residents. In the report, the sliding of the foundation is said to be related to the intrusion of water into the residual soils and greywacke constituting the foundation soils. Detailed investigations were recommended to be carried out to find out the mechanism and identify the domain of the landslide (CGE, 2011).

4.2.5. Directorate of Disaster and Emergency Management (AFAD) Report

The buildings resting on the slope were investigated by AFAD engineers. No severe damage was observed except Güneş Apartment. However, it was recommended that the buildings in the area should be monitored for a while, and in case of an emergency, they should be evacuated. Additionally, it was stated in the report that the excavation of the business center could have been a factor in triggering the landslide (Şeren and İleri, 2011).

4.2.6. Dr. B. KİPER (Bülent Kiper Engineering Co.) Report

Kiper Co., which was hired by the Çankaya Municipality, drilled eight boreholes with depths ranging between 25 m to 35.5 m, and installed inclinometers to each of them between August and September 2011. Figure 4.6 shows the locations of the boreholes. It should be noted that the acronym SK refers to the abbreviation of a borehole (BH) in Turkish. Also, the business center excavation does not appear in the picture since satellite view was taken before the beginning of its construction. The GWT level varied between 1.5 m to 18.5 m depths in the boreholes. Laboratory tests were carried out on the samples retrieved from boreholes.

Figure 4.6. Locations of the boreholes installed by Kiper Co. (Çokça et al., 2011).

The primary rock formation at the site was identified as phyllite (clayey schist), graphitic schist and metagreywacke. Graphitic schist and phyllite are particularly weak. There also exists 1 m to 13 m thick clayey sandy gravelly debris and residual soil layers locally on the surface. When field investigations started, ground movements caused by the heavy rainfall were still ongoing. Readings from inclinometers indicated movements in the direction down the slope (towards west). Displacements ranged between 0.2 cm and 9.5 cm within a depth range of 1 m to 20 m. It was argued in the report that the differences observed in the static GWT levels signify an unstable groundwater regime. However, leaking water from surface and infrastructure pipes (which were partially damaged due to ground deformations) was understood to be retained by the impermeable layers. Besides, due to inundation, near-surface soils reached to plastic and liquid states, leading to decreases in the soil strength and subsequent shallow and deep slides.

In the report, it was stated that the lack of surface drainage system in the area must have particularly aggravated the situation. Therefore, an urgent rehabilitation and extension of the infrastructure in the area are needed. Due to the danger of complete overturning, evacuation of Güneş Apartment was recommended. No additional buildings should be constructed on the slope. It was also recommended that the retaining wall of the business center retaining wall should be extended 50 m towards the north.

4.2.7. METU Geotechnical Division Report

METU Report was prepared upon the request of the Çankaya Municipality. Within the context of the report, data collected from inclinometers of Kiper Co. was evaluated, approximate boundaries of the landslide were defined, and slope stability calculations were conducted. The landslide rate was reported to be classified as very slow to slow. According to the results of the analyses, shallow and deep landslides, consistent with that reported by Kiper Co., existed in the area. Safety factors were calculated for the deep zones around 0.7- 0.8, and 0.65 for the shallow zone. These factors of safety are rather small compared to those in the Kiper Report.

Additional assessments and recommendations in the report included the following: The gas station and the buildings in the vicinity of Güneş Apartment should be evacuated. Residents of those buildings should not be allowed for returning to their homes unless the stability of the slope was ensured. Güneş Apartment should be demolished, and the debris should be removed. Inclinometer readings would be continued. Further investigations, including drilling of additional boreholes, laboratory experiments, and three-dimensional analyses, were required to identify whether the business center foundation excavation had a triggering effect on the landslide.

4.2.8. Kilci Engineering Co. Report

Kilci Co. was employed by Çankaya Municipality for supplementary investigations in compliance with the recommendations given in the METU Report. Within the scope of the study, 11 boreholes were drilled with a range of depths of 20 m to 56 m and inclinometers were installed each of these boreholes. Besides, 2 observation wells were dug, and relevant laboratory tests were conducted over retrieved soil samples. GWT levels varied between 1.7 m to 17.5 m in the boreholes. Slope stability calculations were also performed. Locations of the boreholes, observation wells, and the cross-sections used in the analyses are shown in (Figure 4.7)[6]. The data from boreholes, inclinometers, and slope stability analyses were consequently evaluated.
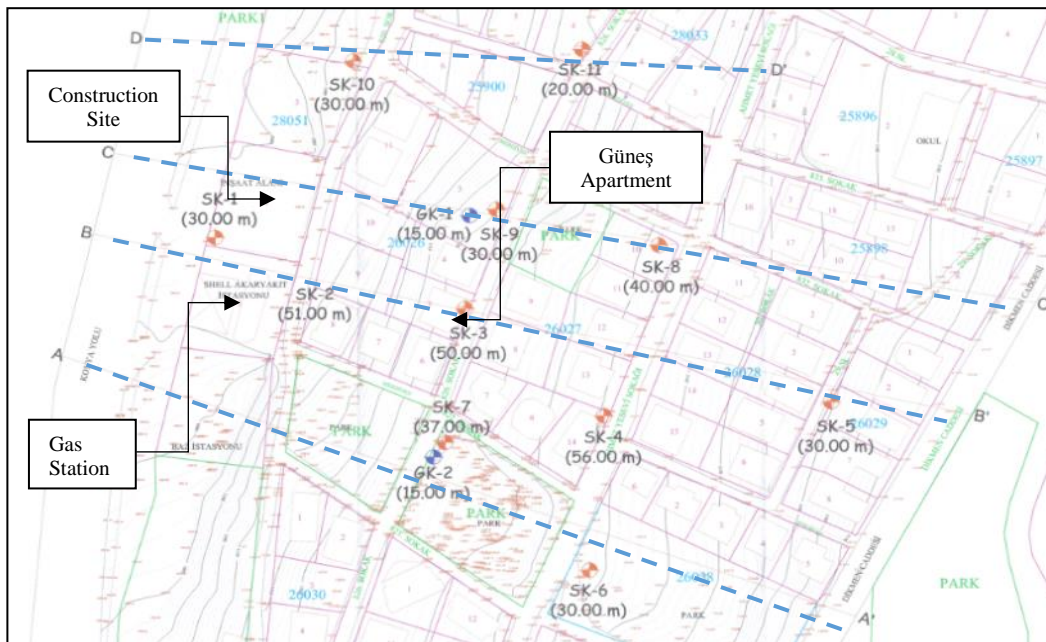
Figure 4.7. Locations of the boreholes drilled and cross-sections used in slope stability analyses by Kilci Co. (Nalçakan et al., 2012).

Slope movements were considerably reduced due to the dry season when the field investigation campaign was launched. Hence, no significant movement was observed

---

[6] Note that "GK" refers to the abbreviation stands for observation well in Turkish.

except for BH7 (Figure 4.7). The general subsurface layering of the site is debris or residual soil, greywacke, schist (phyllite), limestone and schist-limestone mélanges in the increasing order of depth from surface. From laboratory experiments, cohesion intercept and internal angle of shear were determined to range respectively between zero to 10 kPa and between 18º to 26º, whereas the internal angle of shear was identified to be 15.65º (for c=1 kPa) from the back-analysis of the slope (Nalçakan et al., 2012).

4.2.9. Dr. B.S. Bakır (METU) Reports

The first report of Dr. Bakır, which is dated July 2011, is about the investigation and evaluation of the problems encountered following the downpour in the ongoing business center foundation excavation (Figure 4.8). Additional structural support measures were recommended in relation to the tension cracks that were formed in the retaining wall. The surfacing of the road behind the east (uphill) side of the wall should be rehabilitated to prevent further water intrusion into the ground. Damages in the buildings on the slope were not related to excavation, but due to the volumetric deformations of foundation soils caused by the seeping of surface water from the downpour. Cracks formed on the concrete ground surfacing of the gas station were due to the ongoing nearby excavation (Figure 4.9) (Bakır, 2011).

Figure 4.8. View of the business center foundation excavation and support system (Bakır, 2011).

Figure 4.9. Crack formations observed in the gas station due to the ground deformations caused by the foundation excavation (Bakır, 2011).

In his second report, dated January 2012, Dr. Bakır made evaluations concerning the possible effects of the business center foundation excavation on the case landslide. In the report, previous investigations were evaluated, and recommendations were

proposed subsequently. In the AFAD report, it was stated that the excavation of the business center could have been a factor in triggering the landslide. This assertion was considered to be rather premature. The recommendation given in Kiper Report regarding the extension of the retaining wall of the business center 50 m towards north would not affect the stability of the slope since the deep slide surface extends beyond the depth of the wall. The values of safety factors calculated in the METU Report were a bit small for a landslide with a very slow rate. Two-dimensional analyses would be sufficient since such analyses provide lower safety factors compared to the three-dimensional analyses, and that very precise and detailed information would be required besides a much greater effort to obtain a meaningful outcome.

From site investigations and examination of the inclinometer data provided in the Kiper Report, it was inferred that there existed shallow and deep-seated slope failures ongoing in the area. The deformations observed in the Güneş Apartment and twin buildings (located immediately behind the wall) were due to volumetric deformations caused by the saturation of the foundation soils. At the time of heavy rain, depth of excavation of the business center had reached 21 m, and no problem existed in either the retaining wall or the buildings behind it. Following the rain, situation is reevaluated and excavation depth is increased only three more meters. The amount of deformation of the wall measured between the occurrence of the downpour and the completion of excavation was less than four centimeters. On the other side, the reasons behind triggering of the deep slide were the subsequent increase of mass due to saturation of surface soils and possible strength loss due to the rising of the groundwater table at the site.

It was concluded that the business center excavation had no triggering effect on the deep or shallow landslides. Also, as stated in other reports, the non-existence of an effective surface drainage system was a major drawback. The construction purpose of

retaining wall was not stabilization of a potential landslide. Completion of the business center construction would contribute positively to the overall slope stability since a massive load would be exerted on the toe of the slope (Bakır, 2012).

The third report of Dr. Bakır, dated September 2012, was prepared upon the request of Çankaya Municipality and is mainly concerned with the evaluation of Kilci Report. The extensively disintegrated greywacke and schist units could be classified as weak to very weak rock due to their relatively low RQD (Rock Quality Designation) values. Measurements were taken in the dry season and considerable time had passed since downpour. Hence, no significant movements were observed in the inclinometers, with the exception of BH7 (Figure 4.7). This observation verified the proposed reasons for the landslide, which are mass increase and likely partial strength loss due to infiltration of rainwater in the slope surface, besides possible elevation of the groundwater table.

Back analyses were considered to be more realistic rather than shear box tests to obtain the shear strength parameters. The safety factor values calculated in the METU Report were too low for a slow to a very slow-moving landslide. In natural slopes, it would be difficult to obtain reliable strength parameters. Thus, stability analyses should be supported by back-analyses. An effective drainage system was urgently needed in the area. Otherwise, similar problems could be observed again in case of heavy rain. No additional surcharge load should be applied to the slope. The maximum number of floors for the buildings to be newly constructed should be restricted. In addition, piled raft foundations could be obliged for the new buildings. Based on the inclinometer data of Kilci Report, it was concluded that the sliding displacements were practically halted and the situation was no longer critical (Bakır, 2012).

4.3. Evaluation of the Site Inclinometer Data

Measurements were made during August thru October in 2011 in 8 inclinometers installed in the boreholes drilled by Kiper Co. Locations of these inclinometers are shown in Figure 4.6, cumulative displacement plots obtained are provided in detail in Appendix-A, Figure A.1 and the results are summarized in Table 4.2 (Çokça et al., 2011). In the plots, Axis-A represents the slope direction (i.e., uphill − downhill), whereas Axis-B is the orthogonal direction. Slip surfaces were identified within a depth range of 13 m to 34 m from the surface, and significant movements were observed at the inclinometers, except BH-5. Apparently, an error occurred concerning readings of BH-1, since the displacements clearly initiating at 17 m depth, but then become zero at a depth around 10 m.

On the other hand, displacements are observed to initiate immediately at the bottom of inclinometers without a zero-reading zone, except for BH-4, BH-7, and BH-8. This situation points out that the sliding zones are likely to occur at somewhat deeper levels than the extents of the inclinometers. Still, however, the results clearly signify the triggering of a deep-seated landslide.

Table 4.2. *The identification of the slide surface based on the inclinometer readings (Çokça et al., 2011).*

BH No	Approximate Depth of Movements from the BH Top (m)	Elevation of the BH Top (m)	Time Interval of the Measurements	Cumulative Maximum Displacement During the Time Interval (mm)	Average Velocity of Movements (mm/day) *
1	17	1123	17.08-2011-27.10.2011	26	26 mm / 70 days = 0.37

BH No	Approximate Depth of Movements from the BH Top (m)	Elevation of the BH Top (m)	Time Interval of the Measurements	Cumulative Maximum Displacement During the Time Interval (mm)	Average Velocity of Movements (mm/day) *
2	34 (Movements were also observed at 14 m depth in Direction-B)	1116	15.08-2011-27.10.2011	100	100 mm / 72 days = 1.39
3	32	1096	23.08-2011-27.10.2011	36	36 mm / 64 days = 0.56
4	13-14 (Movements were also observed at 31 m depth in Direction-B)	1098	05.09-2011-29.10.2011	40	40 mm / 54 days = 0.74
5**	21	1123	08.09-2011-27.10.2011	2.5	2.5 mm / 49 days = 0.05
6	22	1083	14.09-2011-27.10.2011	8	8 mm / 43 days = 0.19
7	13	1083	17.09-2011-27.10.2011	8	8 mm / 40 days = 0.20
8	14	1084	23.09-2011-27.10.2011	8.5	8.5 mm / 34 days = 0.25

*	Velocities of the movements were calculated based on the difference between the first and the last displacements and are considered as average values. During the time interval, they may have increased and decreased. According to Cruden and Varnes (1996) study the velocities of the case landslide are classified as "Very Slow" and "Slow".
**	It was inferred that problems in the BH-5 readings had taken place because displacements in the buildings and the surface around the BH-5 signify more serious displacements than the measurements. The reason behind the problem may be either insufficient installation depth or problems at the installation.
Note:	The existence of movements in Direction-B at BH-2 and BH-4, and rotation of the buildings (like Güneş Apartment) around themselves, signify movements in Direction-B or a certain angle (crosswise) to the downhill.

Locations of the 11 inclinometers installed later by Kilci Co. are presented in Figure 4.7. Readings were taken from these inclinometers during June and July of 2012. Cumulative displacement plots are given in Appendix-A, Figure A.7, and the results

are presented in summary in Table 4.3. Notably, the recorded displacements were much smaller compared to those from the previous set of boreholes (drilled by Kiper Co.). This difference is attributed to the alleviating of the effects of downpour in time, besides the fact that the measurements were made in the dry season. The other important observation is that the zero reading zones were observed in each case on the plots. Hence, it is recognized that the slip surfaces, which varied between 7 m and 38 m depths from the surface, were reliably identified. Consistent with the Kiper Co. set of boreholes, results validate the triggering of a deep slide. On the other hand, the peculiar displacement trend observed in the normal direction (Direction-B) in BH-7 reveals that the slope movement can locally have a considerable lateral component as well.

Table 4.3. *Inclinometer data from Kilci Co. boreholes (Nalçakan et al., 2012).*

Inclinometer (BH) No	Inclinometer Depth	Potential Slide Depths as of 28.07.2012 Date
1	28	18.0-19.0 m
2	50	37.0-38.0 m
3	50	27.0-28.0 m
4	55	No movement
5	30	No movement
6	30	17.0 m
7	37	19.0 m
8	40	No movement
9	30	25.0 m
10	30	10.0-12.0 m
11	20	7.0 m

4.4. Velocity-Time Graphs from Inclinometer Data

In this section, slip velocity variations are constructed along the inclinometer depths using recorded data. The approach followed here consists of the extraction of recorded

inclinometer data from the hard copies of cumulative displacement plots using the computer program Web Plot Digitizer, which allows users to import data from images.

Once the data is digitized, cumulative displacements can be interpolated for any specific depth and variation of displacement rates can be calculated. Examples of such plots showing the outcomes in Direction-A obtained for BH-2 of Kiper Co. and BH-7 of Kilci Co. are presented in Figure 4.10, and Figure 4.11, respectively, and the plots constructed for other boreholes installed by Kiper Co. are presented in Appendix-A.

When the two plots are examined, shallow zones are observed to have higher velocities in general. Also, the slip rates in the case of BH-2 are much greater (approaching 10 mm/day near the ground surface), compared to those of BH-7, due to the reasons explained in the previous section. A sharp reduction trend is observed in the slip velocities of BH-2 in time, which can be related to the lessening effects of the downpour.
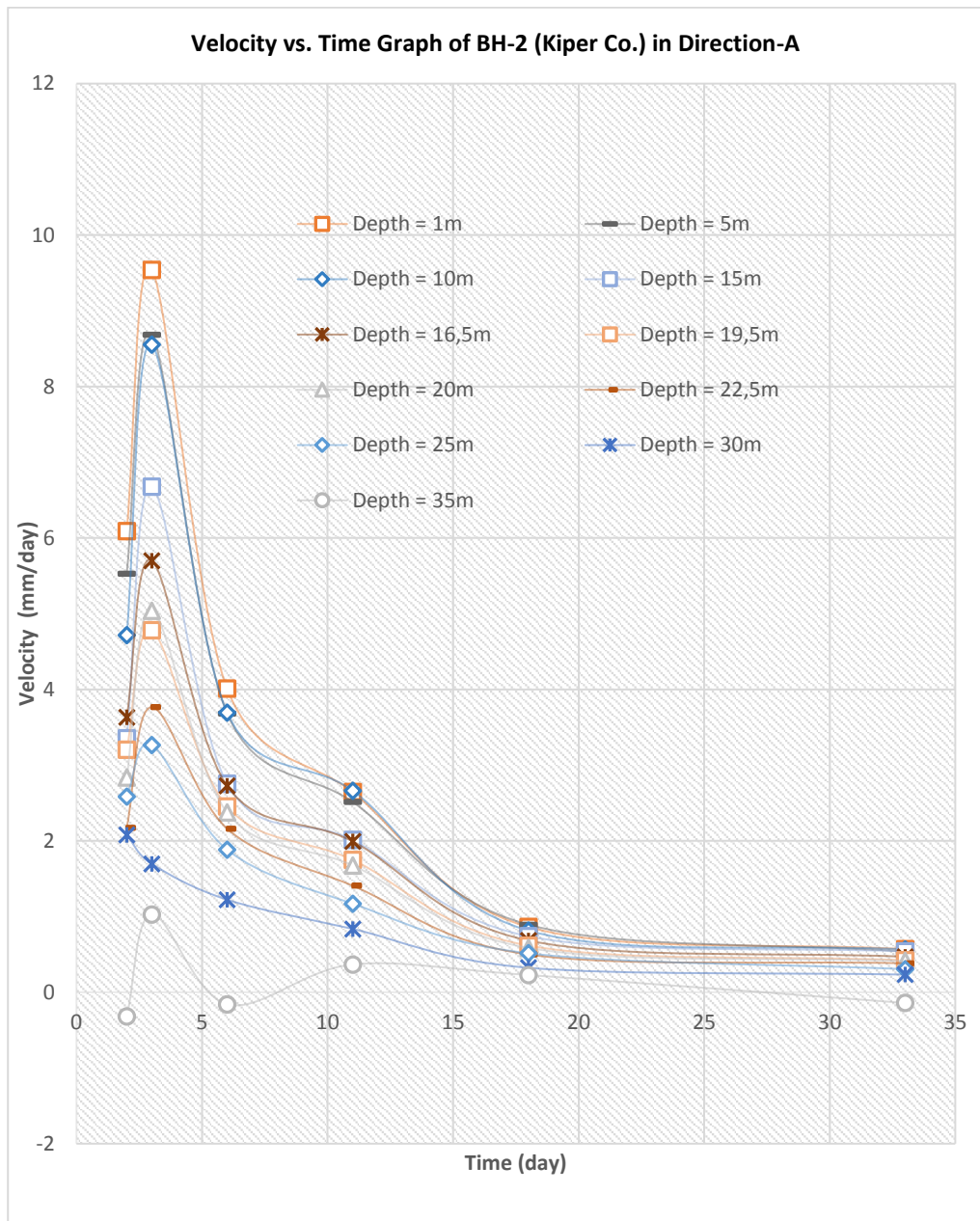
Figure 4.10. Velocity vs. time graph of BH-2 (Kiper Report) in direction-A.
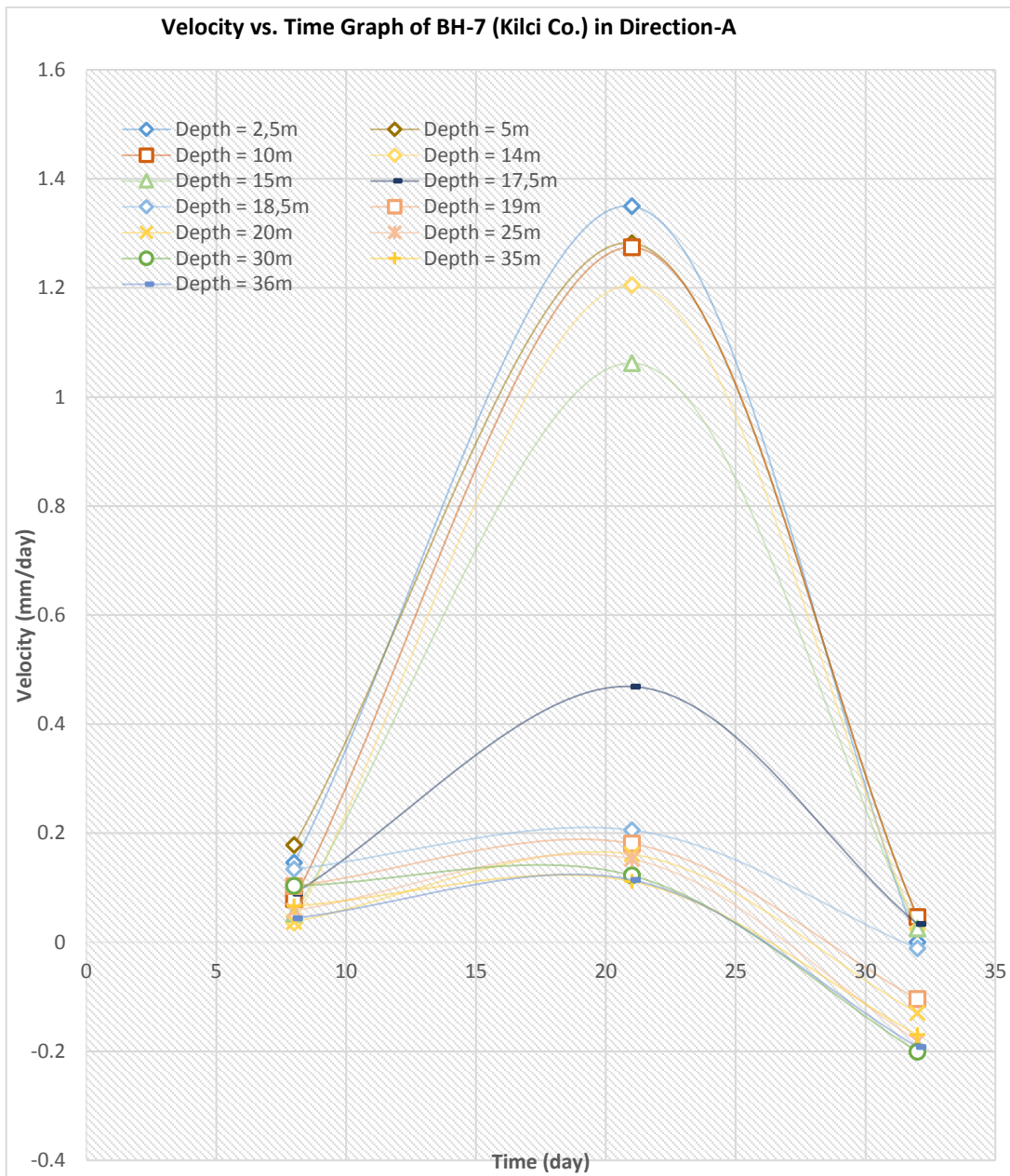
Figure 4.11. Velocity vs. time graph of BH-7 (Kilci Co.) in direction-A..

CHAPTER 5

STATIC ANALYSES OF THE CASE SLOPE

In this chapter, the modeling and analyses of the case slope with two-dimensional limit equilibrium, two and three-dimensional finite element approaches are presented.

The stability of the case slope was investigated previous to this study by Kiper Co., METU Civil Engineering Department and Kilci Co. These earlier studies are introduced first. Subsequently, the methodology followed within the framework of this study is explained and then analyses and results are presented.

5.1. Previous Analyses

LE grid search analyses have been carried out by Kiper Co., using SLIDE software. Following soil parameters, which were obtained from direct shear tests, were used in the analyses: cohesion, c = 8 kPa, internal friction angle, ϕ =20°, and unit weight γ = 17.65 kN/m^3. The retaining wall of the business center foundation excavation was modeled as a rigid block in the analyses. This rigidity is provided by using relatively high shear strength parameters for the wall material. The GWT level in the models was positioned in accordance with the observations made in the boreholes, which varied between 1.5 m to 18.5 m depths. The outcome of the analyses is shown in Figure 5.1. The critical sliding surface is observed to be rather shallow with a factor of safety of 1.042, indicating a marginal equilibrium condition.
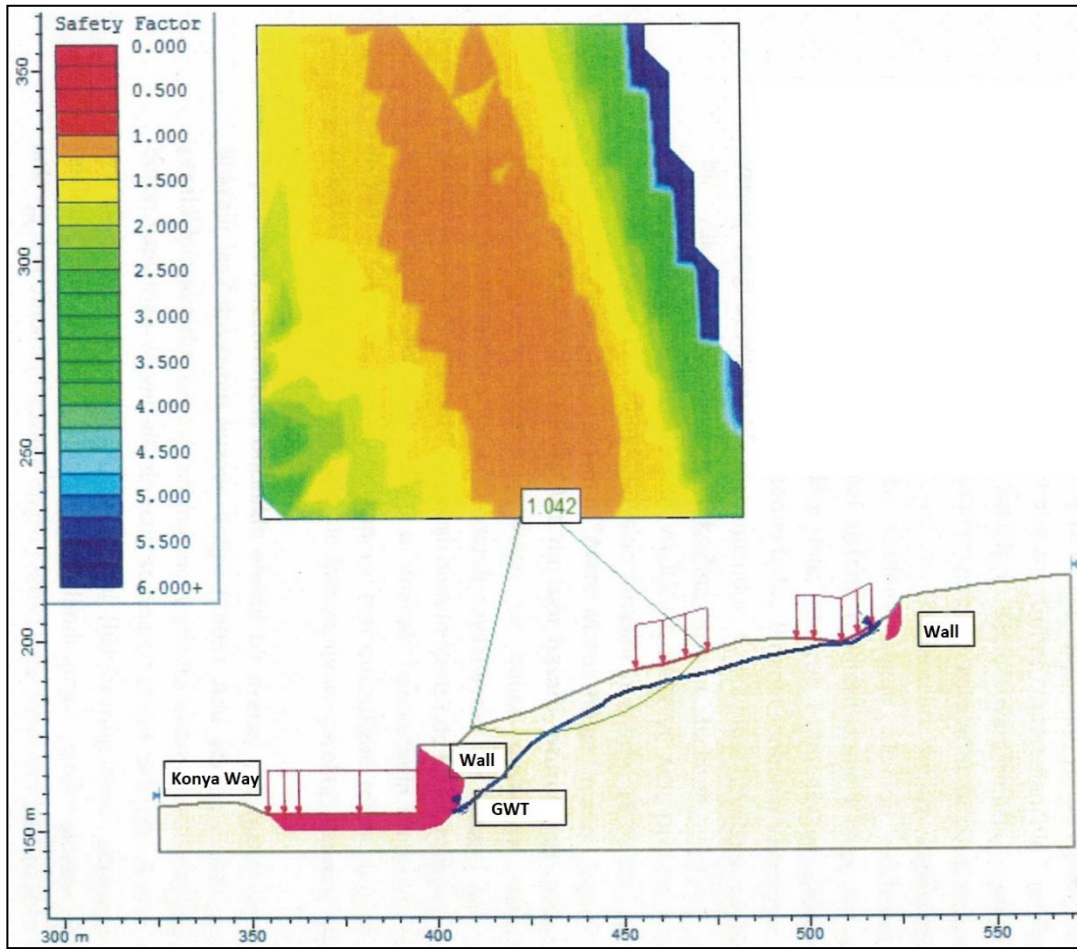
Figure 5.1. The outcome of limit equilibrium analyses (Kiper,2011).

Kilci Co. has conducted a series of back-analyses over four sections with LEM using SLIDE Software. Locations of the analyzed cross-sections are shown in Figure 4.7 The GWT levels, which were measured between 1.6 m to 17.5 m depths in the boreholes, were implemented accordingly in the models. The outcome for the cross-section C-C', which cuts through the business center construction site, is shown in Figure 5.2. The identified critical slip surface is deep, passing beneath the business center excavation.

Unit Weight: 26 kN/m3
Cohesion: 1 kPa
Friction Angle: 14.4 degrees
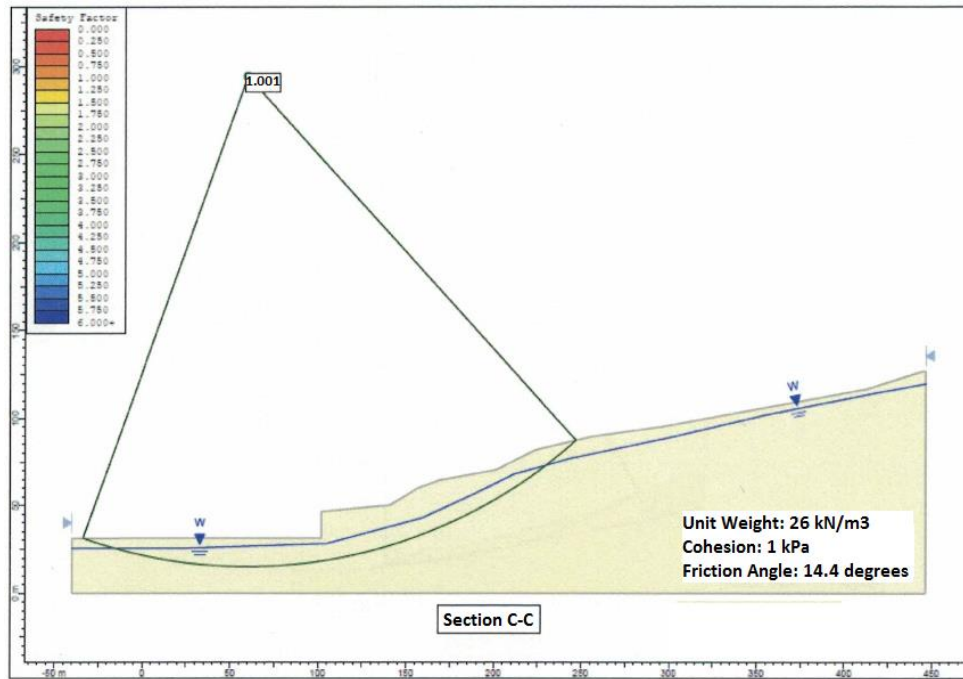
Section C-C

Figure 5.2. The outcome of back-analysis for Section C-C' (Nalçakan et al., 2012).

From the back-analyses of four cross-sections, the average long-term strength parameter is calculated as ϕ_r =15.65° (residual). Whereas, it was stated in Kilci Report that the direct shear test results carried out over a number of undisturbed specimens extracted from various depths yielded strength parameters between ϕ_r = 18° - 26° (residual). The strength parameters obtained from direct shear tests are noted to be quite high compared to that calculated from back-analyses. Moreover, the back-calculated internal friction angle is significantly low compared with Kiper Co.'s analysis as well. Reasons for difference between shear strengths could be:

- Samples taken from different depths, not from shear surface of landslide.
- Samples being disturbed.
- Saturation condition in the field vs. in the lab tests.
- Sample preparation issues in the lab tests.

59

Locations of the cross-sections analyzed in the METU Report are shown in Figure 5.3. Analyses were conducted with SLIDE software using the following material parameters identified with reference to technical literature considering similar soil characteristics: internal friction angle, $\phi' = 17°$, cohesion, $c' = 1$ kPa, and unit weight, $\gamma = 18$ kN/m^3. The retaining wall of the business center foundation excavation was modeled as a rigid block in the analyses. The GWT levels were adopted from the Kiper Report.

Figure 5.3. Cross-section locations analyzed in the METU Report (Çokça et al., 2011).

It is to be noted that the building within the yellow box in Figure 5.3 is the Güneş Apartment. Excavation of the business center does not appear in the figure since it had not started at the time when the picture was taken. The outcome of the analyses for

cross-section A-A', which cuts through both Güneş Apartment and business center foundation excavation, is shown in Figure 5.4.
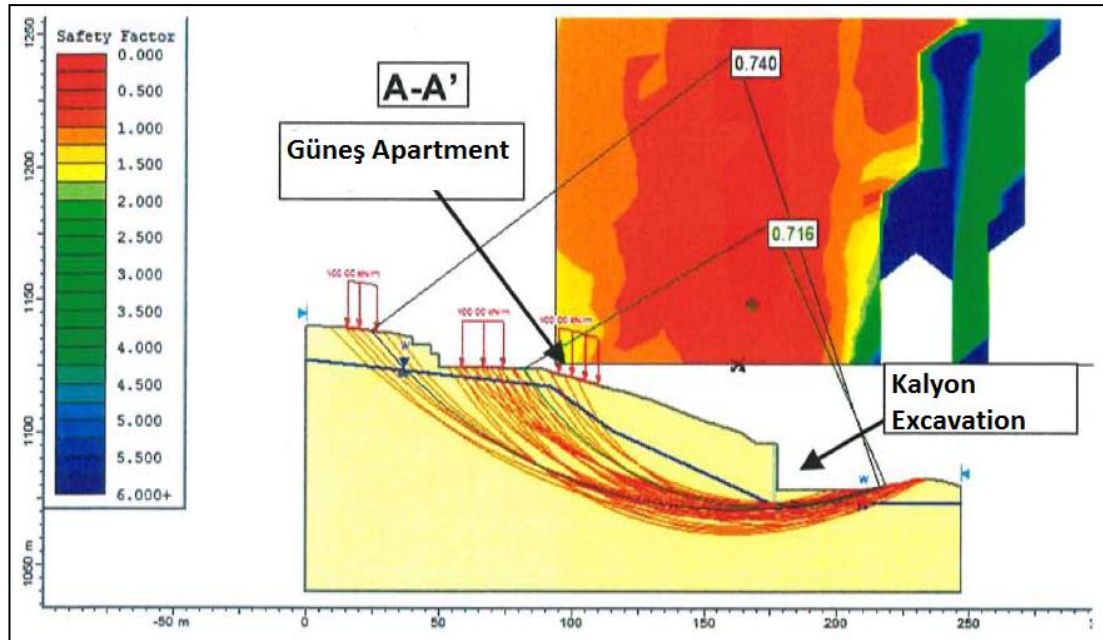
Figure 5.4. Stability analyses results of cross-section A-A' (Çokça et al., 2011).

The ranges of safety factors calculated for all four analyzed cross-sections are presented in Table 5.1. The safety factors in the table are in general representative of deep-seated sliding surfaces. On the other hand, the safety factors, which are by and large around 0.7 – 0.75, are rather low, suggesting that the slope is highly unstable. This, however, is considered to be questionable for a slope failure of very low displacement rate.

Table 5.1. *The ranges of factors of safety of the analyzed cross-sections in the METU Report (Çokça et al., 2011).*

Section	Factor of Safety
A-A'	0.716 - 0.740
A-A' (without Güneş Apartment)	0.732 - 0.742
B-B'	0.750 - 0.812
C-C'	0.696 - 0.713
E-E'	0.881 - 0.887

5.1.1. Methodology

In this section, the possible mechanism and influence of the flooding; the potential effect of business center excavation on the slope stability will be investigated. Bearing in mind the difficulty of obtaining representative strength parameters for the stability assessment of natural slopes by laboratory tests, the parameters will be estimated through back-analyses. For the case modeling, section A-A' of the METU Report has been selected, since it spans through the business center foundation excavation as well as the Güneş Apartment.

At the outset, back-analyses were conducted on the case slope based on geotechnical circumstances previous to the landslide. The possible influence of the excavation of business center foundation on the stability of the case slope will be searched through consideration of the following circumstances:

1. Presence of the business center excavation only.
2. Non-presence of the business center excavation (i.e., natural state of the slope).
3. Fully constructed business center building.

Influence of the downpour will be investigated through consideration of the following short-term geotechnical consequences:

1. GWT has risen one meter.
2. Formation of a one-meter thick saturation zone below the slope surface.

Analyses for the above-mentioned circumstances and short-term effects will be carried out using two-dimensional limit equilibrium and finite element approaches. Subsequently, a three-dimensional analysis of the slope will be carried out under static loading using FEM. Finally, the results to be obtained from this series of analyses will be compared and discussed.

5.2. Input Parameters

The unit weights were distinguished as "dry" and "saturated" to model the zones which lie above and below the GWT. Data from the boreholes drilled by Kiper Co. have been utilized in the analyses. For the dry zone, the unit weights of the samples varied between 17.9 and 18.5 kN/m^3, whereas for the saturated zone, the unit weights were identified between 21 and 22 kN/m^3 (Appendix- Table B.1). In this study, the dry and saturated unit weights of the soil have been idealized as 17 kN/m^3 and 21 kN/m^3, respectively. The elastic modulus and Poisson's ratio were assigned as 50 MPa and 0.4 with reference to the technical literature for similar soils.

Regarding the shear strength parameters, which are to be calculated from the series of back-analyses, Abramson et al. (2001) point out that the solution can be provided through combinations of various sets that satisfy equilibrium. The magnitudes of these parameters should be consistent to an extent with the laboratory or field test data. Thus, for the assessment of initial values of strength parameters, direct shear test results provided in Kiper Report (available for the shallow zone) and in Kilci Report (available for the deep zone) have been considered. These values are tabulated in Table 5.2, and summary of test results can be found in Appendix-B.

Table 5.2. *Direct shear test results used as initial values for deep and shallow zones in the analyses.*

Report Name	Sample Depth (m)	c' (kPa)	ϕ' (°)
Kiper Co.	3,00-3,50	9,6	20
Kiper Co.	3,00-3,50	6,2	17
Kilci Co.	17	8	23
Kilci Co.	25	6	26

The initial values of the soil parameters consequently used in the analyses are presented in Table 5.3. The wall was modeled as a rigid block in the analyses by assigning rather high strength parameters for the wall material.

Table 5.3. *Initial assignment of the parameters.*

Soil Layer	Drained Cohesion-c' (kPa)	Drained Internal Friction Angle-ϕ' (°)
Residual Soil	6	17
Greywacke	8	23
Phyllite	6	26

It should also be noted that there can be some uncertainties regarding the shear strength of soil layers, displacement dependence of the shear strength, GWT level, saturated/unsaturated shear strength conditions.

5.3. Two-Dimensional Limit Equilibrium Model and Analyses

5.3.1. Definition of Two-Dimensional Limit Equilibrium Model

In the previous studies of the case slope, the subsurface was represented by a single homogenous layer. In this study, to model the subsurface conditions more realistically, the subsurface profile has been divided into three distinct soil layers based on the information gained from earlier ground investigations. These soil layers, from top to bottom, namely are residual soil, greywacke, and phyllite. The layered cross-section is shown in Figure 5.5:
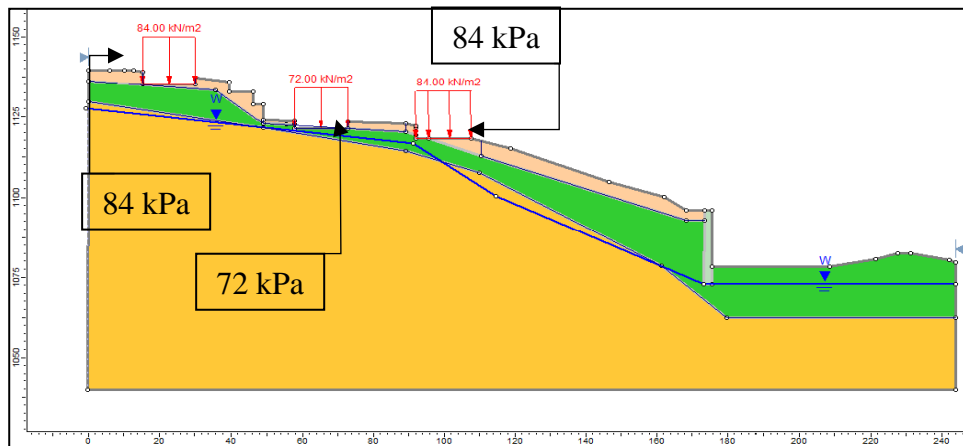
Figure 5.5. Layering of the case slope cross-section.

The groundwater table has been modeled as a piezometric line. The presence of buildings has been represented by uniform surcharge loads applied at cuts (having appropriate foundation depths) on the slope surface.

When calculating the foundation pressures for the residential buildings on the slope, 12 kPa per storey is presumed to be transmitted to the ground, whereas 15 kPa is assumed per storey for the business center building. Raft foundations of the buildings are assumed to have 50 cm thickness, which approximately corresponds to 12 kPa surcharge load.

Soil behavior is represented by the Mohr-Coulomb material model. Rock and soil tend to behave in a highly non-linear manner under loading, and this behavior can be represented at various levels of complexity. Mohr-Coulomb model can be considered as the first-order approximation of real soil behavior. Accordingly, the soil behavior is elastic-perfectly plastic and rigid-perfectly plastic, in the case of finite element and limit equilibrium type of analyses, respectively. Bishop's Simplified Method is utilized in the limit equilibrium analyses in this study.

65

5.3.2. Two-Dimensional Limit Equilibrium Analyses

Series of back-analyses have been conducted to identify the strength parameter sets for the sublayers corresponding to the marginal stability condition (i.e., a factor of safety just above unity) of the slope previous to the downpour. The groundwater level in the model is presumed to represent that of before the downpour at this stage. The outcome for the marginal stability condition is shown in Figure 5.6.
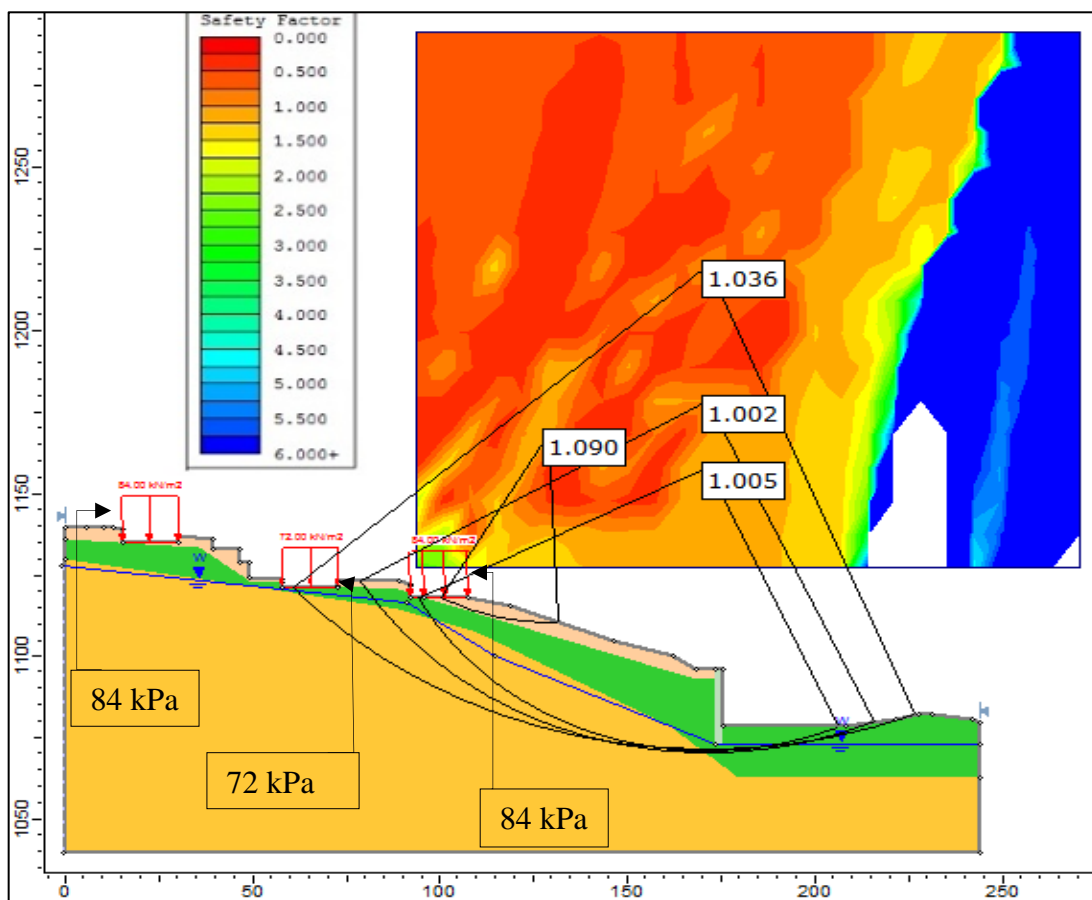
Figure 5.6. The outcome of limit equilibrium analysis representing the marginal stability of the slope previous to the heavy rain.

The set of residual shear strength parameters attained from the back-analysis calculations is tabulated in Table 5.4. The back analysis has been conducted by

66

lowering the initial shear strength parameters gradually and simultaneously for the three layers. This set of shear strength parameters will be presumed to be valid for the three-layer subsurface model. The marginal stability condition has appeared to be provided for shallow and deep zones with the parameters relatively close to the laboratory residual shear strength results.

Table 5.4. *Residual shear strength parameter set identified following back-analysis.*

Soil Layer	Drained Cohesion-c' (kPa)	Drained Internal Friction Angle-ϕ' (°)
Residual Soil	2	17
Greywacke	7	19
Phyllite	1	22

Following the downpour, the groundwater table is assumed to have risen temporarily about one meter from the marginal stability condition. In addition, the ground is presumed to become saturated within a thickness of 1 m on the surface. The temporary shallow saturation zone has been modeled by defining a pore pressure coefficient R_u, which is described by Bishop and Morgenstern (1960) as the ratio of pore water pressure to the overburden pressure. Regarding R_u value, Fredlund and Barbour (1986) stated that "*There is no theory available to predict the pore pressure coefficient. Rather the value for the pore pressure coefficient is assumed, based on experiments. Design values generally range from 0.3 to 0.45. Experience has shown that problems with instability generally occur when the pore pressure coefficient exceeds approximately 0.35.*" Thus, 1 m of temporary saturation zone has been defined to the top layer with a R_u value of 0.35. Analyses were carried out with these modifications, and the outcome is shown in Figure 5.7.
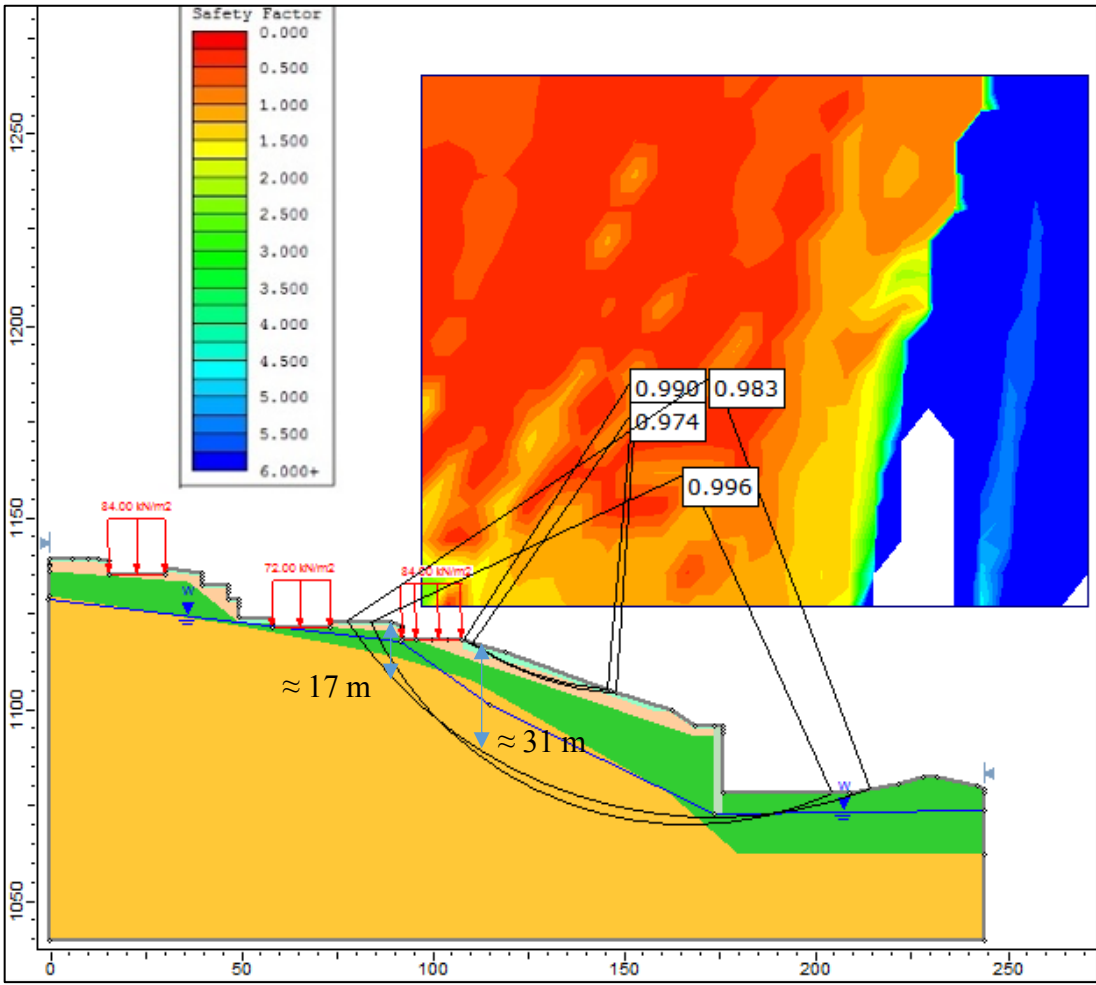
Figure 5.7. SLIDE outcome of the flood condition.

It is seen from Figure 5.7 that the safety factors for shallow and deep slide surfaces (shown as a number of query surfaces) are reduced to slightly below unity. Accordingly, the rise in the water table and saturation of surface soils destroyed the marginal equilibrium state, and hence the slope instability is initiated in deep and shallow zones. The shallow slide surface for which the safety factor is below unity in the figure occurs immediately in front of the Güneş Apartment. The depth of this sliding surface is observed to be consistent with the slide depth observed in the inclinometer installed in front of the Güneş Apartment. Following the downpour, GWT at the site fluctuated between 1 m and 2.5 m depths based on the measurements

68

taken from 2016 thru 2018 (Professor H. Sarıhan, personal communication, December 3, 2019).

Whether the foundation excavation of the business center was a triggering factor of the deep-seated landslide was of concern. Accordingly, flood condition (1 m GWT rise + 1 m saturation zone at the surface) has also been analyzed without the existence of business center foundation excavation. The relevant model and the outcome of the analyses are shown in Figure 5.8. It is observed that although the flooding circumstances cannot trigger a deep-seated slide, there still exists a shallow landslide independent from the foundation excavation.
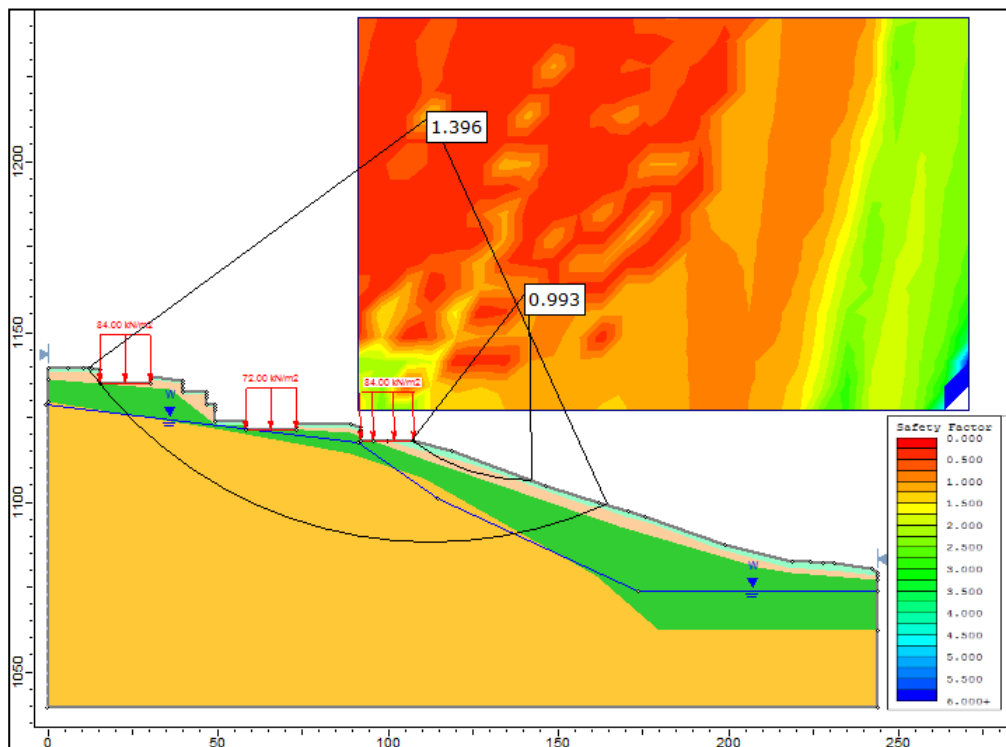
Figure 5.8. SLIDE outcome of the flood + no excavation condition.

The last case analyzed with the static limit equilibrium approach consists of the presence of business center building, presuming its construction is fully completed,

for the flood condition. The business center was planned to have 15 stories. Hence a surcharge pressure of 225 kPa is calculated to act at the foundation level. The relevant section and the outcome are presented in Figure 5.9.
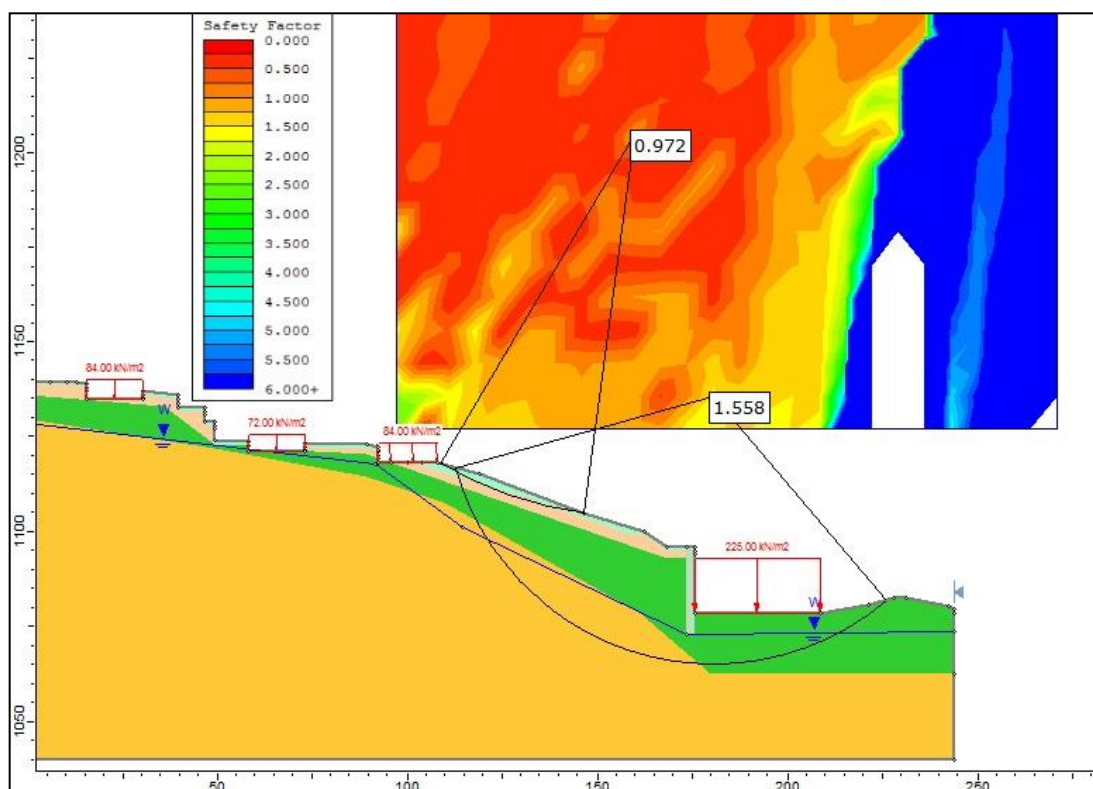
Figure 5.9. SLIDE outcome of the flood condition with the business center being fully completed.

As can be observed, although the existence of shallow landslide was not affected, the presence of the business center building appears to improve the stability of the deep-seated failure surface.

5.4. Two-Dimensional Finite Element Model and Analyses

5.4.1. Definition of Two-Dimensional Finite Element Model

The multi-layered section utilized in LE analyses in the previous section has been reconstructed by applying proper boundary conditions and meshing for use in FE analyses. The mesh type is uniform, and the element type is a 6-noded triangle (Figure 5.10). As it was mentioned in Chapter 3, FEM finds the smallest strength reduction factor anywhere in the model. Therefore, the area of interest should be specified by an SSR search area on the model to focus on the case situations.
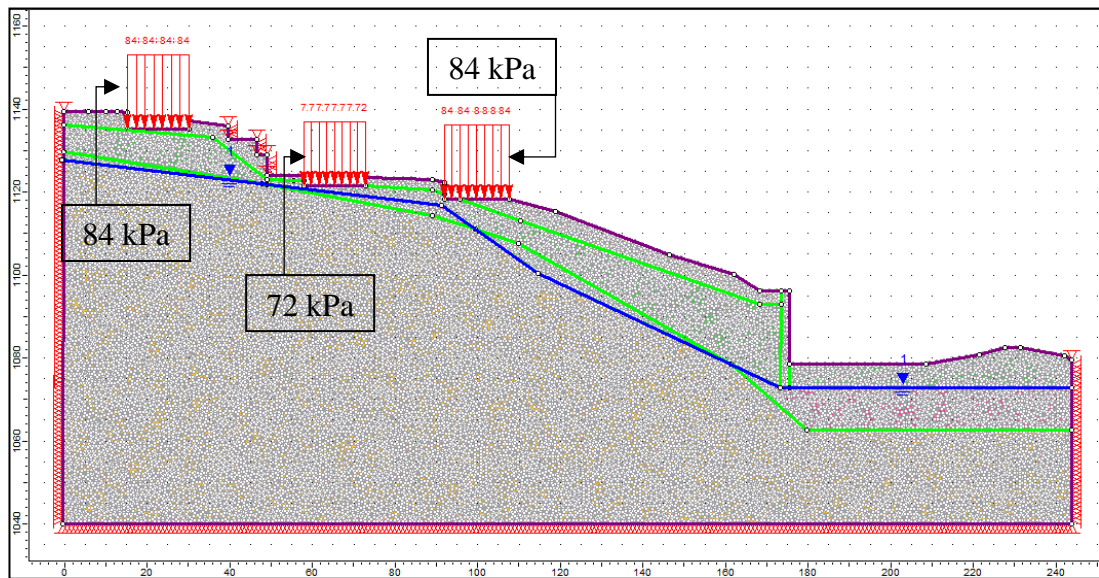
Figure 5.10. Reconstructed finite element version of the case slope section.

The Mohr-Coulomb model requires three additional input parameters in FEM to define the elastic soil response, namely Young modulus, Poisson's Ratio and dilation angle. Same shear strength parameters calculated in the back-analyses of the previous section used in LEM analyses (Table 5.4) have also been used in FEM analyses, whereas the additional three parameters were determined with reference to technical literature for similar soils as 50 000 kPa for Young's modulus, 0.4 for the Poisson's ratio and zero for the dilation angle.

71

Groundwater has been modeled as a piezometric line, which is the same as in the limit equilibrium models. Additionally, in RS2, unlike the SLIDE, it is necessary to differentiate the saturated and dry zones of an individual layer by dividing it as if two materials exist with different unit weights (saturated and dry state), all other properties being the same.

5.4.2. Two-Dimensional Finite Element Analyses

The finite element model of the section given in Figure 5.10 has been analyzed by defining an SSR search area to focus on the potential deep-seated slip surfaces. The mentioned search area and the outcome are shown in Figure 5.11. It is seen that the critical SRF is 0.87 and the approximate location of the deep slide is identified through maximum shear strain distribution.
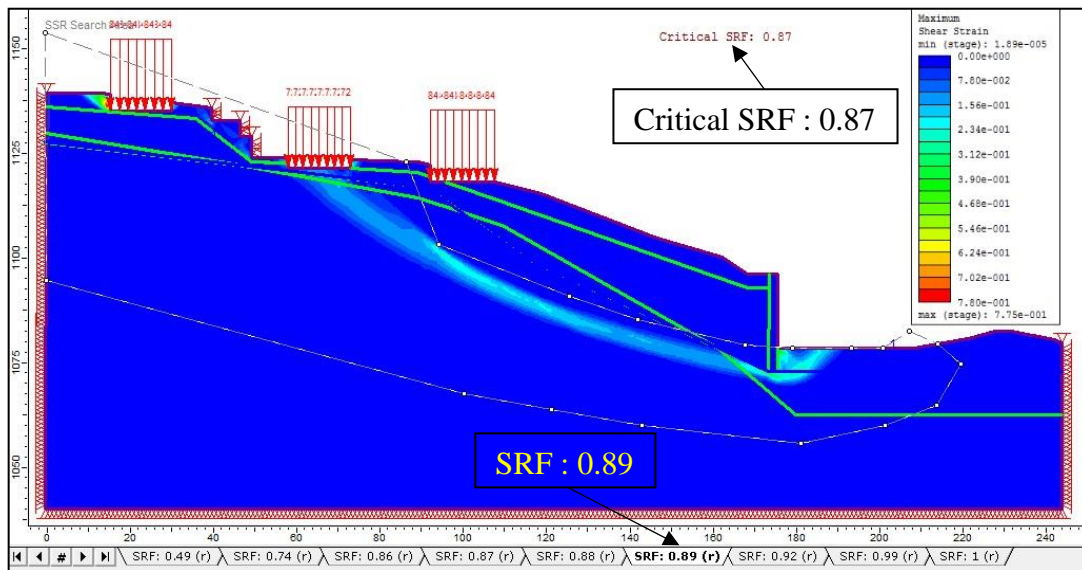
Figure 5.11. RS2 outcome (SSR=0.89) for the marginal stability condition of LEM.

When the model representing the flood condition (1m saturation zone + 1m GWT rise) is analyzed, the critical SRF has decreased to 0.72 (Figure 5.12). This is owing to the fact that the SSR search area encompasses some saturation zone. The critical SRF

values calculated through FEM are noted to be lower than those calculated through LEM, in general. This is because the failure surfaces are not limited to circular shapes in the case of FEM, and hence more realistic failure patterns are obtained with respect to LEM.
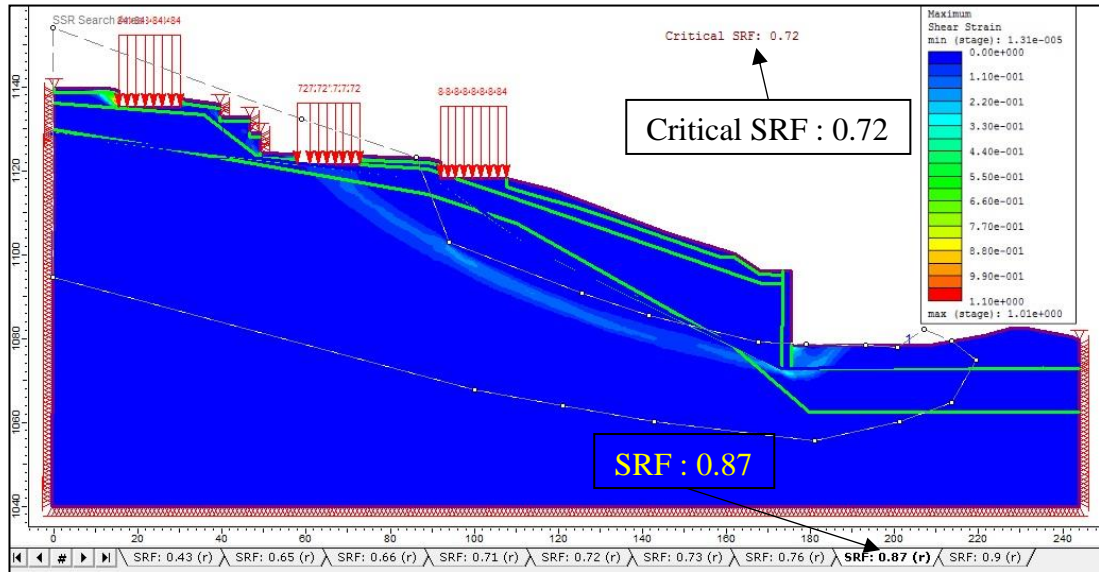
Figure 5.12. RS2 outcome for the deep slide surface under flood condition.

To inspect the stability in the vicinity of Güneş Apartment, an SSR search area which encircles the shallow zone has been specified. The search area and the outcome are shown in Figure 5.13:

73
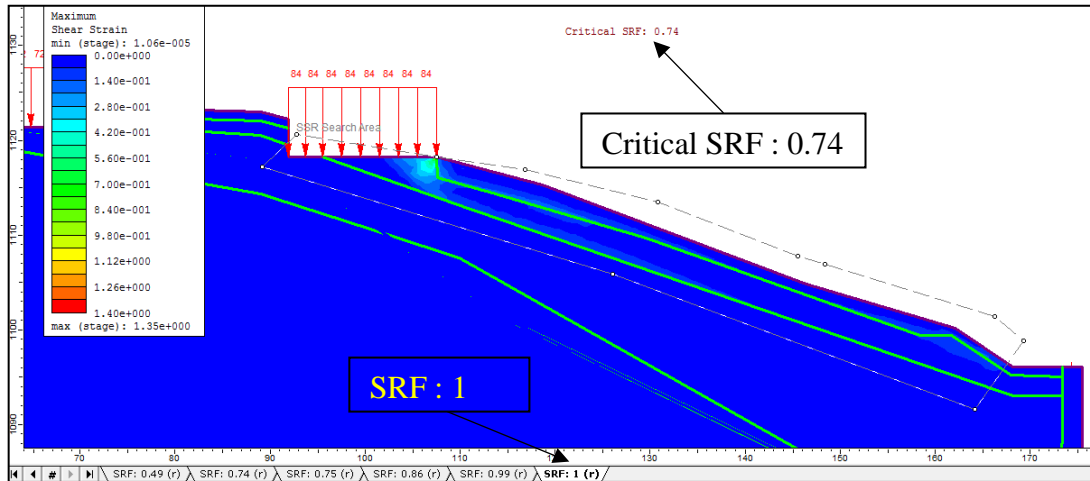
Figure 5.13. RS2 outcome for the flood condition (SSR=1) in the shallow zone.

The critical SRF is calculated as 0.74, and the location of failure surface is immediately beneath the downslope side of the Güneş Apartment foundation. The critical SRF values calculated through FEM are again lower compared to those of LEM.

Regarding the stability of the slope for the flood condition in case the business center excavation did not exist, it is evident that the stability of the deep zone would improve due to the unexcavated mass of soil on the toe, as it was also observed in LEM analyses. In this case, the SSR search area has been defined directly to the deeper zone, and critical SRF is calculated to be 1.23, which is well above unity (Figure 5.14).
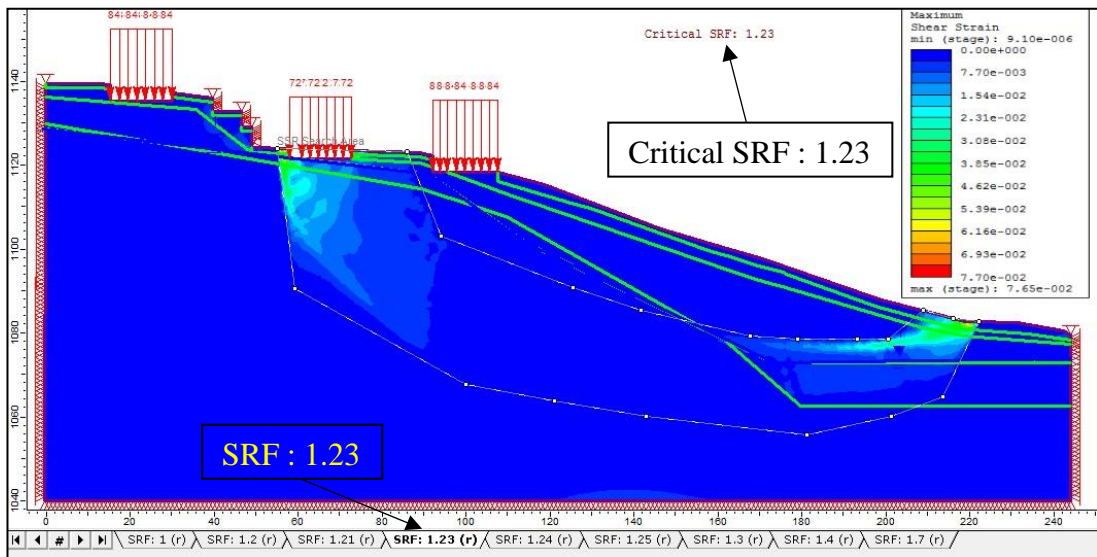
Figure 5.14. RS2 outcome for no excavation + flood condition.

The effect of presence of the fully completed business center building on the stability of slope was investigated also with FEM. Relevant outcome of the analysis from RS2 is shown in Figure 5.15.
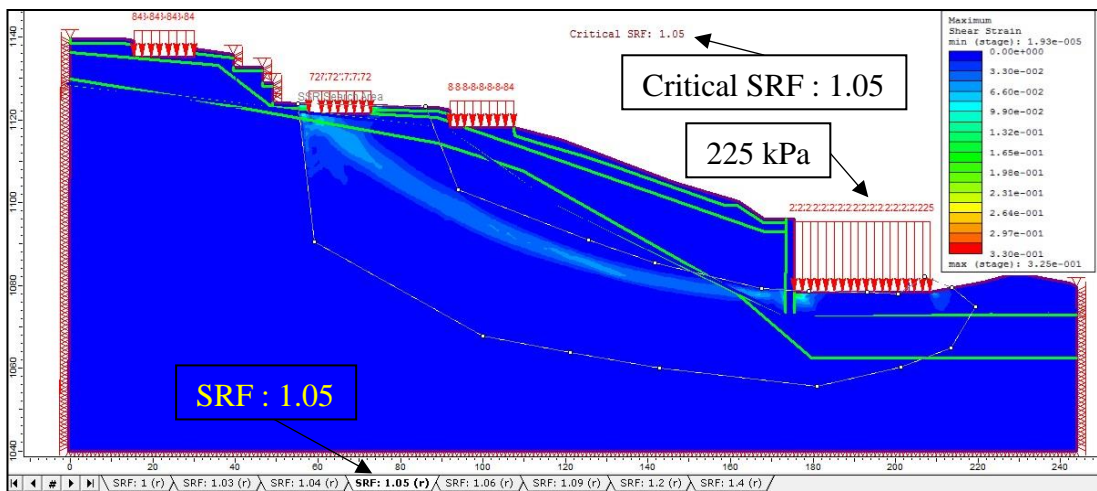
Figure 5.15. RS2 outcome for building surcharge + flood condition.

The critical SRF for the deep zone is 1.05.

5.5. Three-Dimensional Finite Element Model and Analyses

5.5.1. Definition of Three-Dimensional Finite Element Model

Conduction of three-dimensional analyses of the case slope were recommended in the METU Report. Accordingly, a three-dimensional model of the slope, enclosing the Güneş Apartment and the business center foundation excavation is formed using the two cross-sections, namely, section A-A′ (Figure 5.4) and section C-C′ (Figure 5.16) given in METU Report, and analyzed in this part of the study.
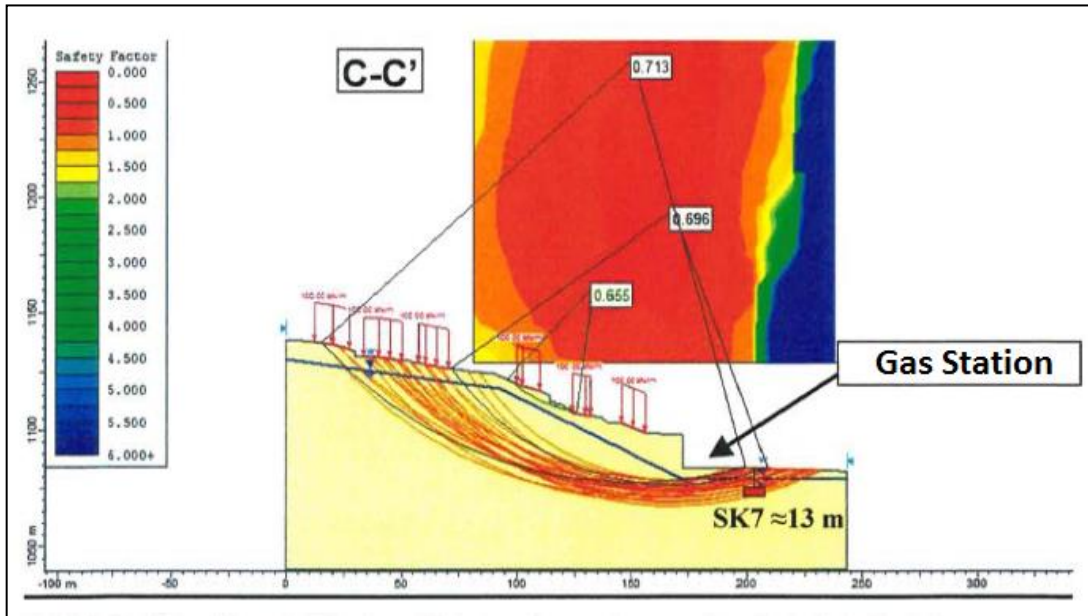
Figure 5.16. Cross-section C-C' (Çokça, et al., 2011).

The satellite view of the model area and the buildings remaining inside the boundaries are presented in Figure 5.17. It should be noted that building 7 in the figure is the Güneş Apartment which does not appear in the figure since it had been demolished before the picture was taken.

76

Figure 5.17. Satellite view of the three-dimensional model area (Google,2019).

With reference to the sections A-A′ and C-C′, ground surface (Figure 5.18) has been constructed by making use of the AutoCAD program. The surface is the combination of many '3DFace[7]'s. Building foundations have been designated as cuts on the surface. The three-dimensional surface is then imported into RS3 program Figure 5.19.

---

[7] In the Autocad program "3DFACE" command creates a three-sided or four-sided surface in 3D space.
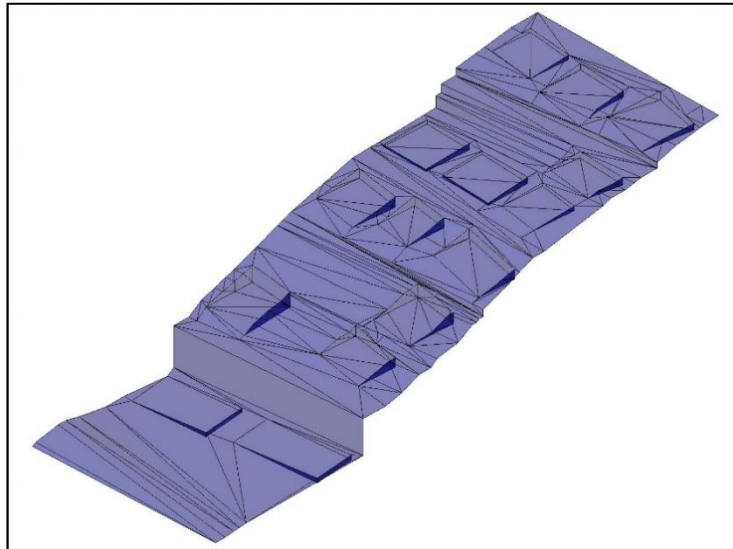
Figure 5.18. The 3D surface constructed from AutoCAD.
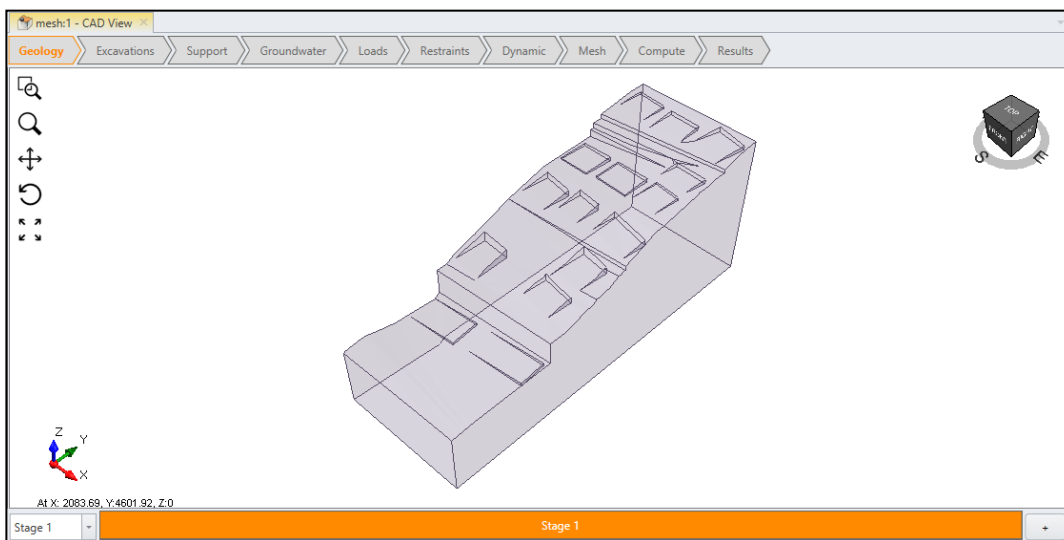
Figure 5.19. Three-dimensional slope model.

Six of the boreholes, namely BH-1 through BH-6, drilled by Kiper Co., were located inside the boundaries of the model. These boreholes, the locations of which are shown in Figure 4.6, were used to construct the subsurface profile (Figure 5.20) of the model using Borehole Manager Software, which was mentioned earlier in Chapter 3. The

inverse distance interpolation method was selected as the surface reconstruction setting.
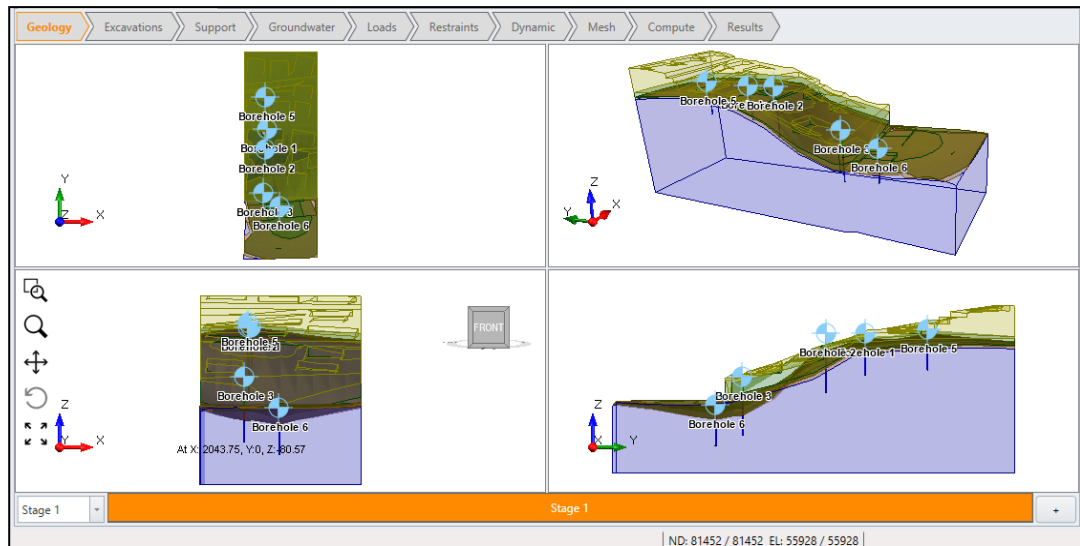
Figure 5.20. Various views of the 3D model.

As can be seen from the figure, soil layers have been formed as three-dimensional solid masses and the groundwater table is designated by a surface (instead of a piezometric line as in the two-dimensional model). The constraints in x, y, and z-directions in the model have been defined into right-left-back-front-above faces. Cuts and faces of foundation excavations of the apartment buildings on the sloping surface are restrained by proper boundary conditions in x, y, and z-directions, which are shown in Figure 5.21. A rigid liner mass has been defined to the front surface of the business center excavation retaining wall. Loads due to buildings have been defined in accordance with the assumptions stated in Section 5.3.1. The relevant illustration is given in Figure 5.22. The same material properties, as in the case of the two-dimensional finite element model are used (Section 5.2 and Table 5.4).
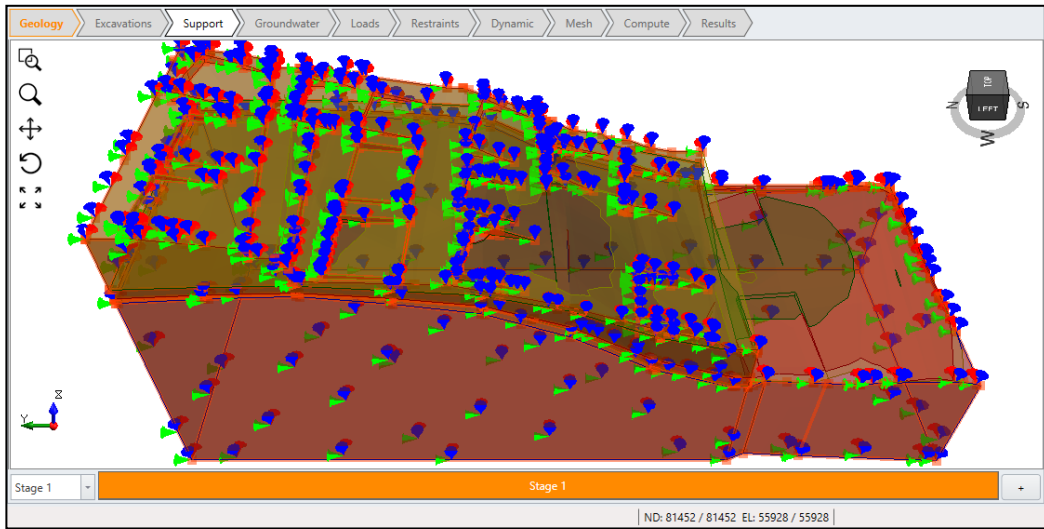
Figure 5.21. Constraints in x, y, and z-direction.
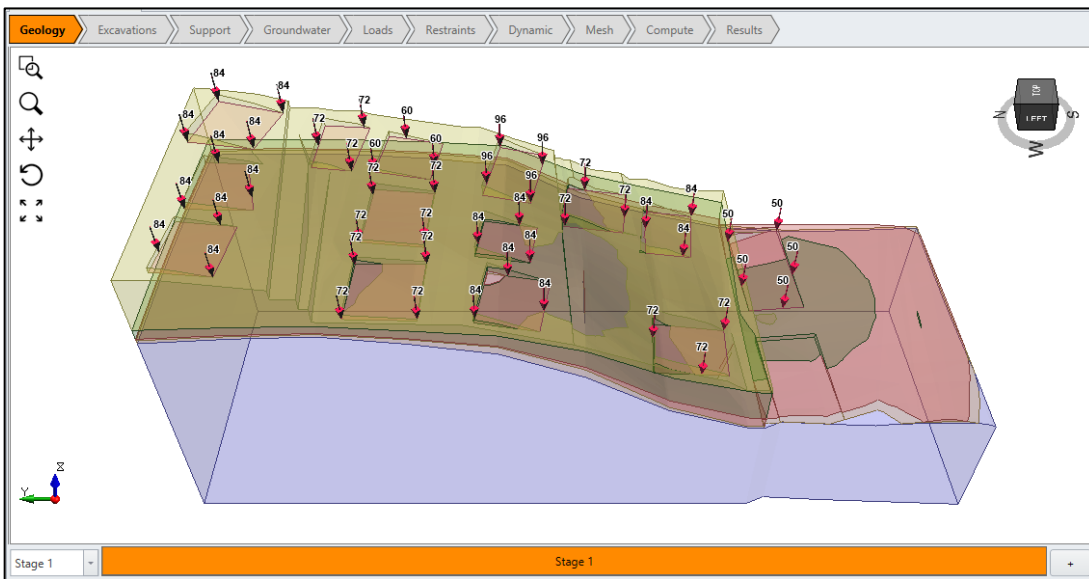
Figure 5.22. Building surcharge loads in the 3D model.

Finally, to construct a three-dimensional FE mesh, additional properties have to be defined. These are presented in Table 5.5. The constructed three-dimensional mesh is shown in Figure 5.23.

Table 5.5. *Mesh settings of the three-dimensional model*

Element Type	10-Noded Tetrahedra
Mesh Gradation	Uniform
Mesh Density	Medium
Element Size (m)	6.2
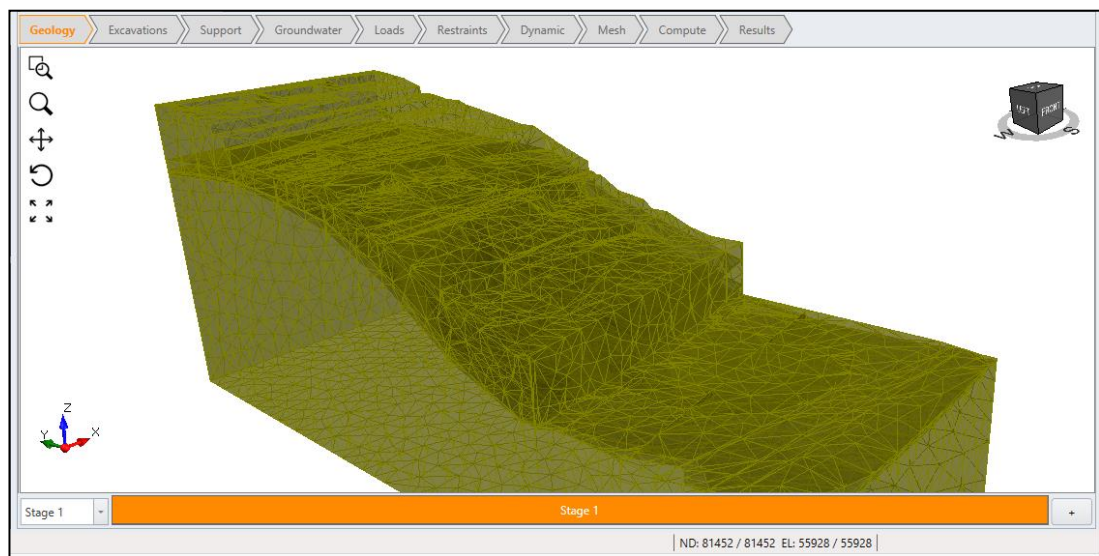
Figure 5.23. The three-dimensional mesh of the slope.

5.5.2. Three-Dimensional Finite Element Analyses

Following the analysis, the critical strength reduction factor was calculated to be 1.11. The distribution of shear strains corresponding to SRF of 1 is shown in Figure 5.24.
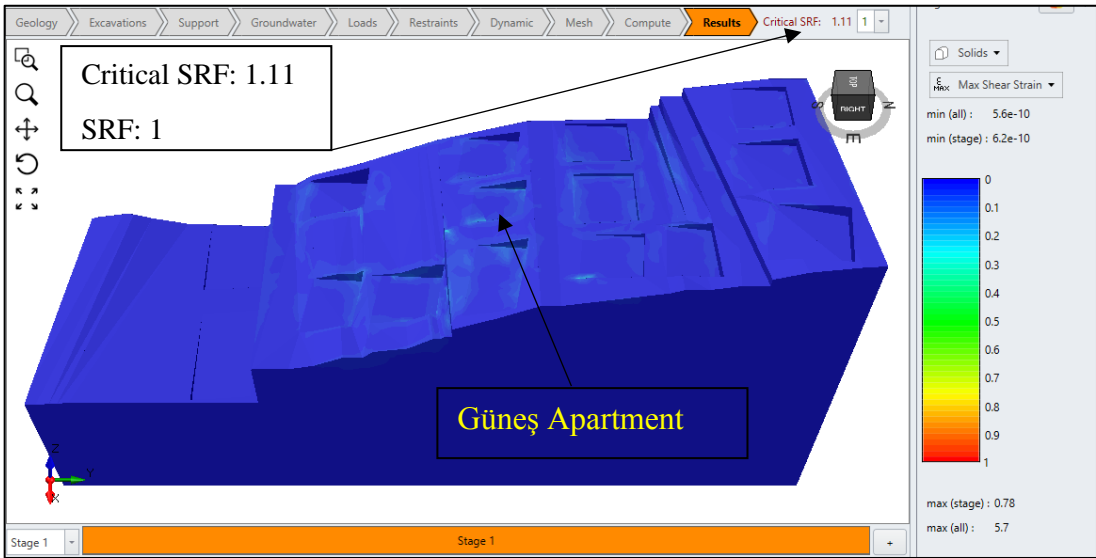
Figure 5.24. Distribution of shear strains following three-dimensional analyses at SRF of 1.

At the critical SRF (1.11), shear strains were observed to accumulate within a zone around the Güneş Apartment (Figure 5.25).

Figure 5.25. Strain accumulation zones at the critical SRF.

Distribution of total displacements on the ground surface is shown in Figure 5.26. Whereas the contours of total displacement and shear strain are presented in Figure 5.27 and Figure 5.28, respectively.
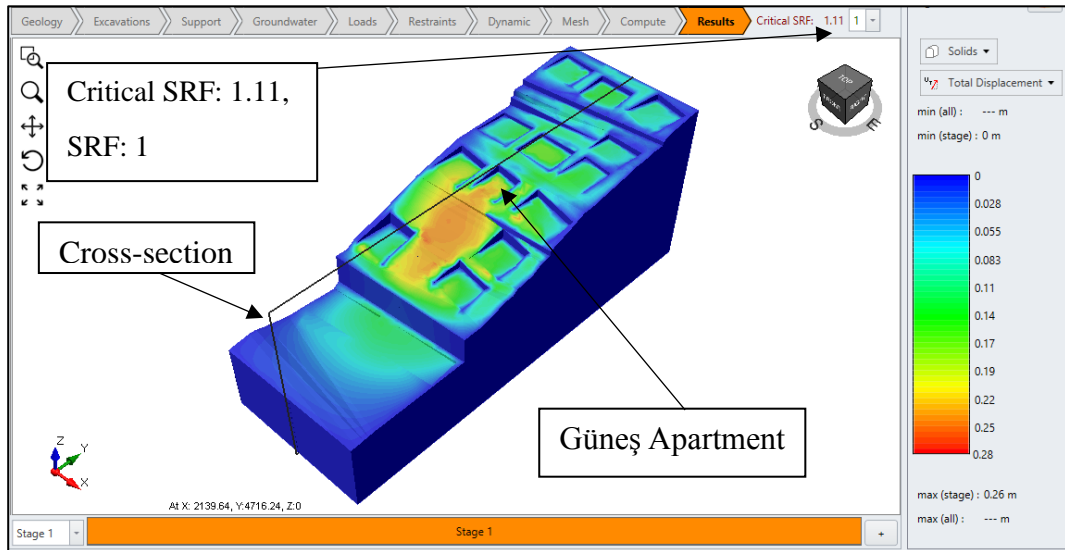
Figure 5.26. Distribution of total displacements on the ground surface.
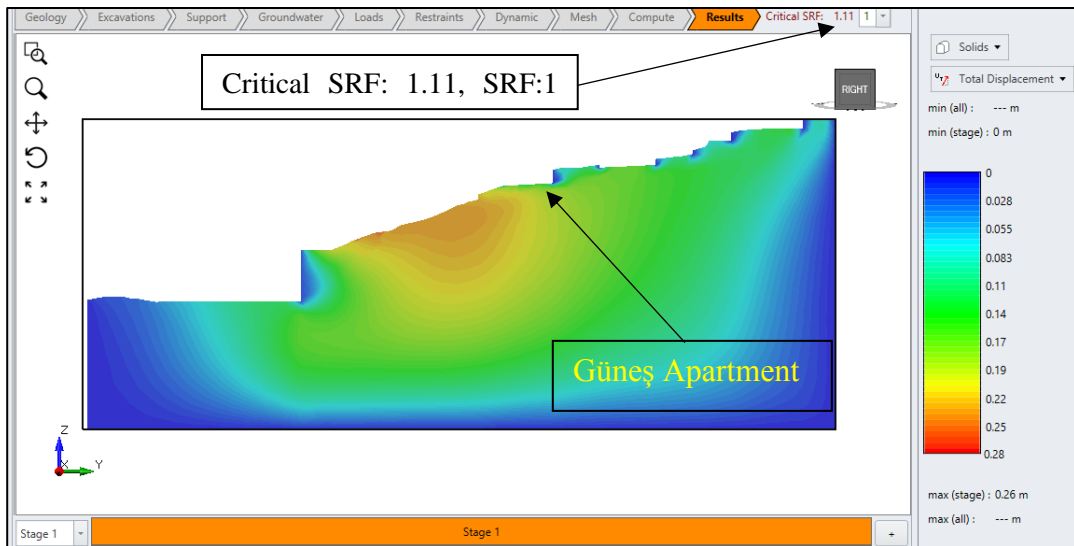
Figure 5.27. Total displacement contours on the cross-section.
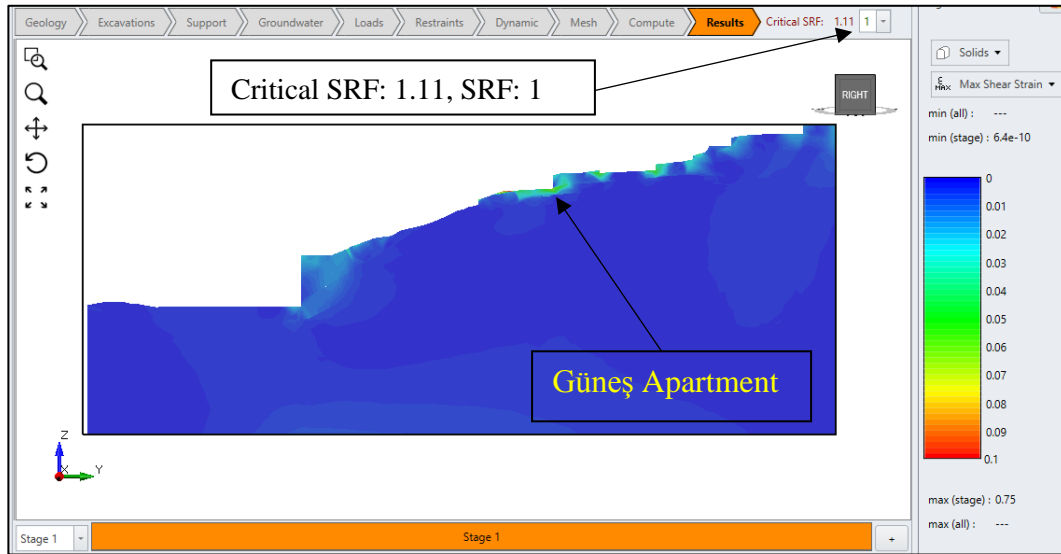
Figure 5.28. Shear strain contours on the cross-section.

The most critical part of the slope appears to be the shallow zone surrounding the Güneş Apartment from 3D model study. Relevant SRF is higher than those calculated by 2D models. Calculations in the deep zones may not have been finalized due to the fact that 3D slope stability analysis software is still under development. Consequently, considering the effort required for the model preparation and the results obtained, the efficiency and benefits of the 3D approach for the case in hand is deemed to be questionable.

CHAPTER 6

DYNAMIC ANALYSES OF THE CASE SLOPE

In this chapter, potential effects due to probable seismic events on the case slope will be investigated through two-dimensional models. Pseudo-static coefficients for 2D-LEM; pseudo-static coefficients and time-history analysis methods for 2D-FEM have been utilized for dynamic calculations.

6.1. Selection of the Strong Ground Motion

The location of Ankara is shown on the Seismic Hazard Map of Turkey (Figure 6.1), which is an integral part of the most recent Building Earthquake Code of Turkey issued in 2018. Clearly, the most significant source of danger for Ankara is the North Anatolian Fault, which is one of the major fault lines throughout the World and crossing the Country east to west.
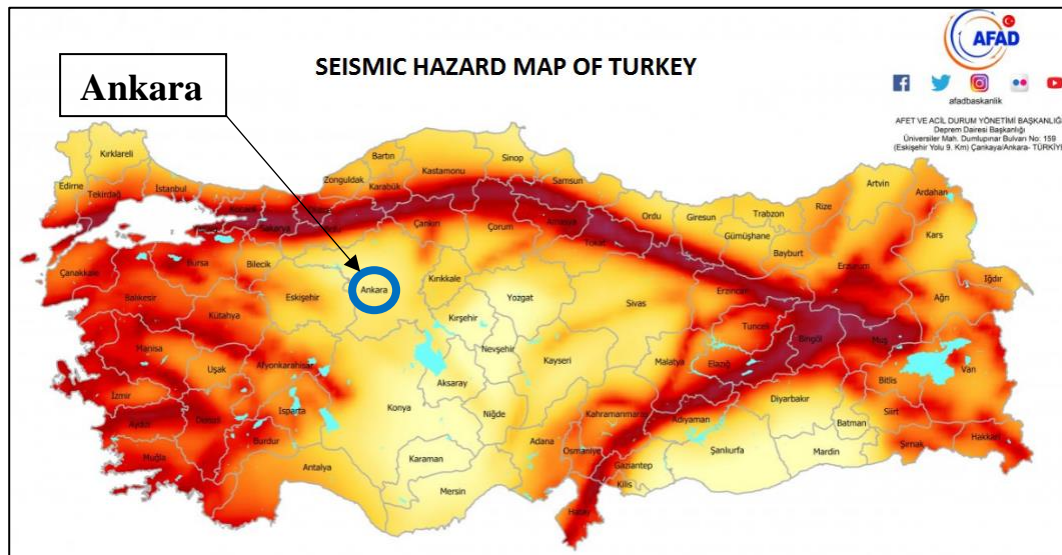
Figure 6.1. Seismic Hazard Map of Turkey (AFAD, 2019).

Strong Ground Motion Database of Turkey, which is prepared by AFAD, was examined to find appropriate ground motion(s) to represent the probable seismic events on the case slope. An earthquake occurred in Kalecik, a county of Ankara, with a magnitude of $M_w = 4.2$ on August 2, 2016. The focal depth of the earthquake was 12.2 km (Figure 6.2). The earthquake was recorded by Center Station in Çankırı, the neighboring city on the north-east of Ankara. Information about the station is provided in the AFAD website as shown in Figure 6.3. Plots of the accelerograms and other relevant information are provided in Figure 6.4.
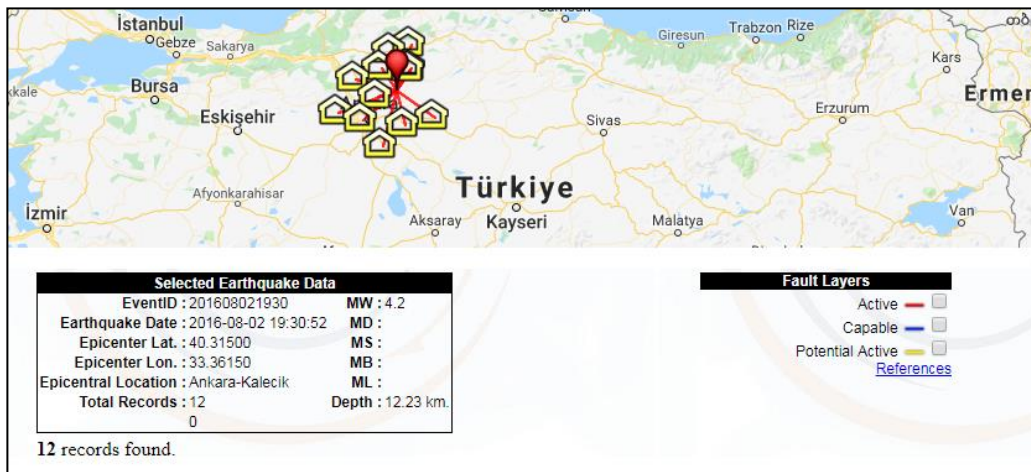
Figure 6.2. Data regarding the selected representative seismic event (AFAD, 2019).
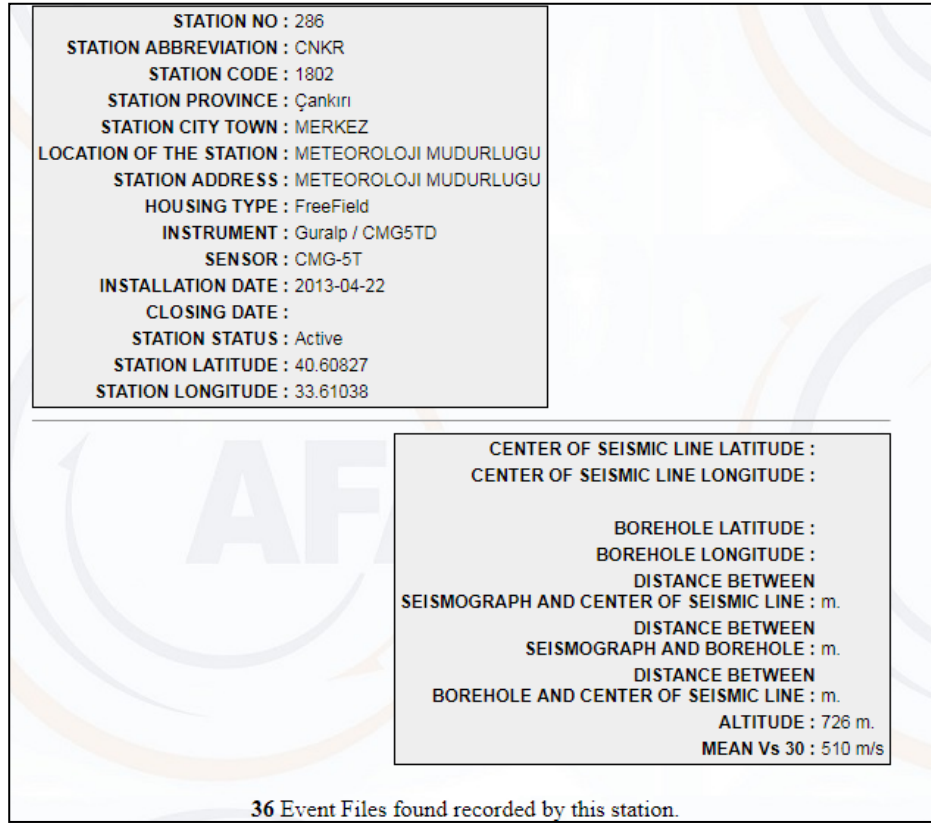
Figure 6.3. Information about Çankırı Center Station (AFAD, 2019).
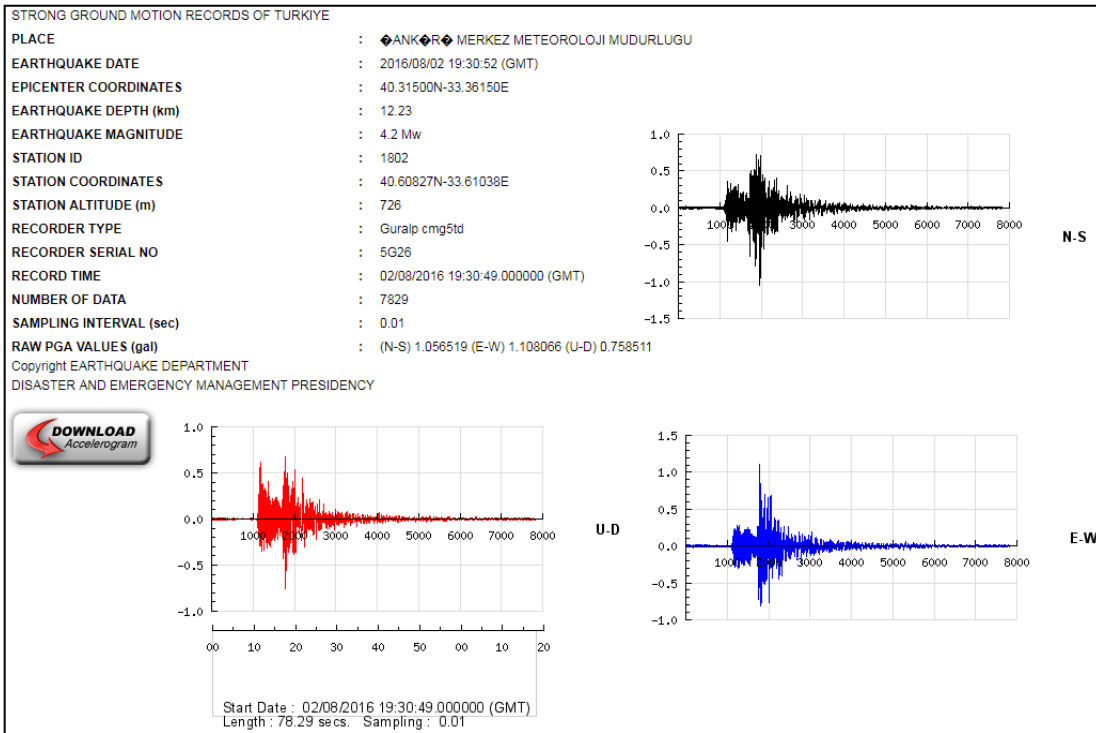
Figure 6.4. Plots of the accelerograms and other relevant information (AFAD, 2019).

6.2. Analyzed Cases and Conditions

The peak ground acceleration (PGA) of Kalecik earthquake is 1.108 gals (cm/s^2) in the E-W direction (Figure 6.4). This value corresponds approximately to 0.001g, which is rather small to induce any significant seismic effect at the slope site. In view of that, the recorded accelerogram was scaled before using as input to investigate the response of the case slope under seismic loading. Accordingly, the recorded time history was scaled to the following PGA values:

- PGA=0.05g
- PGA=0.075g
- PGA=0.1g

The stability of the pre-downpour (static) state of the site was assumed to be represented by an SRF of 1.1, and the material parameters were assigned accordingly. Two-dimensional LE and FE models of the slope have been analyzed through the pseudo-static method, while time history analyses have been conducted with FEM. Drained and undrained parameters (i.e., long-term and short-term parameters), have both been utilized in the models to search the difference in between.

6.3. Definition of Two-Dimensional Seismic Slope Models

The geometry of the multilayered FE model introduced in Section 5.4.1 has been revised by smoothing the sharp edges in the vicinity of building foundations to prevent possible stress concentrations. The retaining wall of the foundation excavation in the FEM model has been supported by a combination of triangular and uniformly distributed loads. Unlike previously, this support has been defined to investigate the displacements likely to occur in the slope during seismic shaking. Surcharge load due to the business center has been applied as 45 kPa since its construction was halted by the decision taken by the local court, and its most recent condition was the foundation raft plus two-floor slabs. Models of LEM and FEM with drained parameters utilized in dynamic response analyses are shown in Figure 6.5 and Figure 6.6, respectively.
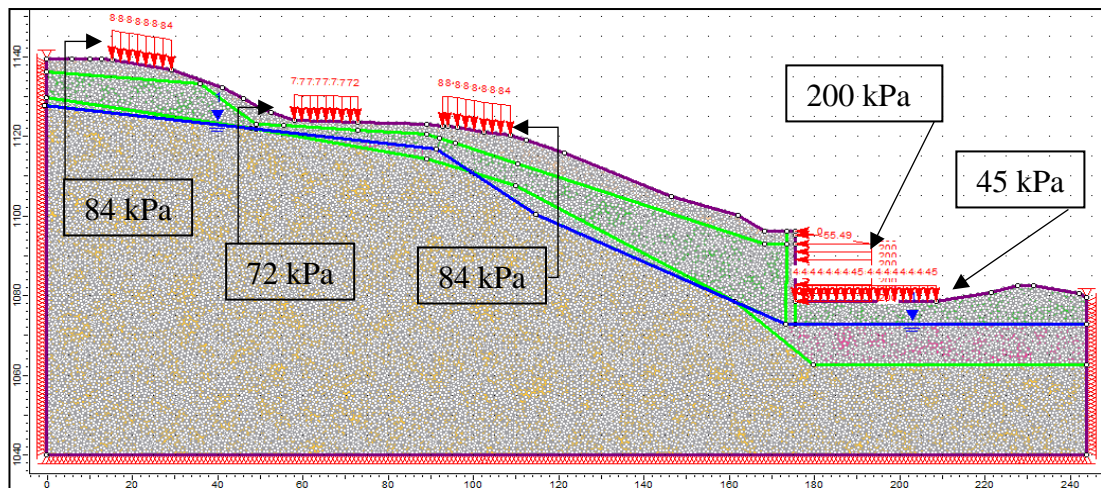
Figure 6.5. Reconstructed seismic model of the case slope.
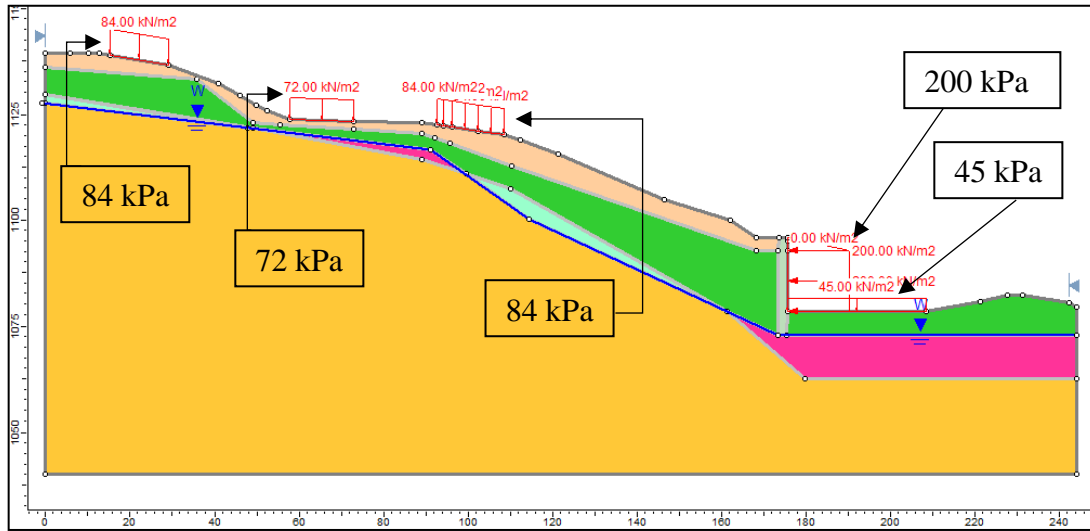
Figure 6.6. Limit equilibrium model with drained parameters.

6.4. Selection of Material Parameters

For the drained condition, cohesion and internal friction angle have been found by the trial-error process, which satisfies SRF of 1.1. For the undrained case, standard penetration test values (SPT-N) provided in the Kiper Report have been used, and the undrained cohesion is assessed through correlation proposed by Sowers (1979). Undrained friction angle has been taken as 4°, which is very close to the UU (Unconsolidated-Undrained) test results in the Kiper Report (Appendix Table-A.1). Young's moduli of the subsoils have been calculated from the following parameters: Poisson's ratio, unit weight, and empirical shear wave velocity profile, which was constructed using Ohta and Goto (1978) approach since no wave velocity measurement was taken on the site.

Ohta and Goto (1978) introduced a series of empirical shear wave velocity equations, which consist of various combinations of indexes, which are SPT-N value, soil type, geological epoch, and depth. Among them, the one which has the lowest probable

90

error (19.7%) and the highest correlation coefficient (0.86), is the equation that contains all of those indexes (Equation 6.1).

$$V_s' = 68.79 * N^{0.171} * H^{0.199} * \begin{pmatrix} 1.000 \\ 1.303 \end{pmatrix}_E * \begin{pmatrix} 1.000 \\ 1.086 \\ 1.066 \\ 1.135 \\ 1.153 \\ 1.448 \end{pmatrix}_F \qquad (6.1)$$

where

$$\begin{pmatrix} Alluvium \\ Diluvium \end{pmatrix}_E, \begin{pmatrix} Clay \\ Fine\ Sand \\ Medium\ Sand \\ Coarse\ Sand \\ Sand\ and\ Gravel \\ Gravel \end{pmatrix}_F, H = \text{Depth (m) and } N = \text{ SPT} - \text{N value}$$

The geological epoch of the residual soil has been selected as alluvium; whereas, greywacke and phyllite as diluvium. The soil type of residual soil has been selected as medium sand since it is of sand and clay mixture. Greywacke and phyllite are have been designated as gravel due to the weak rock nature. Calculated values of shear wave velocity are presented in Table 6.1. These values are observed to be consistent with the SPT blow counts of local soil classes tabulated in Building Earthquake Code of Turkey (AFAD, 2018) (Table 6.2):

Table 6.1. *Average SPT-N values and calculated shear wave velocities.*

Layer Name	Average SPT-N	V_s' Mean (m/s)
Residual	13	130
Greywacke	56	346
Phyllite	57	425

Table 6.2. *Local Site Soil Classes (AFAD, Building Earthquake Code of Turkey,2018).*

Local Site Soil Class	Soil Type	Average in the upper 30 meters depth		
		$(V_s)_{30}$ [m/s]	$(N_{60})_{30}$ [blow/30 cm]	$(C_u)_{30}$ [kPa]
ZA	Solid, hard rocks	> 1500	-	-
ZB	Slightly decomposed, moderately hard rock	760-1500	-	-
ZC	Very dense sand, gravel, and stiff clays or decomposed, fissured weak rocks	360-760	>50	>250
ZD	Moderately dense-dense sand, gravel or very dense clays	180-360	15-50	70-250
ZE	Loose sand, gravel or soft - dense clays or soft clays ($C_u <$ 25 kPa) satisfying Plasticity Index (PI) > 20 and w>40% whose thickness is greater than 3m in total.	< 180	< 15	<70
ZF	Soils that require site-specific investigations: 1) Soils having potentials of collapse or fail under earthquake effects (liquefying soils, highly sensitive clays, collapsible weak cemented soils, etc.). 2) Soils having peat or highly organic content whose thickness greater than 3m in total. 3) Clays having high plasticity (PI>50%) whose thickness is higher than 8m in total. 4) Very thick (>35 m) soft or moderately dense clays.			

Young's moduli of subsoils are calculated using the following relationship between shear wave velocity and Young's modulus (Equation 6.2):

$$E = (V_s')^2 * 2 * (1 + \mu) * \rho \tag{6.2}$$

where $V_s^{'}$: Mean Shear Wave Velocity

μ: Poisson's Ratio

ρ: Unit Weight

Poisson's ratio is presumed to be 0.4 for all soil layers. Calculated values of Young's moduli for the soil layers are summarized in Table 6.3.

Table 6.3. *Calculated Young's moduli values for the soil layers.*

Layer Name	$V_s^{'}$ Mean (m/s)	μ	ρ	E (GPa)
Residual	130	0.4	1.73	82
Greywacke	346	0.4	2.14	720
Phyllite	425	0.4	2.14	1085

Correlation between SPT-N and undrained shear strength proposed by Sowers (1979), shown in Figure 6.7 is utilized to determine the undrained cohesion of the soil layers. The soil type is considered to be silty clay at the site (Appendix Table-B.1) and the critical SRF is presumed to be 1.1 in the pre-downpour state. The values of undrained cohesion thus calculated are presented in Table 6.4.
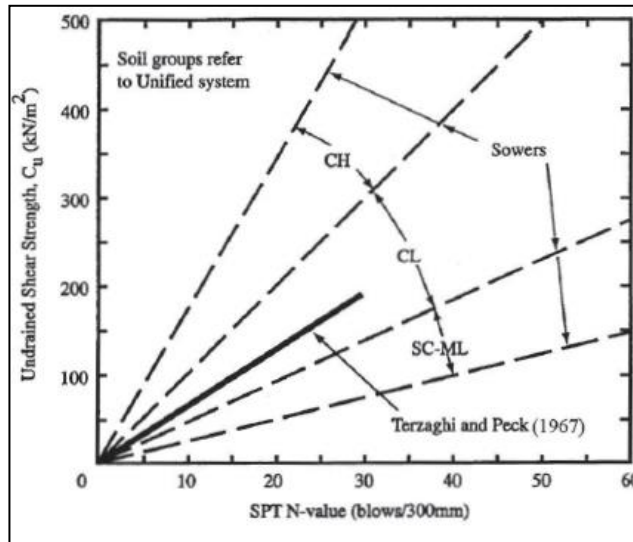
Figure 6.7. Correlation between undrained shear strength and SPT-N (Sowers, 1979).

Table 6.4. *Corresponding undrained shear strength values with respect to SPT-N.*

Layer Name	SPT-N Value	Undrained Shear Strength (kPa)
Residual	13	31
Greywacke	56	140
Phyllite	57	141

Consequently, the material parameters for FE modeling of seismic loading are tabulated in Table 6.5. Shear strength parameters given in the table have also been used in the pseudo-static limit equilibrium analyses.

Table 6.5. *Drained and undrained material parameters used in seismic response analysis.*

Drained Parameters Model Layer Name	Cohesion (kPa)	φ (°)	E (GPa)	μ	ψ (°)
Residual	7	20	82	0.4	0
Greywacke	8	21	720	0.4	0
Phyllite	1	23	1085	0.4	0

94

Undrained Parameters Model Layer Name	Cohesion (kPa)	φ (°)	E (GPa)	μ	ψ (°)
Residual	31	4	82	0.4	0
Greywacke	140	4	720	0.4	0
Phyllite	141	4	1085	0.4	0

6.5. Two-Dimensional Seismic Analyses with Limit Equilibrium Method

Seismic analyses have been conducted with the pseudo-static approach for both drained and undrained conditions using horizontal pseudo-static coefficients of 0.001 (actual), 0.05, 0.075, and 0.1. Simplified Bishop's method is selected as the method of analysis.

Analyses with Drained Parameters

Results of the analyses with pseudo-static coefficients of 0.001 and 0.1 have been selected for presentation here and the respective outcomes are shown in Figure 6.8 and Figure 6.9.
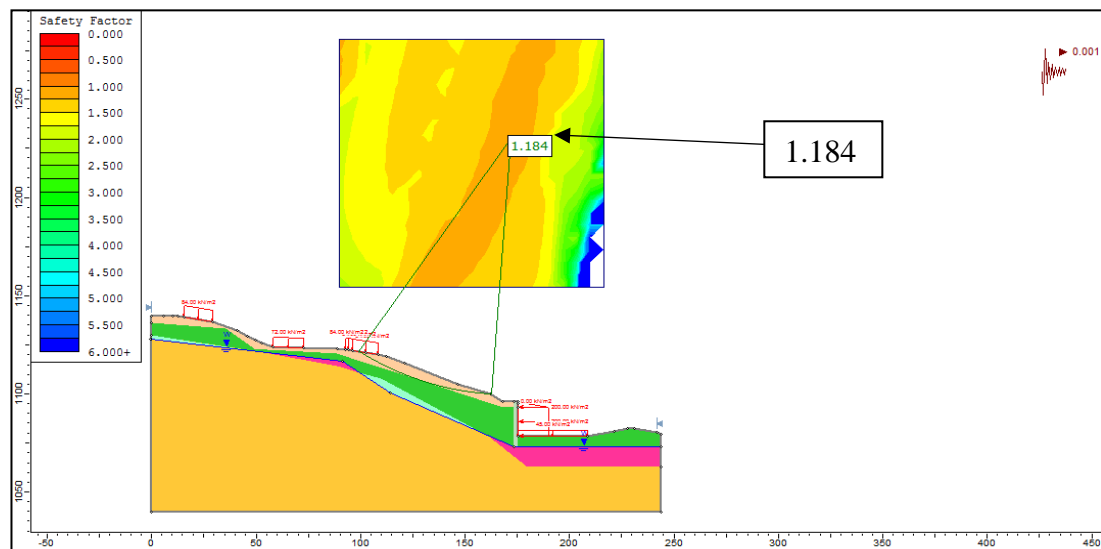
Figure 6.8. LEM analysis result with drained parameters and horizontal pseudo-static coefficient of 0.001.
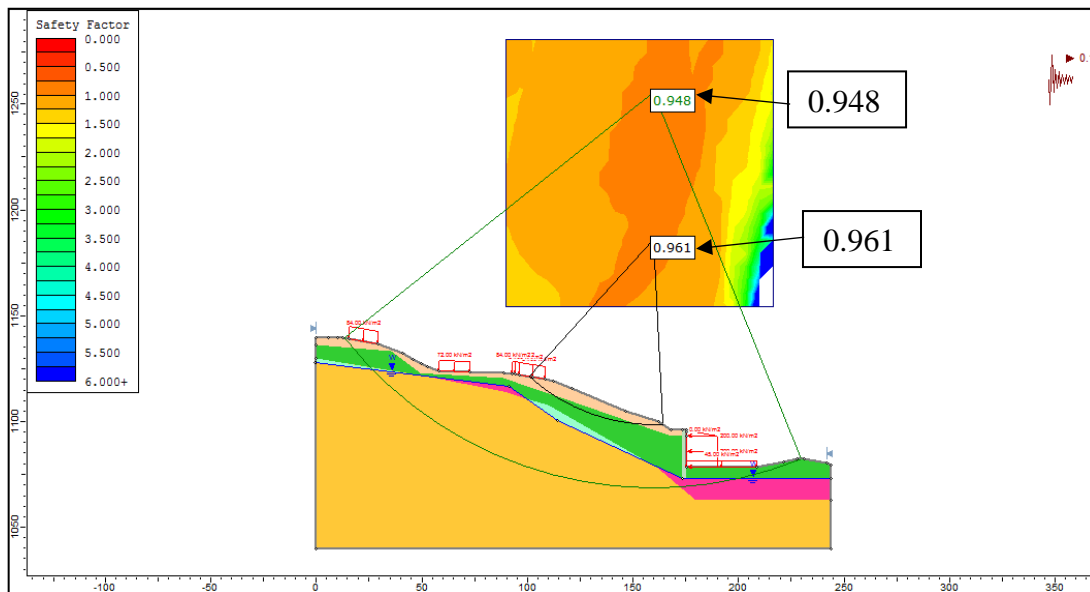
Figure 6.9. LEM analysis result with drained parameters and horizontal pseudo-static coefficient of 0.1

The pseudostatic analysis with the coefficient of 0.001 practically yields the same result with the static analysis. The critical safety factors for pseudo-static coefficients of 0.001, 0.05, 0.075 and 0.1 are calculated as 1.184, 1.06, 1.01 and 0.948, respectively.

Analyses with Undrained Parameters

Critical safety factors for pseudo-static coefficients of 0.001, 0.05, 0.075 and 0.1 are calculated as 1.22, 1.04, 0.97 and 0.91, respectively, from the analyses with undrained parameters. The undrained LE modeling is observed to display relatively greater sensitivity to changes in the pseudo-static accelerations compared to drained modeling. If FS of unity is considered to represent the boundary of stability, the critical pseudo-static acceleration appears to be 0.075g for the case slope.

6.6. Two-Dimensional Seismic Analyses with Finite Element Method

Analyses are conducted with dynamic finite element models using pseudo-static and time history approaches and for both, drained and undrained parameters.

6.6.1. Pseudo-Static Finite Element Analyses

Horizontal pseudo-static coefficients of 0.001 (actual), 0.05, 0.075, and 0.1 have been used again, as in the case of pseudo-static LEM analyses.

Analyses with Drained Parameters

Results of the analyses with pseudo-static coefficients of 0.001 and 0.1 have been selected for presentation here and the respective outcomes are shown in Figure 6.10 and Figure 6.11.
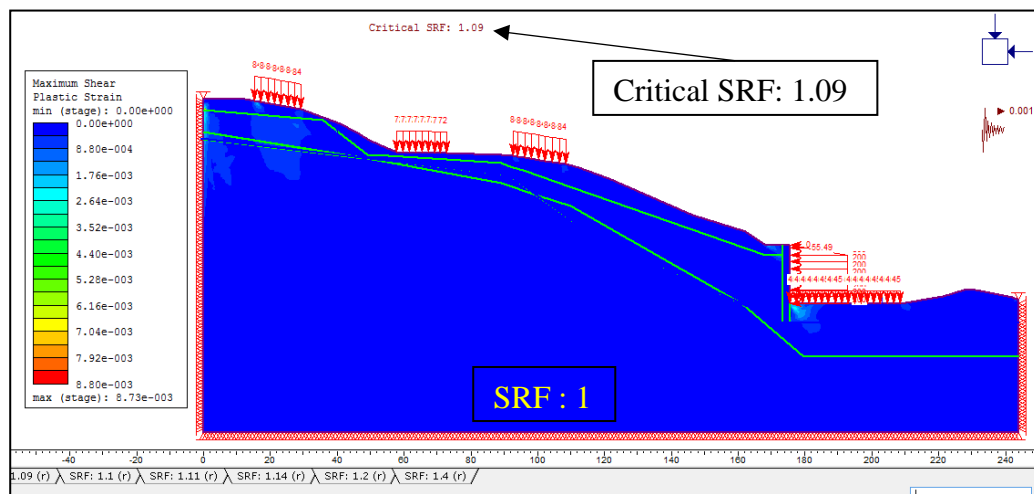
Figure 6.10. FEM analysis result with drained parameters and horizontal pseudo-static coefficient of 0.001.
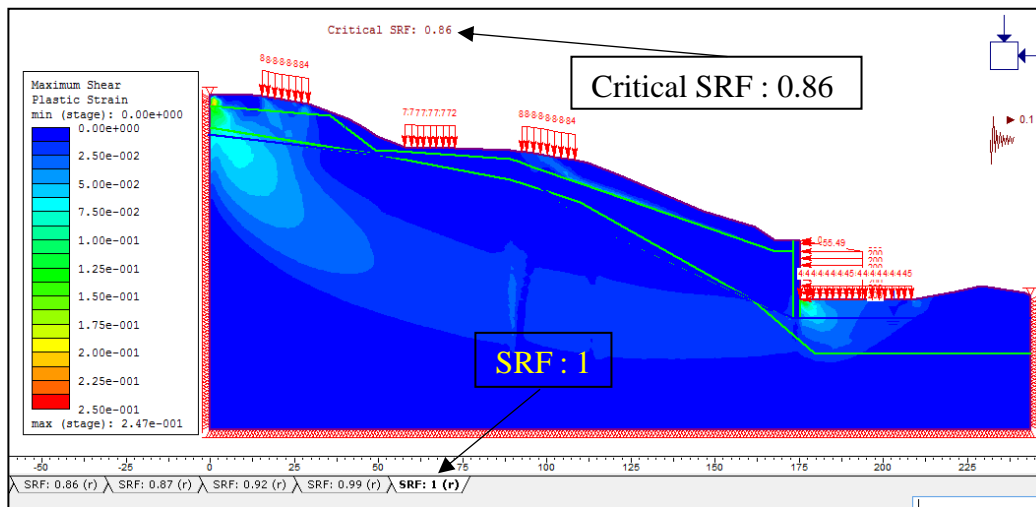
Figure 6.11. FEM analysis result with drained parameters and horizontal pseudo-static coefficient of 0.1.

The pseudostatic analysis with the coefficient of 0.001 practically yields the same result with the static analysis. The critical SRFs calculated for pseudo-static coefficients of 0.001, 0.05, 0.075 and 0.1 are 1.09, 0.995, 0.92 and 0.86, respectively.

Analyses with Undrained Parameters

The critical SRFs for pseudo-static coefficient of 0.001, 0.05, 0.075 and 0.1 are 1.16, 1, 0.93 and 0.86 respectively. The undrained FE modeling has shown more sensitivity to change in the pseudo-static accelerations compared to drained FE modeling. If SRF below unity is considered as theoretical instability region, the critical pseudo-static acceleration can be treated as 0.05g for the case. Consequently, FEM has provided smaller safety measures compared to LEM.

6.6.2. Time-History Analyses

Before it can be used in response analyses, the input accelerogram should be filtered from noise and the baseline must be corrected. These modifications have been done using SeismoSignal 2016 software. Subsequently, the accuracy of the wave transmission should be checked. Lysmer and Kuhlemeyer (1973) criteria, which was

98

mentioned in Chapter 2, will be used for this purpose. The input motion was filtered to work with the optimum mesh size without losing significant power.

RS2 allows users to define Rayleigh damping in the models to simulate the cyclic behavior of the soil during an earthquake. As it was mentioned earlier in Chapter 2, this is done by introducing damping through frequency-dependent Rayleigh formulation using viscous damping consistent with the level of strain induced by the earthquake.

Appropriate boundaries have been defined on the model for dynamic analyses; dynamic stages and time query points have been defined to observe the dynamic process properly.

Filtering of the Input Motion

Lysmer and Kuhlemeyer (1973) criteria for the accurate representation of wave transmission through a model is:

$$Element\ size\ \leq\ \frac{\lambda}{10}$$

Where λ is the wavelength associated with the highest frequency component which contains considerable energy. This inequality can be expressed in terms of shear wave velocity and frequency, considering:

$$\lambda = \frac{V_s'}{frequency} \tag{6.3}$$

$$Element\ size\ \leq\ \frac{V_s'}{10*frequency}$$

$$frequency\ \leq\ \frac{V_s'}{10*Element\ size}$$

From finite element models of the slope, the maximum element size has been measured as 2.5 m. Using the mean shear wave velocities calculated for the three soil layers from Table 6.1, the limiting frequency components for the layers can be calculated (Table 6.6).

Table 6.6. *The calculated frequency components for the layers.*

Layer Name	V_s' Mean (m/s)	10 * Element Size	Frequency
Residual	130	25.44	5.1
Greywacke	346	25.44	13.6
Phyllite	425	25.44	16.7

Accordingly, the greatest frequency value to satisfy the Lysmer and Kuhlemeyer (1973) criterion for all the soil layers is 5.1 Hz. Thus, the input motion will be filtered by removing the frequencies above 5.1 Hz from the record. Figure 6.12 shows the power spectrum of the Kalecik earthquake accelerogram filtered to 8 Hz.
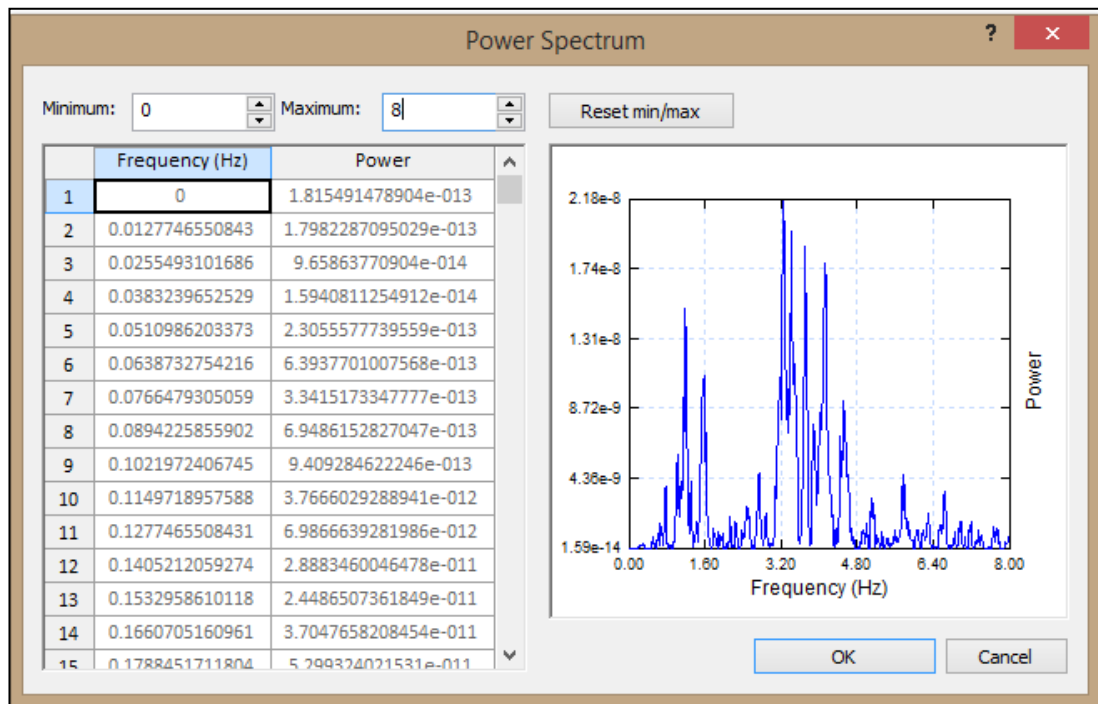
Figure 6.12. Power spectrum of the input motion filtered to 8 Hz.

It is seen from the figure that the significant part of the power of accelerogram occurs below 5.1 Hz. Therefore, the maximum frequency component of the record can be filtered to 5.1 Hz without loss of essential features.

Rayleigh Damping Parameters

From the Compute Natural Frequencies option of the program, damping versus frequency curves have been constructed to get 5% average system damping for both drained and undrained models (Figure 6.13. and Figure 6.14). As can be seen from the figures, the curves are Rayleigh parameters (α_M and β_K) dependent. Since Rayleigh damping is proportional to mass and stiffness, both drained and undrained models have the same α_M and β_K values because they have the same mass and stiffness. Consequently, **α_M=0.141** and **β_K=0.0011** were used for both, drained and undrained models.
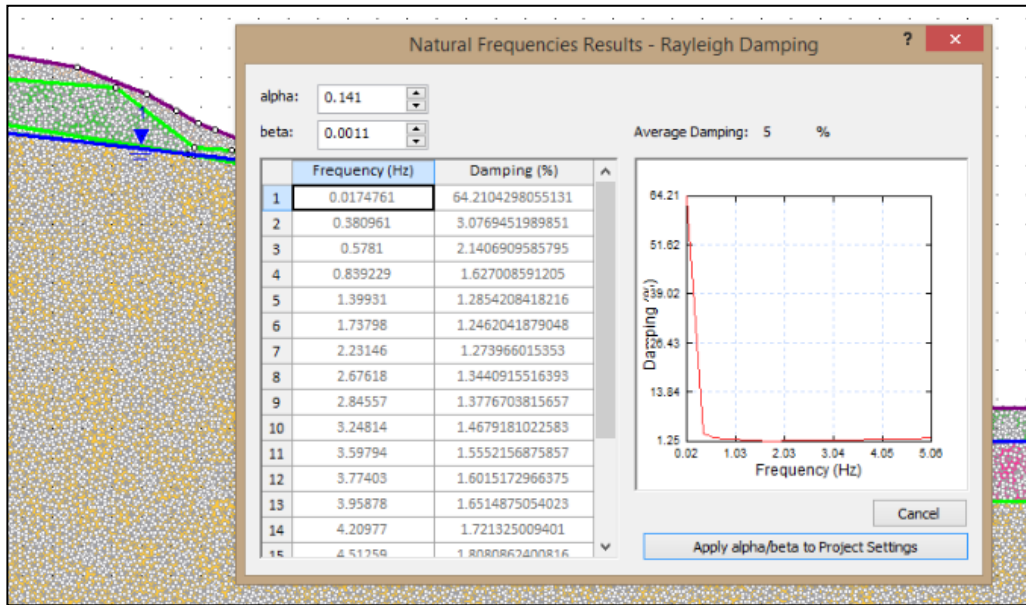
Figure 6.13. Natural frequencies results (Rayleigh damping) for the drained model.
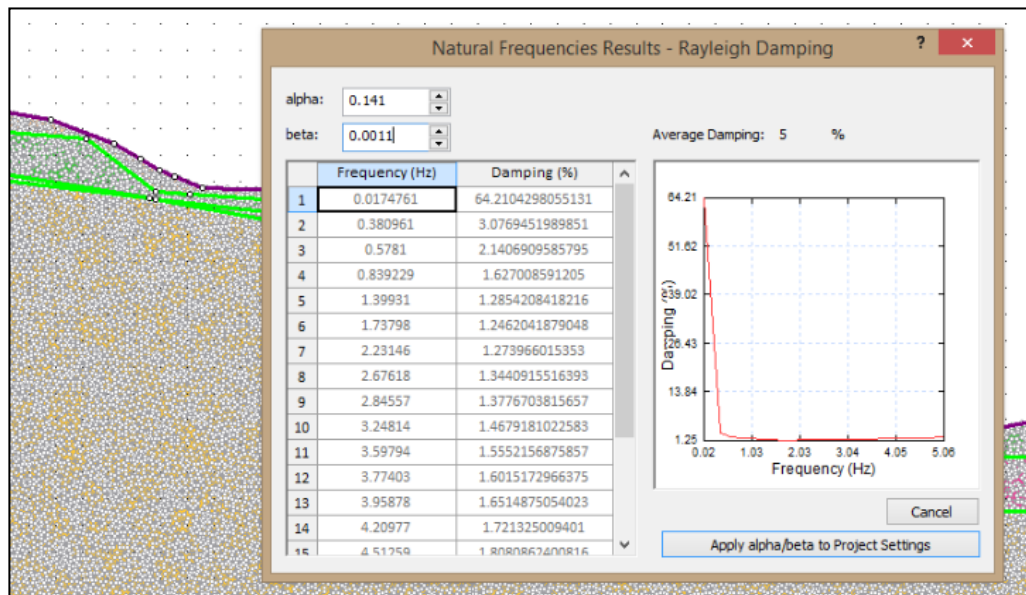
Figure 6.14. Natural frequencies results (Rayleigh damping) for the undrained model.

Dynamic Stages

By default, the first stage is the static condition; other stages may be defined as dynamic stages. Kalecik earthquake record (Figure 6.4) has a duration of 78.29 seconds and the time interval used is 0.01 s. Following five additional dynamic stages are defined:

- 5 second (Intermediate 1)

- 10 second (Intermediate 2)

- 45 second (Intermediate 3)

- 76 second (Intermediate 4)

- 100 second (Intermediate 5)

Dynamic Boundaries and Time Query Points

Transmitting boundary conditions to the lateral sides; absorbing boundary conditions to the base have been assigned. Additionally, 12 time query points have been defined in the model as shown in Figure 6.15 to see the response in terms of acceleration, velocity, and displacement with respect to time.
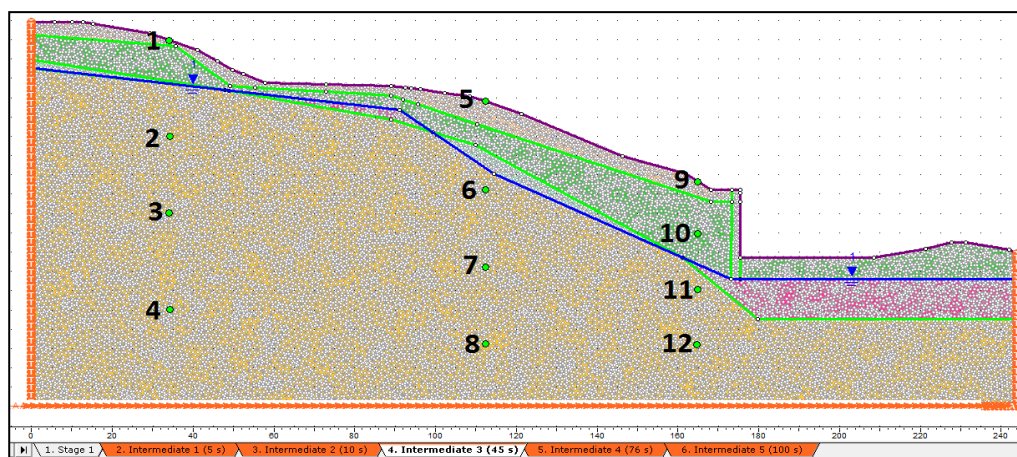
Figure 6.15. Locations and the numbering of the time query points.

Analyses with Drained Parameters

Batch computation of the drained model with PGA values of 0.001g (actual), 0.05g, 0.075g, and 0.1g has been conducted. The outcome for PGA of 0.075g has been selected here for presentation. Total displacements (elastic + plastic) which occur in the section at various stages of the analysis starting from the static condition are shown Figure 6.16, Figure 6.17, and Figure 6.18.
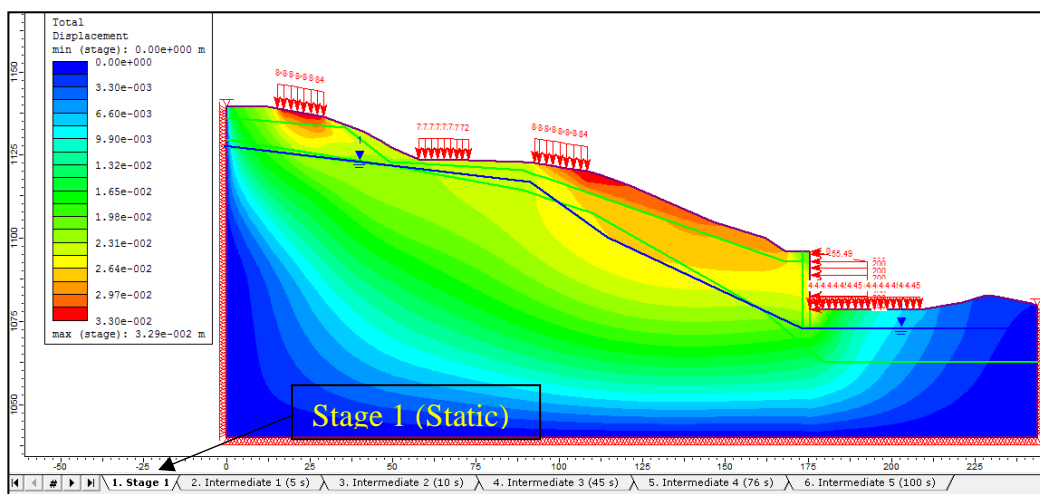
Figure 6.16. Static displacements for the drained model.
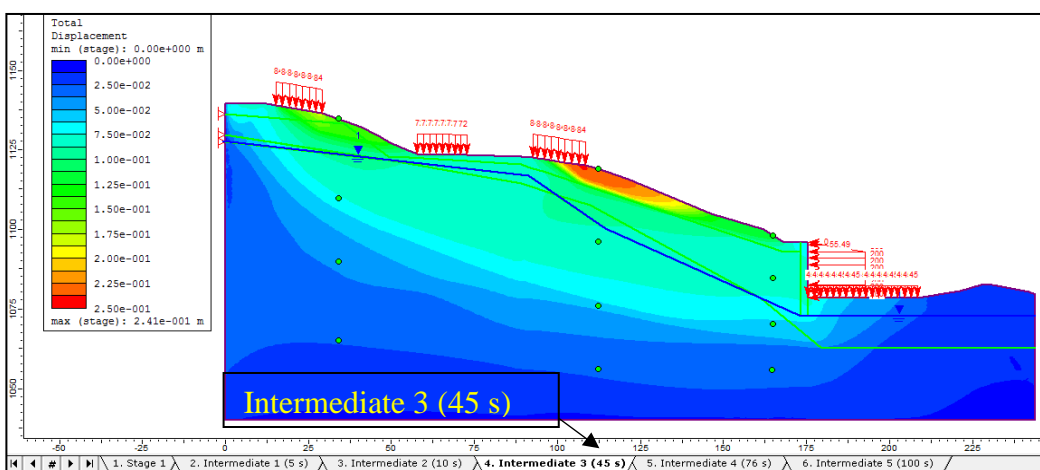
Figure 6.17. End of the 45 s displacements for the drained model.
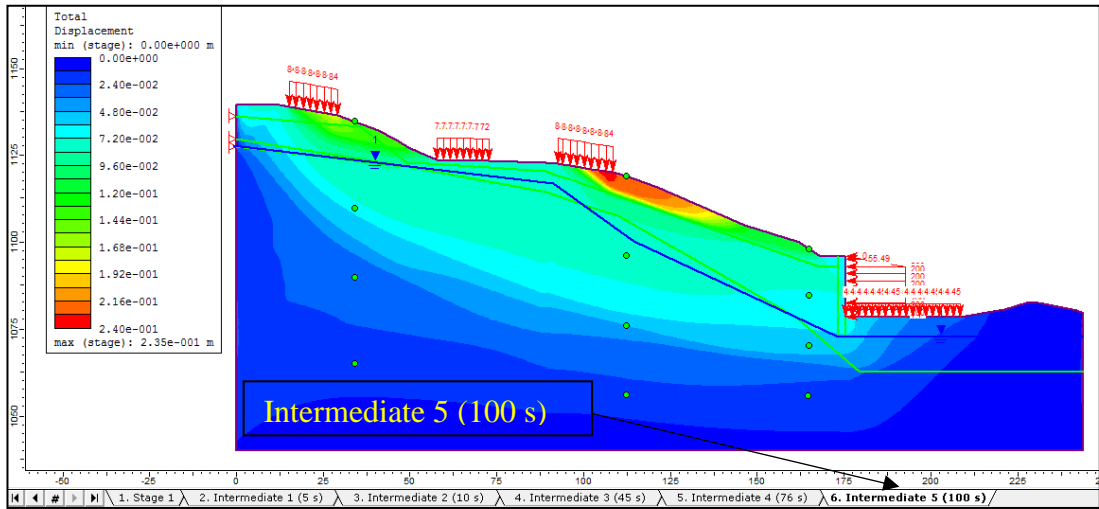
Figure 6.18. End of the 100 s displacements for the drained model.

It can be seen from the figures that the displacements start from stage intermediate 3 (end of 45 s) and are located near the query point 5. The maximum plastic shear strains are illustrated in Figure 6.19. Clearly a shallow slope failure has taken place in the vicinity of Güneş apartment (i.e., near the time query point 5).
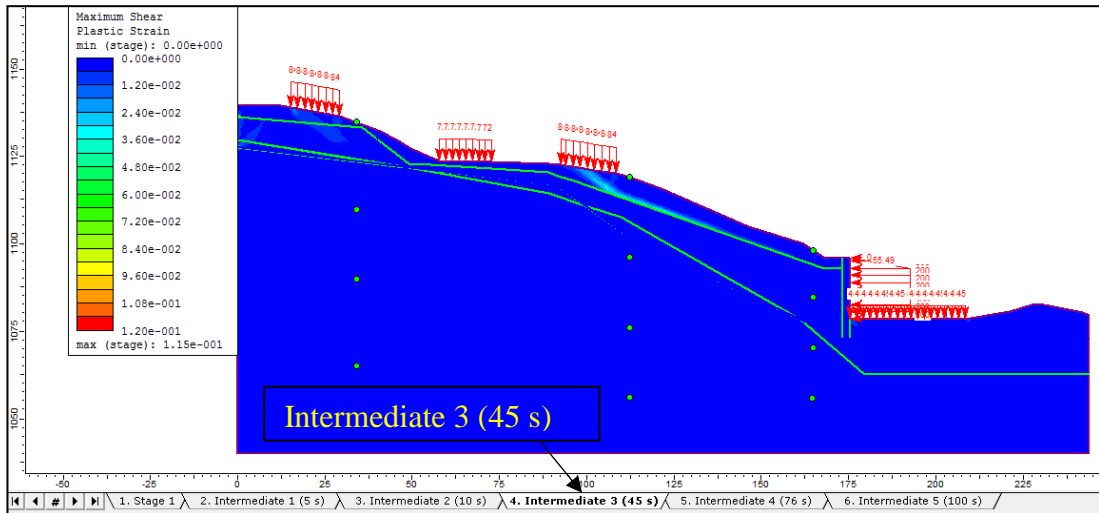
Figure 6.19. Maximum plastic shear strain contour at the end of the 45 s for the drained model.

105

Time query data of point 5 has been plotted as x-displacement versus time (Figure 6.20) and x-acceleration versus time (Figure 6.21).
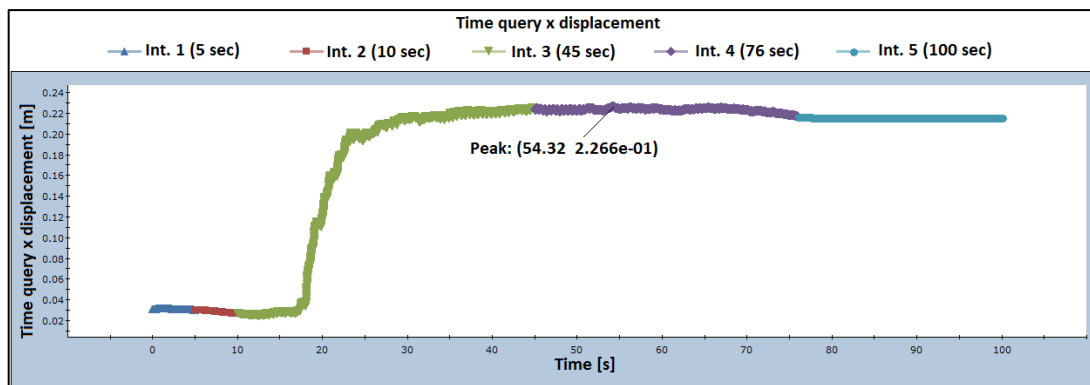
Figure 6.20. Drained model, time query x-displacement data at point 5.
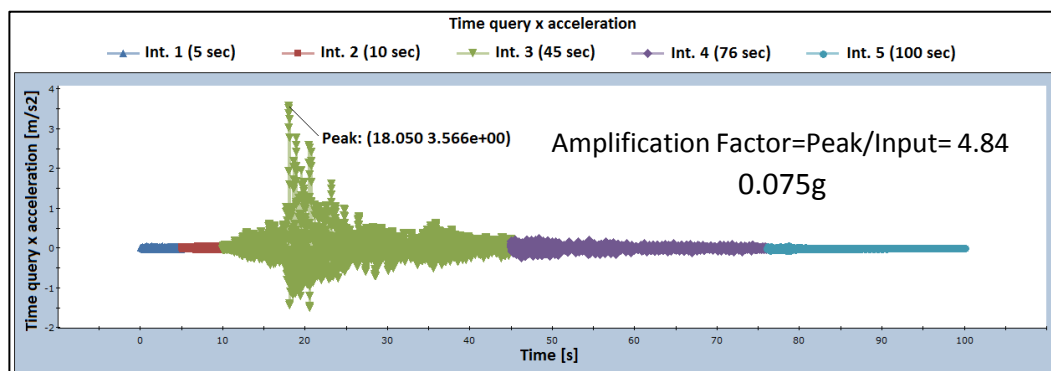
Figure 6.21. Drained model, time query x-acceleration data at point 5.

The essential response parameters are peak accelerations, amplification factors, initial displacements, peak displacements and end of earthquake plastic displacements. At query point 5, these parameters are 0.36g, 4.84, 0.0312 m, 0.23 m and 0.19 m, respectively. Those parameters are provided for all of the query points in Appendix-C.

106

Analyses with Undrained Parameters

Batch computation of the undrained model with PGA values of 0.001g (actual), 0.05g, 0.075g, and 0.1g has been conducted. The model with PGA of 0.075g has been selected to show the outcome here. Total displacements (elastic + plastic) that occur in the section at various stages of the analysis starting from the static condition are shown in Figure 6.22, Figure 6.23, and Figure 6.24.
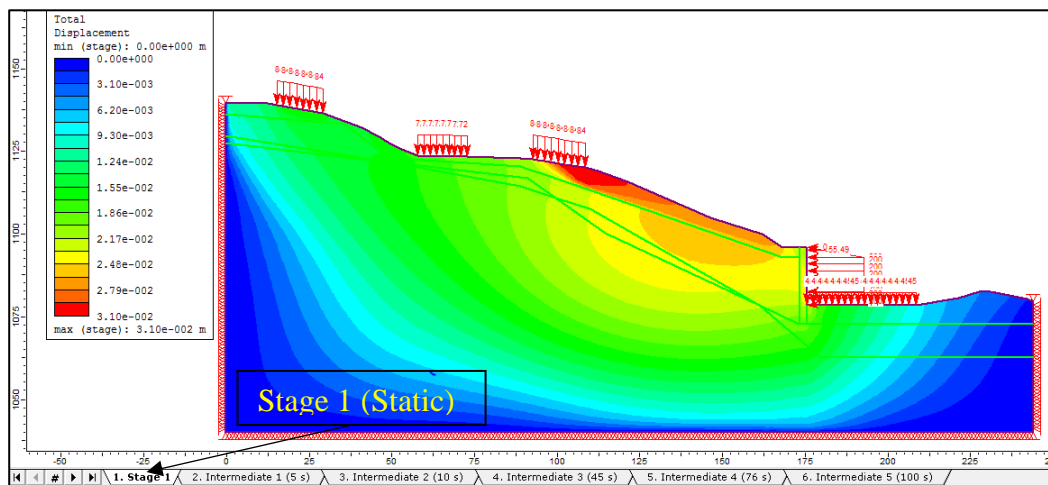
Figure 6.22. Static displacements for the undrained model.
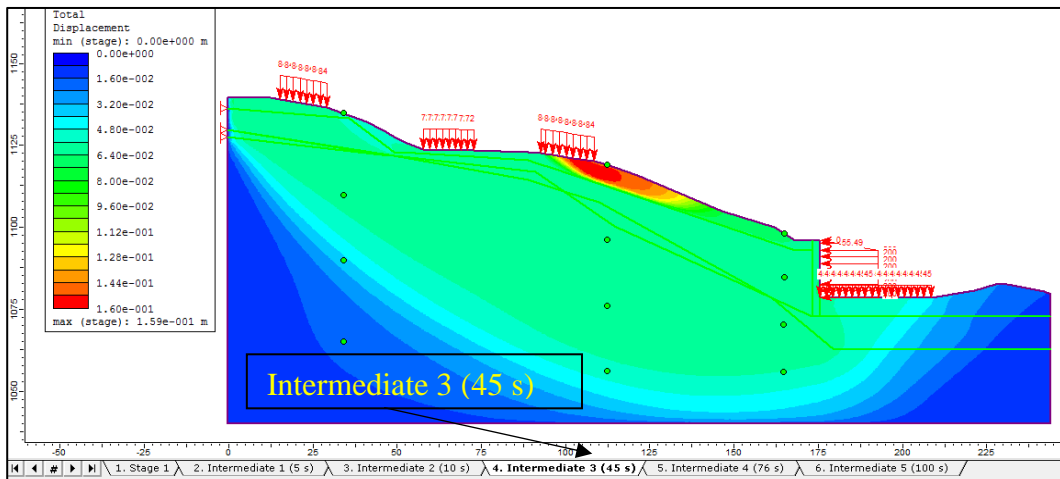
Figure 6.23. End of the 45 s displacements for the undrained model.
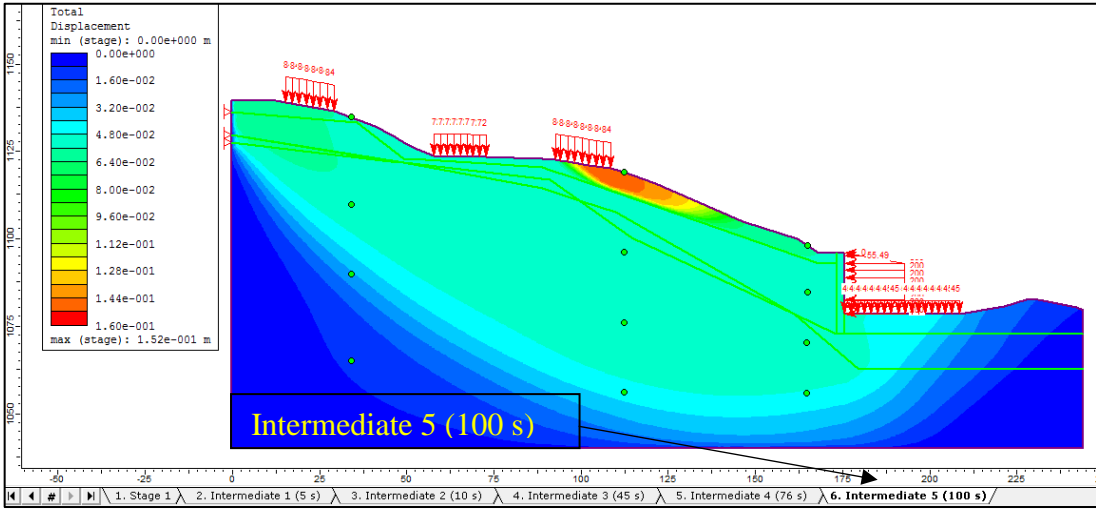
Figure 6.24. End of the 100 s displacements for the undrained model.

The displacements start to increase from stage intermediate 3 (at the end of 45 s) and are located near the time query point 5. The maximum plastic shear strains have been illustrated in Figure 6.25. It has been observed from the maximum plastic shear strains contours that a failure has taken place in the vicinity of Güneş Apartment (i.e., near the time query point 5).
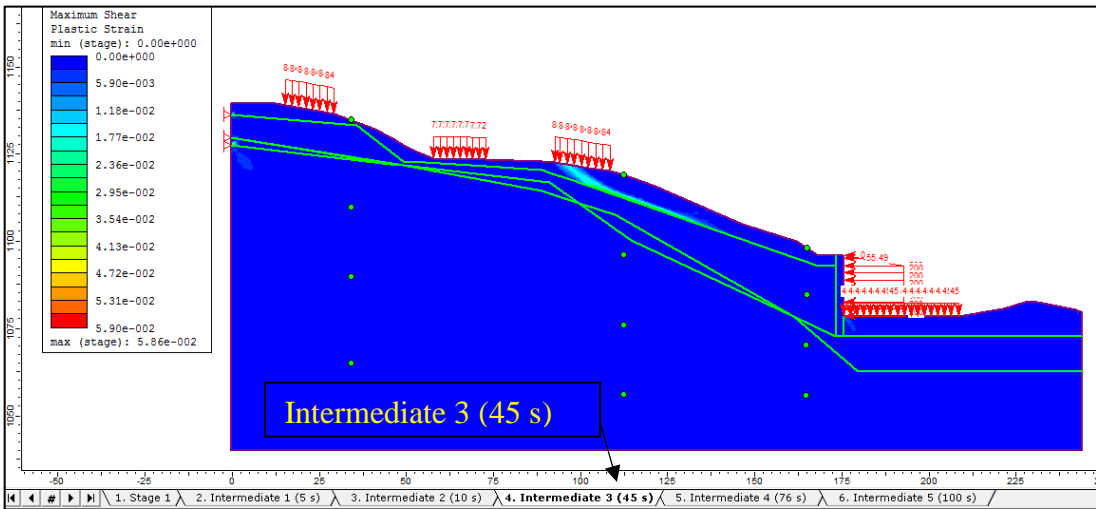
Figure 6.25. Maximum plastic shear strain contour at the end of the 45 s for the undrained model.

108

Time query data of point 5 has been plotted as x-displacement versus time (Figure 6.26) and x-acceleration versus time (Figure 6.27).
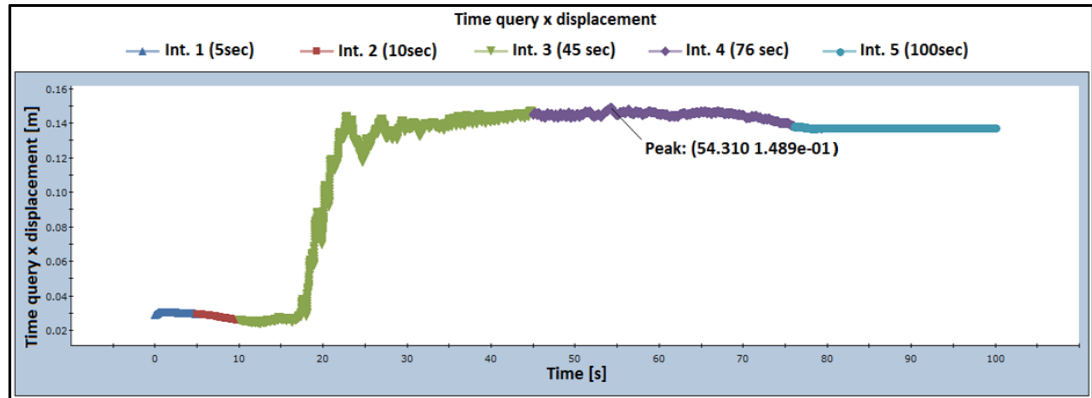
Figure 6.26. Undrained model, time query x-displacement data of point 5.
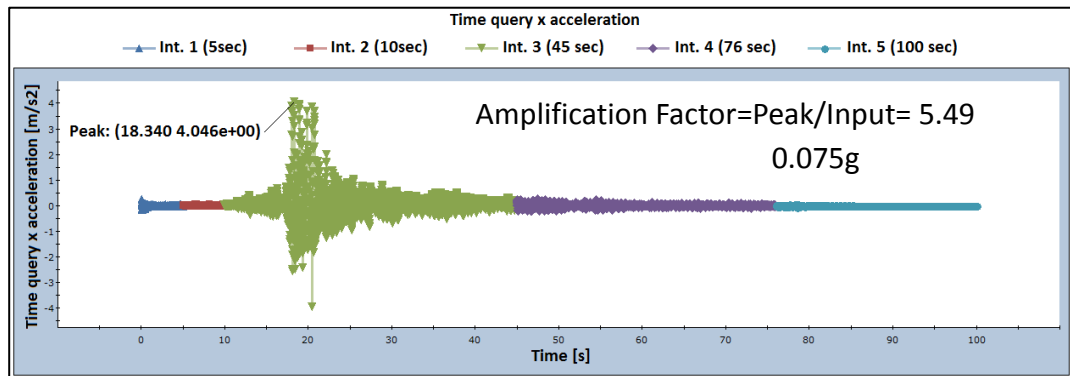
Figure 6.27. Undrained model, time query x-acceleration data of point 5.

In this example, peak acceleration, amplification factor, initial displacement, peak displacement, and end of earthquake plastic displacement are 0.41g, 5.49, 0.03 m, 0.15 m and 0.12 m, respectively. The essential parameters of the plots are provided in Appendix-C for all the query points. Regarding displacements, analysis with drained parameters yielded greater values, while greater accelerations and amplification factors were obtained from the analyses carried out with undrained parameters.

CHAPTER 7

RESULTS AND DISCUSSION

In this chapter, the overall results are presented and discussed. Velocity-time graphs of the site inclinometer data indicate deep and shallow landslides with sharp decreases in displacement rates in time. This is considered to be due to the lessening effects of the downpour. The static analyses results have been summarized in Table 7.1, Table 7.2, and Table 7.3.

.

Table 7.1. *Results of the two-dimensional LE analyses.*

Analyzed Condition	FS Search Zone	Critical FS
Stability margin	Overall	1
Flood	Shallow	0.97
Flood	Deep	0.98
No excavation and flood	Shallow	0.99
No excavation and flood	Deep	1.4
Excavation, surcharge (fully constructed business center) and flood	Shallow	0.97
Excavation, surcharge (fully constructed business center) and flood	Deep	1.56

It is seen from Table 7.1 that the flood condition has decreased safety factors below unity for shallow and deep zones.

Analyses results appear to confirm that the business center foundation excavation on the toe of the slope has a negative effect on the stability of deep potential failure surfaces, whereas the surcharge load due to fully constructed building or non-presence

of excavation appears to have a positive influence. However, neither excavation nor building surcharge does not affect the stability of the shallow zone.

Table 7.2. *Results of the two-dimensional FE analyses.*

Analyzed Condition	SSR Search Zone	Critical SRF
Stability margin	Deep	0.89
Flood	Overall	0.72
Flood	Deep	0.87
Flood	Under Güneş Apartment (Shallow)	0.74
No excavation+ flood	Deep	1.23
Excavation, surcharge (fully constructed business center) and flood	Deep	1.05

The two-dimensional FE static analyses results in Table 7.2 show similar trends with those of limit equilibrium results, with the following two differences:

1. Critical SRFs are approximately 10% below the critical FS's.

2. Critical SRF for the shallow slide in flood circumstances decreases more significantly than the LE condition.

The three-dimensional FE static analyses results are shown in Table 7.3.

Table 7.3. *Results of the three-dimensional finite element analyses.*

Analyzed Condition	SSR Search Zone	Critical SRF
Surcharge (business center)	Overall	1.11

Results of the 3D model analysis clearly validate the domain of shallow slide adjacent to the Güneş Apartment. However, critical SRFs are higher than those of two-dimensional models. Strains in the deep zones may not have been properly calculated due to fact that the 3D slope stability software is in the development stage as yet. Besides, considering the effort required for model preparation and post-processing of the outcome, the efficiency of 3D approach becomes questionable for the case slope. The findings of the research can be summarized as shown in Table 7.4.

Table 7.4. *Summary of the findings (marginal equilibrium state).*

Method	Measure of Safety Assessment	Degree of Safety
2D Limit Equilibrium Method	FS	1
2D Finite Element Method	SRF	0.89
3D Finite Element Method	SRF	1.11

Possible effects of the potential seismic events on the case site have been investigated by 2D models. Results of the pseudo-static analyses are presented in Table 7.5, Table 7.6, Table 7.7, and Table 7.8. Regarding seismic analyses, both, LEM and FEM models with undrained parameters showed greater sensitivity to variations in pseudo-static acceleration coefficient compared to those with drained parameters.

Table 7.5. *Results of pseudo-static LEM analysis with drained parameters.*

Material Behavior	Horizontal Pseudo-static Acceleration Coefficient	Critical FS
Drained	0 (Static)	1.18
Drained	0.001	1.18
Drained	0.05	1.06
Drained	0.075	1.01
Drained	0.1	0.95

Table 7.6. *Results of pseudo-static LEM analysis with undrained parameters.*

Material Behavior	Horizontal Pseudo-static Acceleration Coefficient	Critical FS
Undrained	0 (Static)	1.22
Undrained	0.001	1.22
Undrained	0.05	1.04
Undrained	0.075	0.97
Undrained	0.1	0.91

Table 7.7. *Results of pseudo-static FEM analysis with drained parameters.*

Material Behavior	Horizontal Pseudo-static Acceleration Coefficient	Critical SRF
Drained	0 (Static)	1.09
Drained	0.001	1.09
Drained	0.05	1
Drained	0.075	0.92
Drained	0.1	0.86

Table 7.8. *Results of pseudo-static FEM analysis with undrained parameters.*

Material Behavior	Horizontal Pseudo-static Acceleration Coefficient	Critical SRF
Undrained	0 (Static)	1.16
Undrained	0.001	1.16
Undrained	0.05	1
Undrained	0.075	0.93
Undrained	0.1	0.86

The dynamic time-history analysis results have been summarized in Table 7.9, Table 7.10, Table 7.11, and Table 7.12. Data regarding the query points from 5 thru 8 (Figure 6.15) obtained from the analyses carried out with drained parameters are given in Table 7.9 and Table 7.10. These query points are located in front of Güneş Apartment from the top to the bottom. Both, the greatest amplification factor and displacement occur at the top as would be expected.

Table 7.11 and, Table 7.12 summarize the results of the analyses conducted with undrained parameters for the query points from 5 to 8 (Figure 6.15). The greatest amplification factor and displacement are again at the top. The drained model has greater plastic displacements and smaller amplification factors compared to the undrained model.

Table 7.9. *Amplification factors at query points with drained parameter analysis.*

Query Point Number	Material Behavior	PGA (g)	Peak Acceleration at the Query Point (g)	Amplification Factor
5	Drained	0.075	0.363	4.84
6	Drained	0.075	0.134	1.79
7	Drained	0.075	0.125	1.67
8	Drained	0.075	0.128	1.71

Table 7.10. *Displacements at query points with drained parameter analysis.*

Query Point Number	Material Behavior	Initial (Static, Elastic) Displacement (m)	Maximum (Elastic+ Plastic) Displacement (m)	End of Earthquake Plastic Displacement (m)
5	Drained	0.03	0.23	0.19
6	Drained	0.03	0.09	0.05
7	Drained	0.02	0.06	0.03
8	Drained	0.01	0.03	0.02

Table 7.11. *Amplification factors at query points with undrained parameter analysis.*

Query Point Number	Material Behavior	PGA (g)	Peak Acceleration at the Query Point	Amplification Factor
5	Undrained	0.075	0.412	5.49
6	Undrained	0.075	0.143	1.91
7	Undrained	0.075	0.140	1.87
8	Undrained	0.075	0.118	1.57

Table 7.12. *Displacements at query points with undrained parameter analysis.*

Query Point Number	Material Behavior	Initial (Static, Elastic) Displacement	Maximum (Elastic + Plastic) Displacement	End of Earthquake Plastic Displacement (m)
5	Undrained	0.03	0.15	0.11
6	Undrained	0.02	0.06	0.03
7	Undrained	0.02	0.06	0.03
8	Undrained	0.01	0.05	0.03

CHAPTER 8

CONCLUSIONS AND RECOMMENDATIONS

In this study, the landslide which occurred in Akpınar District of Ankara following the heavy rain in June 2011 has been investigated as the case study. At the outset, the geotechnical conditions at the site have been described, data from inclinometers installed at the site has been evaluated and velocity-time graphs were constructed. Subsequently, static analyses including the downpour condition and presence/non-presence of the business center foundation excavation at the toe of the slope have been modeled with LEM and FEM. Finally, the current condition of the case slope has been remodeled to investigate possible effects of earthquake scenarios. The pseudo-static dynamic analysis approach has been utilized for both LEM and FEM in 2D. In addition, dynamic time-history analyses have been conducted with 2D-FEM.

Although there are some uncertainties e.g. regarding the water levels at different times, the shear strength of different soil layers at the site before and after movements, and possibility of the representation of the removal of lateral earth support by the natural soil at the toe by a vertical surcharge load due to building construction etc., based on the assumptions in this study following are the conclusions reached:

- Shallow and deep, two landslides were triggered simultaneously at the site.

- Leaning of the Güneş Apartment was due to the shallow landslide which occurred due to the saturation of near-surface soils following the downpour.

- The business center foundation excavation at the toe of the slope had an adverse influence in triggering of the deep slide, whereas the surcharge to be

exerted by the fully constructed business center building appears to improve the safety factor.

- In the 3D FEM model, the occurrence of the shallow slide has been well-shown. Safety levels are higher than those of the two-dimensional models, contrary to the expectation.

- In 2D static analyses, FEM has resulted in approximately 10% lower safety levels compared to those of LEM. This is due to the fact that in FEM, failure surfaces are not confined to pre-defined geometric forms (circles) as in the case of LEM.

- Concerning the pseudo-static analyses, undrained material behavior is anticipated during an earthquake. In the analyses with undrained parameters, the critical (for which FS $\approx$ 1) pseudo-static horizontal acceleration coefficient is calculated as 0.075 in case of LEM, whereas FEM yields a value of 0.05. Accordingly, FEM results are again less than LEM results.

- In the dynamic time-history analyses with the drained and undrained parameters, amplification and displacements increase towards the ground surface, as expected.

- Overall, the analyses clearly indicate that the case slope has marginal stability and rather sensitive to any additional loading, such as due to saturation of surface soils and water table fluctuations.

Considering continuous development of the state-of-the-art, the recommendations for future research and the general practice are:

- The LEM and the FEM should be both utilized to check the consistency of the results in slope stability analyses.

- Non-homogeneity in the distribution of subsoils in 3D can be better identified and analyzed with three-dimensional slope models.

- More realistic material models for the hysteretic behavior of the soil can be utilized.

- The level of the groundwater table and the thickness of saturation zone can be identified more precisely in flood condition.

REFERENCES

Abramson, L., Lee, T., Sharma, S., and Boyce, G. (2001). *Slope Stability and Stabilization Methods* (2nd ed.). John Wiley and Sons, Inc.

AFAD. (2018). Building Earthquake Code of Turkey 2018 (in Turkish). Turkey: Official Gazette.

AFAD. (2019). *Accelerogram Information on the Selected Earthquake*. Retrieved from Turkish Strong Ground Motion Database: http://kyhdata.deprem.gov.tr/2K/genAcc.php?dst=TU9EVUxFX05BTUU9Z XZ0RmlsZSZNT0RVTEVfVEFTSz1zaG93Jk1PRFVMRV9TVUJUQVNLP UFMTCZNT0RVTEVfVEFSR0VUPW9sZCZUQVJHRVQ9MjAxNjA4MD IxOTMwNTJfMTgwMiZUQVJHRVRfU0VSSUFMPTIyMTM3

AFAD. (2019). *Seismic Hazard Map of Turkey*. Retrieved from https://deprem.afad.gov.tr/deprem-tehlike-haritasi?lang=en

Akbaş, B. (2015). *Probabilistic Slope Stability Analysis Using Limit Equilibrium, Finite Element and Random Finite Element Methods.* Middle East Technical University (METU), Civil Engineering (CE).

Akış (Keklikoğlu), E. (2002). *Stability Analysis of a Highway Embankment Slope Failed During DÜZCE Earthquake.* Middle East Technical University, Civil Engineering.

Bakır, S. (2011). *Investigation and Evaluation Report on the Business Center Construction Site Excavation Shoring System (in Turkish).* Middle East Technical University (METU)- Civil Engineering (CE) Department, Ankara.

Bakır, S. (2012). *Evaluation of Field Investigation and Displacement Measurements about the Landslide Occurred in Dikmen, Akpınar District, 20026 Land*

Parcel, Çankaya Municipality, Ankara (in Turkish). Middle East Technical University (METU)- Civil Engineering (CE) Department, Ankara.

Bakır, S. (2012). *Evaluation of the Landslide Occurred in Dikmen-Akpınar District from the Business Center Foundation Excavation Point of View (in Turkish).* Middle East Technical University (METU)- Civil Engineering (CE) Department, Ankara.

Bishop, A. (1955, 3). The use of the Slip Circle in the Stability Analysis of Slopes. *Géotechnique, 5*(1), 7-17.

Bishop, A., and Morgenstern, N. (1960, 12). Stability Coefficients for Earth Slopes. *Géotechnique, 10*(4), 129-153.

CGE. (2011). *Survey Report on the Landslide Occurred in Dikmen-Keklikpınarı-Akpınar District-826th Street (in Turkish).* The Union of Chambers of Turkish Engineers and Architects (UCTEA)-Chamber of Geological Engineers (CGE), Ankara.

Chopra, A. (1966). *Earthquake Effects on Dams.* University of California, Berkeley, Civil Engineering.

Cruden, D., and Varnes, D. (1996). Landslides: investigation and mitigation. Chapter 3-Landslide types and processes. In D. Cruden, D. Varnes, R. Schuster, and A. Turner (Eds.), *Special Report,247 - National Research Council, Transportation Research Board.* Washington: National Academy Press.

Çokça, E., Huvaj Sarıhan, N., and Özkan, M. (2011). *Evaluation report on the "Geological-geotechnical investigation report on the Dikmen- Akpınar landslide" of Bülent Kiper Geotech. Co. Ltd. (in Turkish).* Middle East Technical University(METU)- Civil Engineering (CE) Department, Ankara.

Dakoulas, P., and Gazetas, G. (1986, 4). Seismic shear strains and seismic coefficients in dams and embankments. *Soil Dynamics and Earthquake Engineering, 5*(2), 75-83.

Duncan, J. (1996). Landslides: investigation and mitigation. Chapter 13-Soil slope stability analysis. In J. Duncan, R. Schuster, and A. Turner (Eds.), *Special Report,247 - National Research Council, Transportation Research Board.* Washington: National Academy Press.

Duncan, J., and Dunlop, P. (1969). Slopes in stiff-fissured clays and shales. *Journal of Soil Mechanics and Foundations Division, 95*(2), 467-492.

Fellenius, W. (1927). *Erdstatische Berechnungen mit Reibung und Kohäsion (Adhäsion) und unter Annahme kreiszylindrischer Gleitflächen.* Berlin: W. Ernst and Sohn.

Fredlund, D., and Barbour, S. (1986). The Prediction of Pore-Pressures for Slope Stability Analyses. *Slope Stability Seminar, the University of Saskatchewan* (p. 33). Saskatoon: University of Saskatchewan.

Google. (2019). *Satellite view of the area of the case study*. Retrieved from https://www.google.com/maps/@39.8582598,32.8097275,340m/data=!3m1! 1e3

Houston, S., Houston, W., and Padilla, J. (1987, 11 6). Microcomputer-Aided Evaluation of Earthquake-Induced Permanent Slope Displacements. *Computer-Aided Civil and Infrastructure Engineering, 2*(3), 207-222.

Huvaj Sarıhan, N. (2019, December 3). Personal communication.

Hynes-Griffin, M.E. and Franklin, A. (1984). Rationalizing the seismic coefficient method. *Miscellaneous Paper GL-84-13, U.S. Army Corps of Engineers Waterways Experiment Station, Vicksburg, Mississippi, 21 pp.*

Janbu, N. (1954a). Application of composite slip surface for stability analysis. *Proceedings of European Conference on Stability of Earth Slopes.* Stockholm (SWEDEN).

Janbu, N. (1954b). Stability analysis of slopes with dimensionless parameters. *Harvard Soil Mechanics Series, 46*, 811.

Janbu, N. (1968). *Slope Stability Computations.* Technical University of Norway, Trondheim.

Janbu, N. (1973). Slope Stability Computations. In N. Janbu, A. Casagrande, R. Hirschfeld, S. Poulos, and G. Bertram (Eds.), *Embankment dam engineering: Casagrande volume.* Wiley.

Jibson, R. (1993). Predicting Earthquake-Induced Landslide Displacements Using Newmark's Sliding Block Analysis. *Transportation Research Record*(1411), 9-17.

Kiper, B. (2011). *Geological-geotechnical investigation report on the Dikmen-Akpınar landslide (in Turkish).* Bülent Kiper Jeoteknik Mühendislik Ltd. Şti., Ankara.

Kocaman, C., and Doğan, A. (2011). *Investigation Report on the Dikmen-Akpınar District-826th Street-No. 15 Building (in Turkish).* The Union of Chambers of Turkish Engineers and Architects (UCTEA)-Chamber of Civil Engineers (CCE), Ankara.

Kramer, S. (1996). *Geotechnical Earthquake Engineering.* Upper Saddle River, NJ, United States: Pearson Education (US).

Kuhlemeyer, R., and Lysmer, J. (1973). Finite element method accuracy for wave propagation problems. *Journal of Soil Mechanics and Foundations Divison, 99*(5), 421-427.

Laera, A. (2015). PLAXIS 2D and 3D applications in geotechnical earthquake engineering. *Plaxis Bulletin* (38), 6-9.

Liu, F., and Zhao, J. (2013, 12). Limit Analysis of Slope Stability by Rigid Finite-Element Method and Linear Programming Considering Rotational Failure. *International Journal of Geomechanics, 13*(6), 827-839.

Lowe, J., and Karafiath, L. (1960). Stability of earth dams upon drawdown. *Proc. 1st Pan American Conference on Soil Mechanics and Foundation Engineering, Mexico City, 1960*, (pp. 537-552).

Makdisi, F., and Seed, H. (1978). Simplified Procedure for Estimating Dam and Embankment Earthquake Induced Deformations. *Journal of Geotechnical Engineering, ASCE, 104*, 849-867.

Marcuson,III, W. (1981). Moderator's report for session on 'Earth dams and stability of slopes under dynamic loads'. *International Conference on Recent Advances in Geotechnical Earthquake Engineering and Soil Dynamics*, (p. 1175). St. Louis, Missouri.

Morgenstern, N., and Price, V. (1965, 3). The Analysis of the Stability of General Slip Surfaces. *Géotechnique, 15*(1), 79-93.

Nalçakan, M., Cavlaz, C., and Taş, S. (2012). *Geotechnical Report on the Landslide Occurred in Akpınar District, 20026 Land Parcel, Çankaya Municipality, city of Ankara (Factual Report) (in Turkish).* Kilci Engineering Co., Ankara.

Newmark, N. (1965, 6). Effects of Earthquakes on Dams and Embankments. *Géotechnique, 15*(2), 139-160.

Ohta, Y., and Goto, N. (1978). Empirical shear wave velocity equations in terms of characteristic soil indexes. *Earthquake Engineering and Structural Dynamics*.

Plaxis. (2019). *PLAXIS Material Models Manual 2019*. Retrieved from https://www.plaxis.com/?plaxis_download=2D-3-Material-Models.pdf

Rocscience. (2019). *Rocscience RS2 Online Help*. Retrieved from https://www.rocscience.com/help/rs2/#t=getting_started%2FRS2_Applicatio ns_Overview.htm

Rocscience. (2019). *Rocscience RS3 Online Help*. Retrieved from https://www.rocscience.com/help/rs3/#t=Getting_Started%2FGetting_Started .htm

Rocscience. (2019). *Rocscience SLIDE Online Help*. Retrieved from https://www.rocscience.com/help/slide2/#t=getting_started%2FGetting_Start ed.htm

Sarma, S. (1973, 9). Stability analysis of embankments and slopes. *Géotechnique, 23*(3), 423-433.

Sarma, S. (1975, 12). Seismic stability of earth dams and embankments. *Géotechnique, 25*(4), 743-761.

Saygı, M. (2010). *Geological Investigation Report (in Turkish)*. Çözüm Jeoteknik, Ankara.

Seed, H. (1979, 9). Considerations in the earthquake-resistant design of earth and rockfill dams. *Géotechnique, 29*(3), 215-263.

Seed, H., and Martin, G. (1966). The Seismic Coefficient in Earth Dam Design. *Journal of the Soil Mechanics and Foundations Division, 92*(3), 25-58.

Snitbhan, N., and Chen, W.-F. (1978, 12). Elastic-plastic large deformation analysis of soil slopes. *Computers and Structures, 9*(6), 567-577.

Spencer, E. (1967, 3). A Method of analysis of the Stability of Embankments Assuming Parallel Inter-Slice Forces. *Géotechnique, 17*(1), 11-26.

Şeren, İ., and İleri, N. (2011). *Geological Investigation Report (in Turkish)*. Republic of Turkey Ministry Of Interior Disaster And Emergency Management Presidency, Ankara.

Tanverdi, A., and Ekici, Ş. (1987). *Ankara Dikmen-Balgat Arası ile İmrahor-İncesu Vadisi Çevresinin Planlanmasına Esas Etüd Raporu ve Mühendislik Jeolojisi Haritası.* İlbank A.Ş., Ankara.

Terzaghi, K. (1950). Mechanism of Landslides. In K. Terzaghi, *Application of Geology to Engineering Practice* (pp. 83-123). New York, N. Y.: Geological Society of America.

USACE. (1970). *Engineering and Design—Stability of Earth and Rockfill Dams. Engineer Manual EM 1110-2-1902.* Department of the Army, Corps of Engineers, Office of the Chief of Engineers, Washington D.C.

USGS. (2019). *Landslide Types and Processes.* Retrieved from Fact Sheet 2004-3072: https://pubs.usgs.gov/fs/2004/3072/

Yandex. (2019). *Dikmen Akpınar Map.* Retrieved from Yandex Maps: https://yandex.com.tr/harita/11503/ankara/?l=satandll=32.810853%2C39.858 023andmode=searchandsll=32.854049%2C39.920756andsspn=0.314484%2 C0.120543andtext=dikmen akpınar mahaleisandz=19

Zienkiewicz, O. (1971). *The Finite Element Method in Engineering Science.* New York: McGraw-Hill.

APPENDICES

A. Kiper Co. and Kilci Co. Site Inclinometer Data and Velocity-Time Graphs
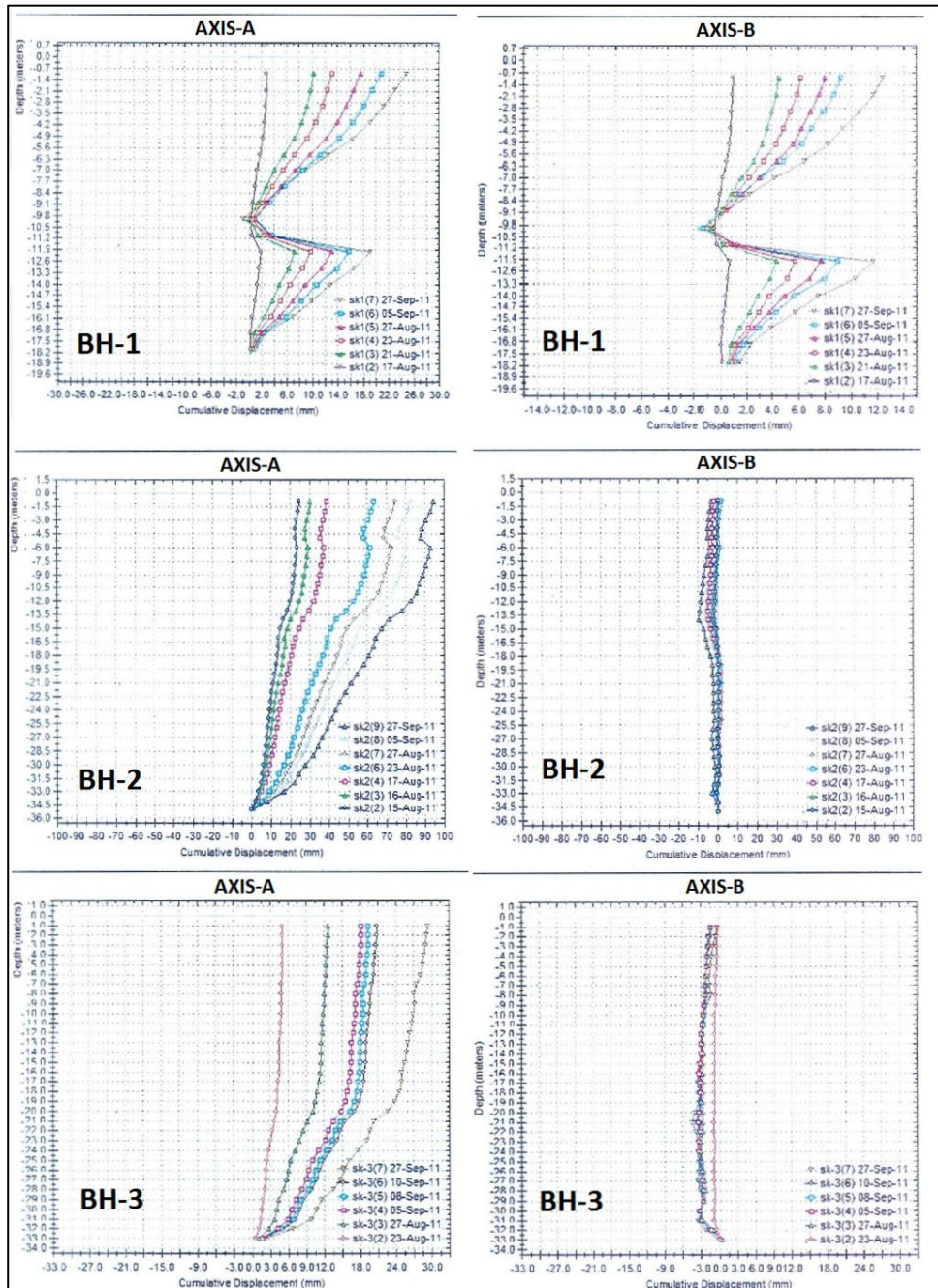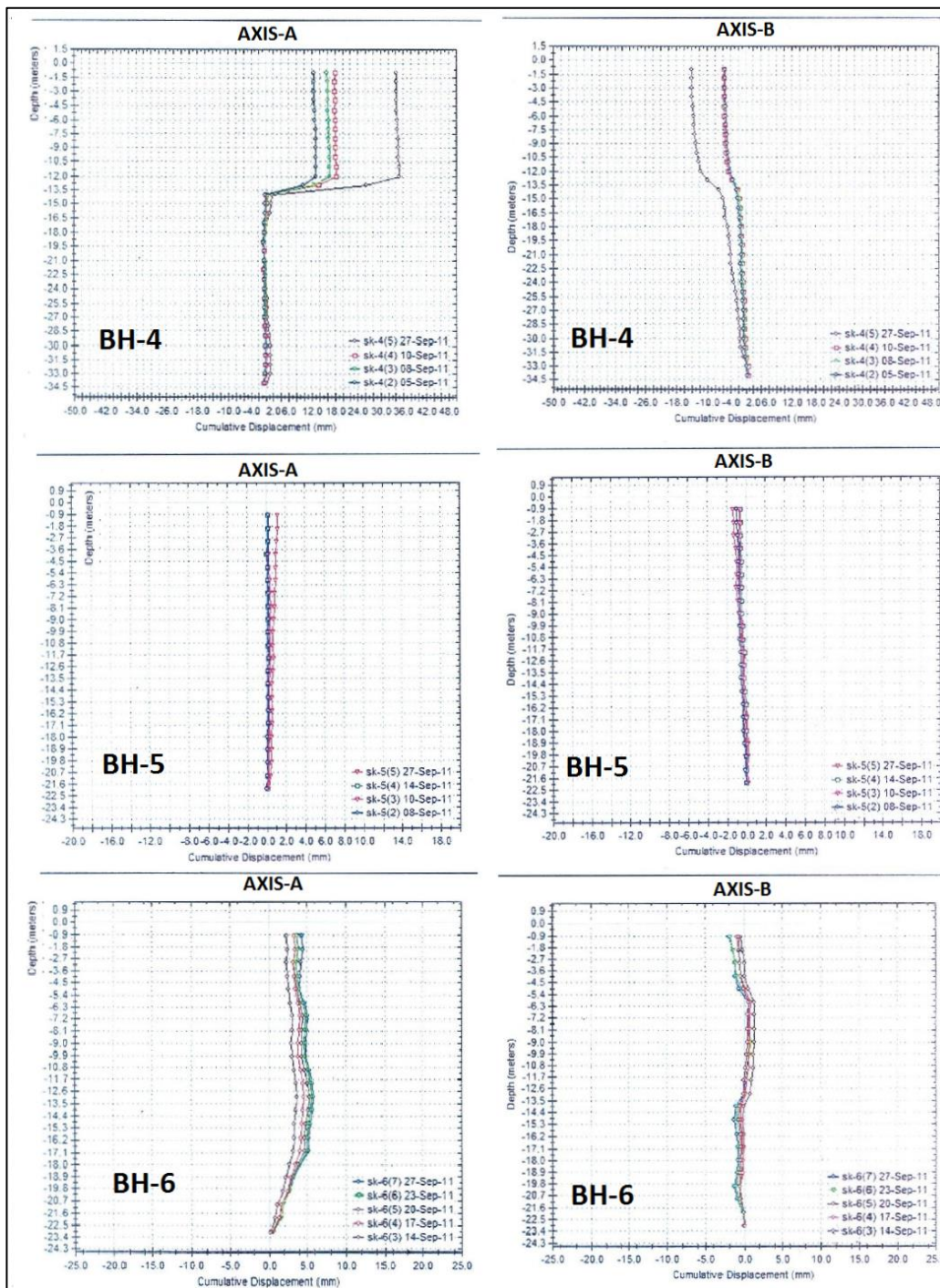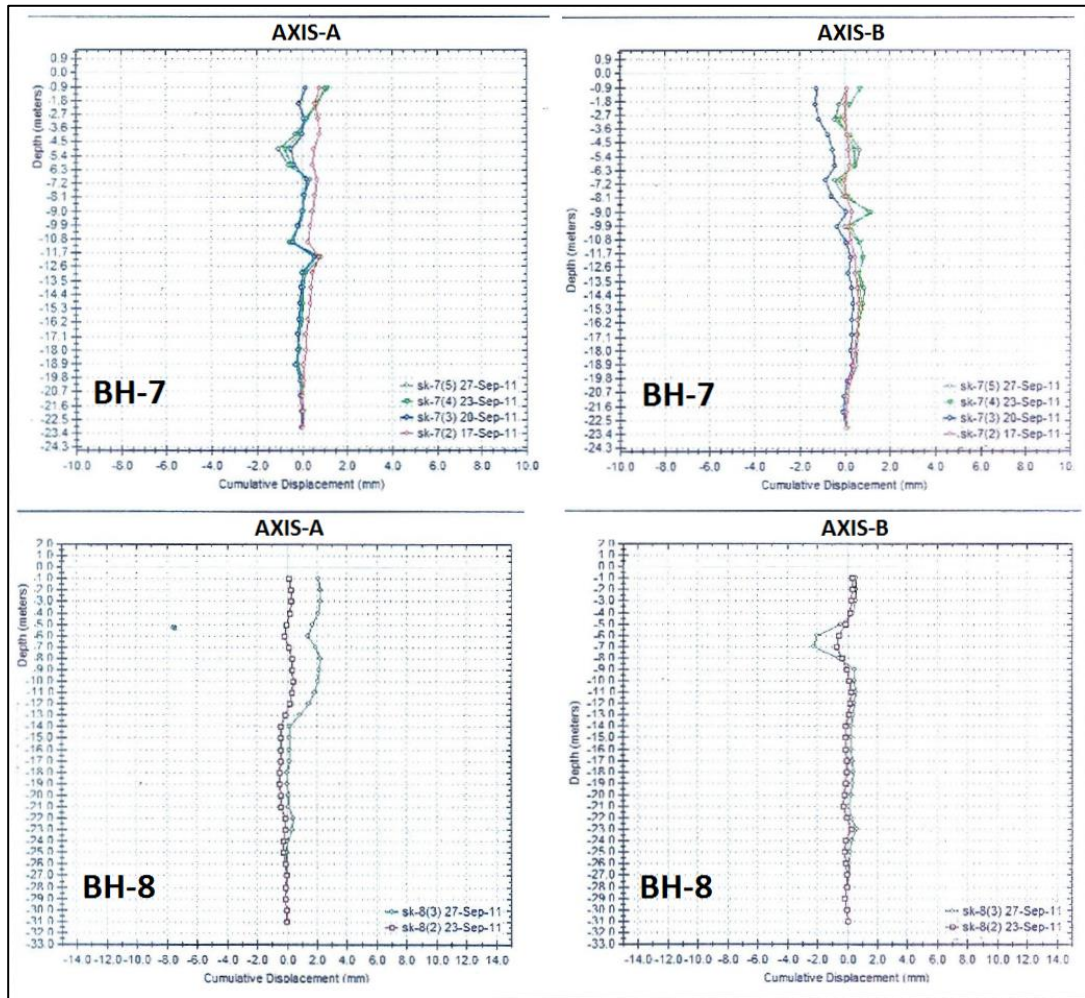
Figure A.1- Cumulative displacements of Kiper Co. boreholes.
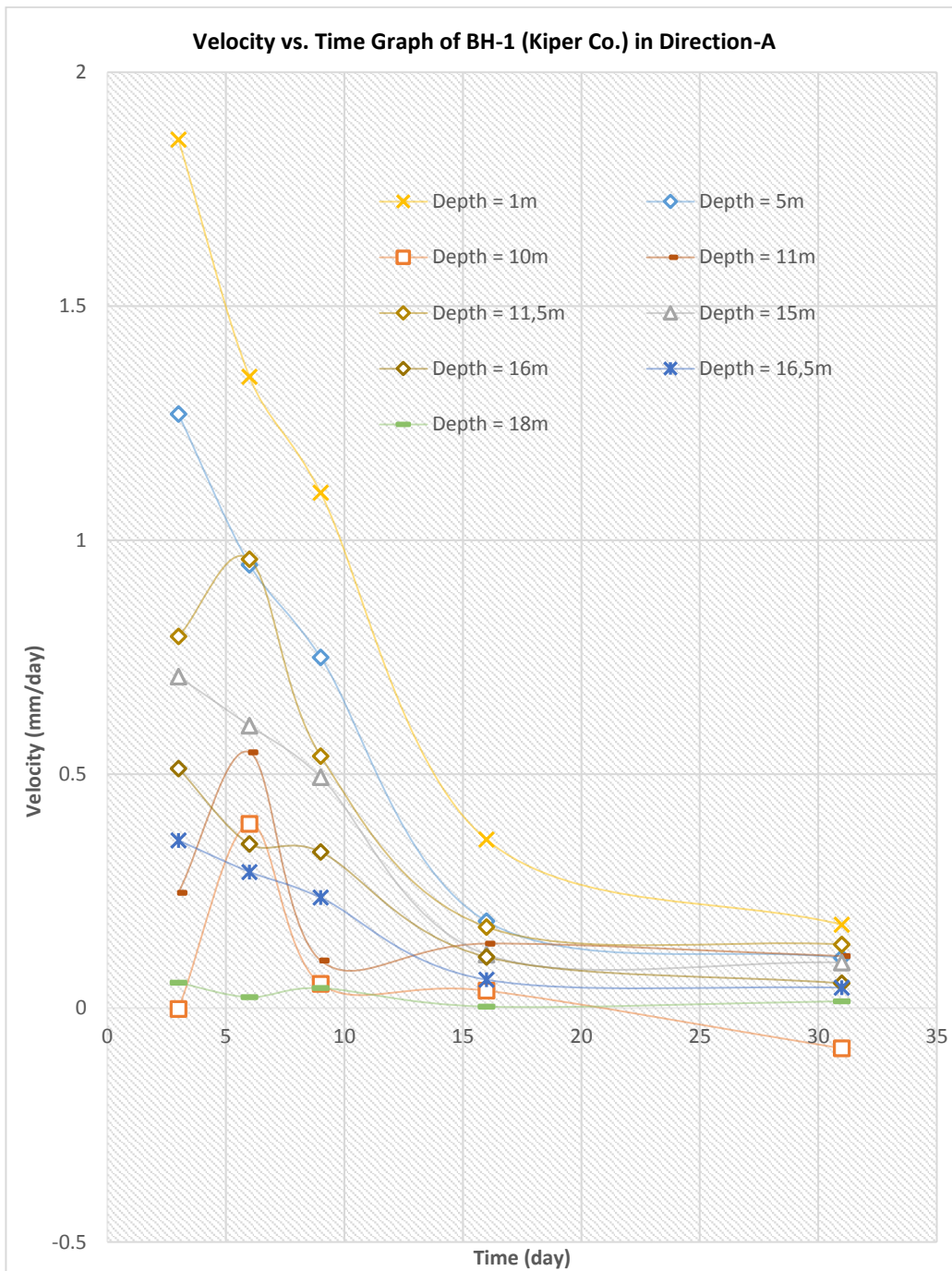
Figure A.2- Velocity vs. Time Graph of BH-1 (Kiper Co.) in Direction-A.
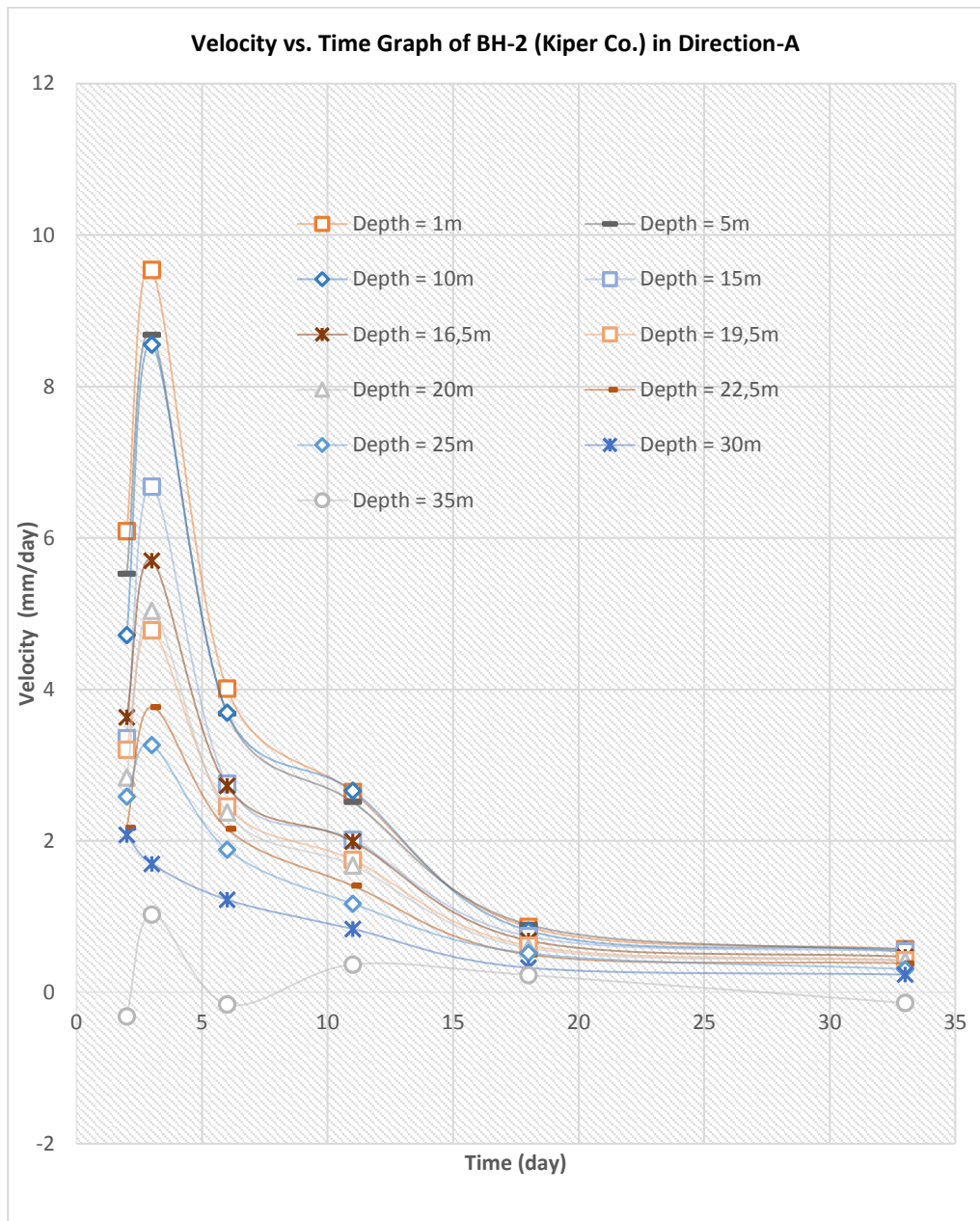
Figure A.3- Velocity vs. Time Graph of BH-2 (Kiper Co.) in Direction-A.
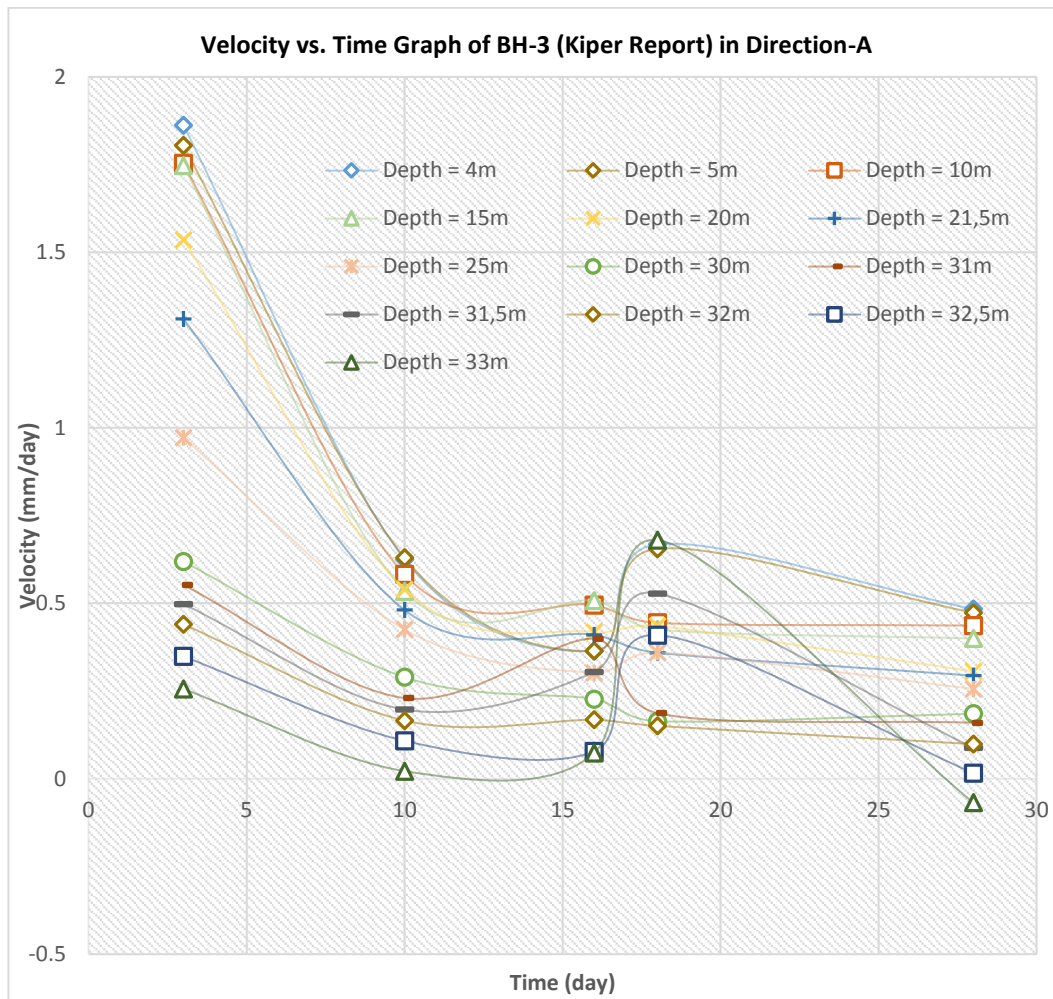
Figure A.4- Velocity vs. Time Graph of BH-3 (Kiper Co.) in Direction-A.
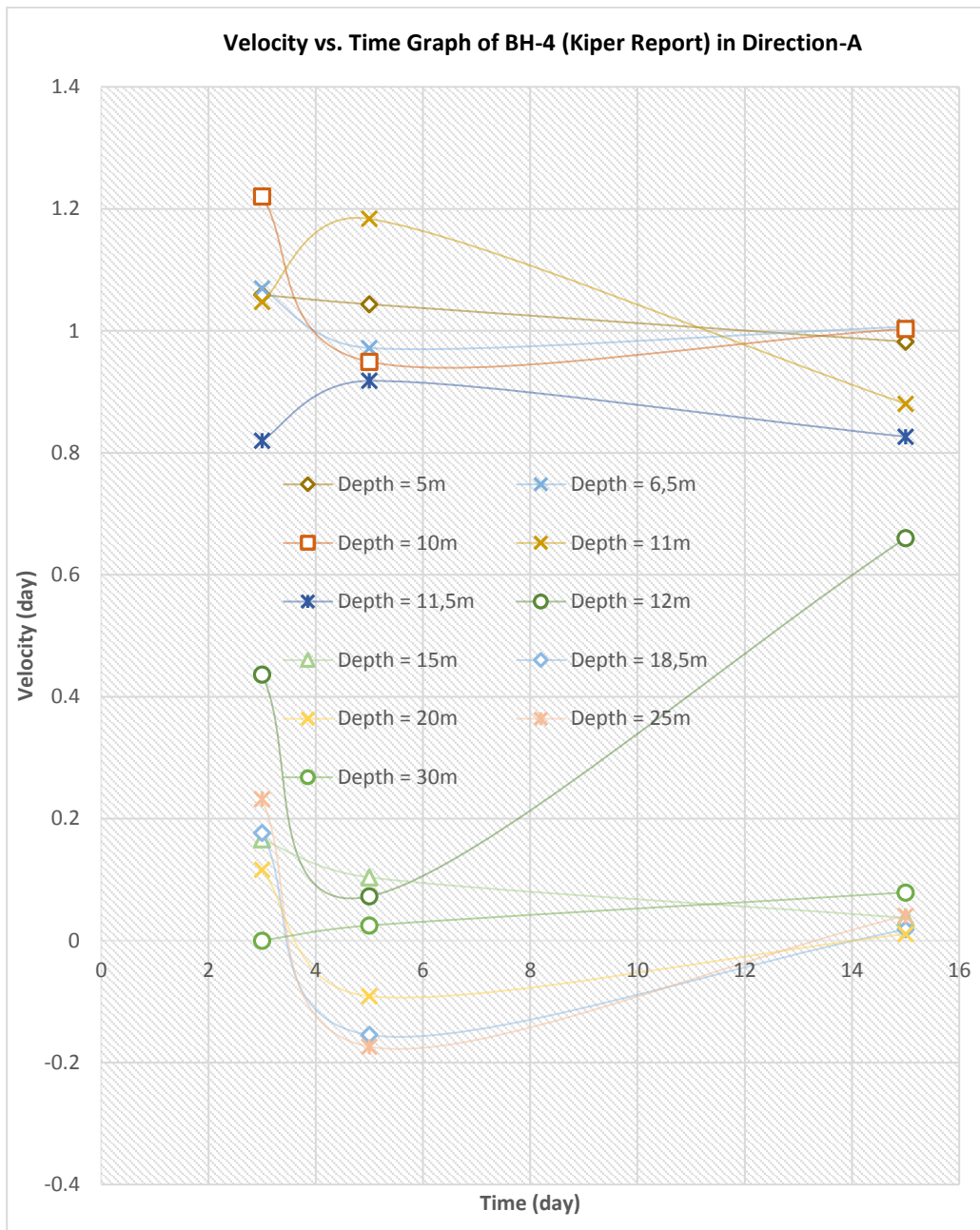
Figure A.5- Velocity vs. Time Graph of BH-4 (Kiper Co.) in Direction-A.
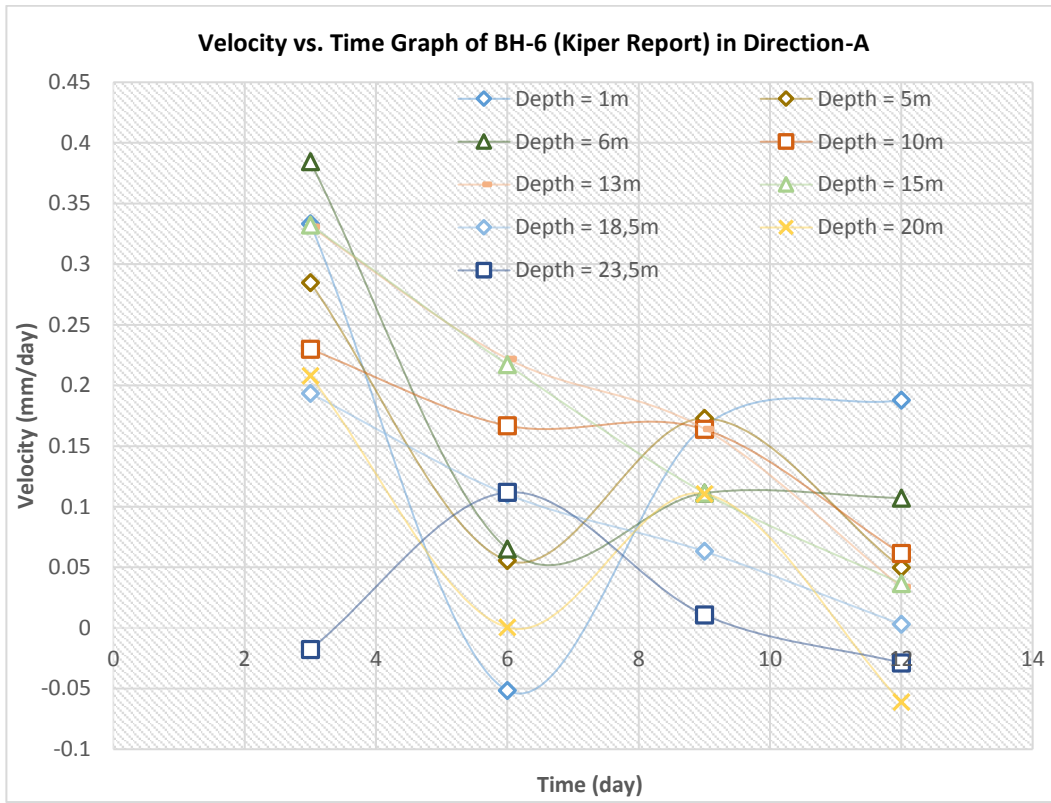
Figure A.6- Velocity vs. Time Graph of BH-6 (Kiper Co.) in Direction-A.

Deflection (mm)

-50 -25 0 25 50

Depth (m)

Cumulative Deflection
Direction A

Cumulative Deflection
Direction B

dikmen, Inclinometer sk-1

Deflection (mm)

-50 -25 0 25 50

LEGEND
initial   21 Jun2012
              3 Jul2012
             17 Jul2012
             28 Jul2012

Depth (m)

Cumulative Deflection
Direction A

Cumulative Deflection
Direction B

dikmen, Inclinometer sk-2

137

Cumulative Deflection
Direction A

Cumulative Deflection
Direction B

dikmen, Inclinometer sk-3

LEGEND

initial

	8 Jun2012
	15 Jun2012
	21 Jun2012
	28 Jun2012
	17 Jul2012
	28 Jul2012

Ref. Elevation m

Cumulative Deflection
Direction A

Cumulative Deflection
Direction B

dikmen, Inclinometer sk-4

LEGEND

initial

	3 Jul2012
	18 Jul2012
	27 Jul2012

138

dikmen, Inclinometer sk-5

dikmen, Inclinometer sk-6

139

dikmen, Inclinometer sk-7

dikmen, Inclinometer sk-8

dikmen, Inclinometer sk-9

dikmen, Inclinometer sk-10

141

Figure A.7- Cumulative displacements of Kilci Co. boreholes.
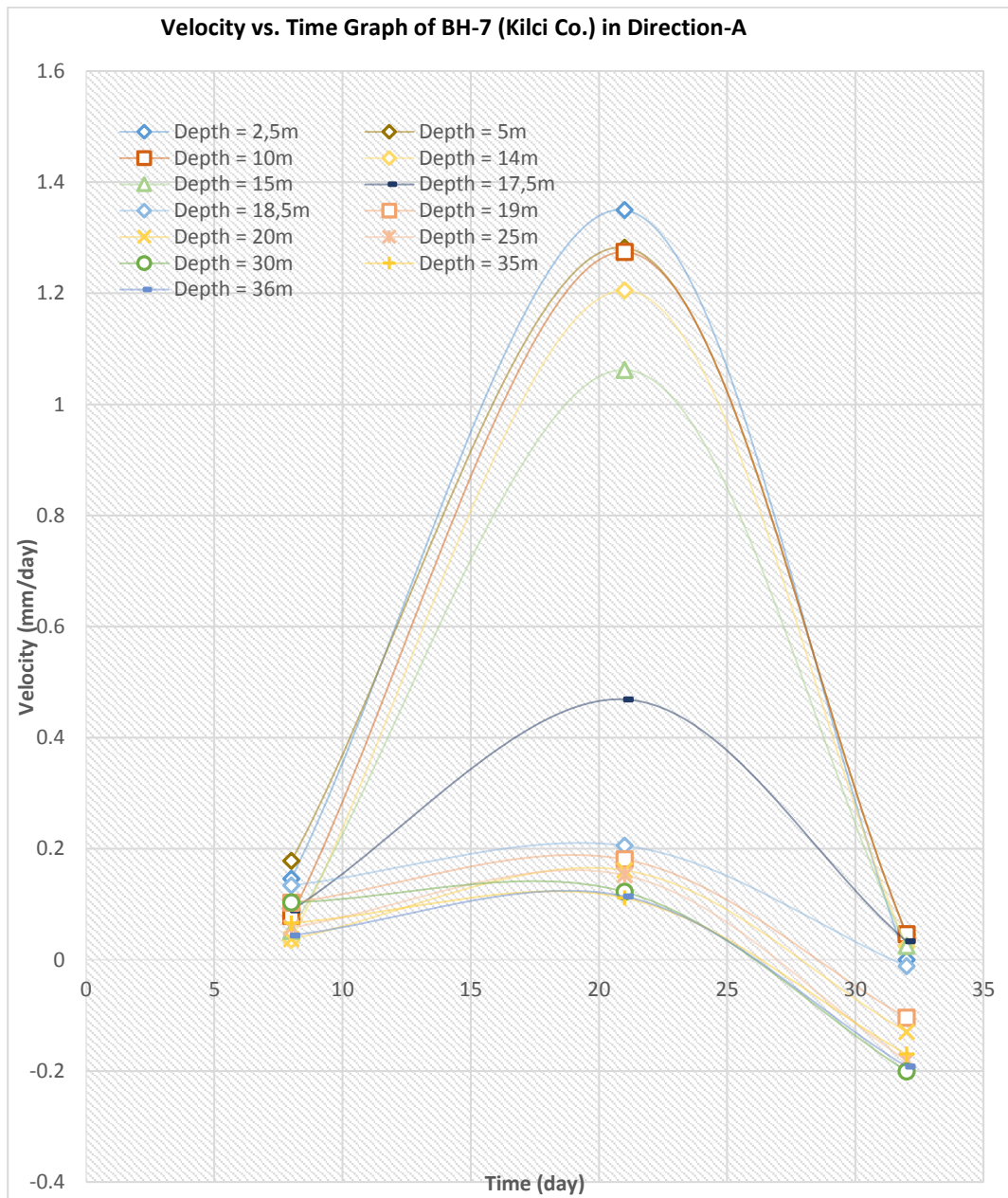
Figure A.8- Velocity vs. Time Graph of BH-7 (Kilci Co.) in Direction-A.

B. Laboratory Reports

Table B.1- *Libra Zemin Laboratory Test Results (Kiper Report)*

DENEY SONUÇLARI TABLOSU / TABLE OF TEST RESULTS

PROJE / PROJECT: KONYA YOLU HEYLANI
MÜŞTERİ / CLIENT: PETRA MÜHENDİSLİK MÜŞAVİRLİK VE İNŞ.LTD.ŞTİ

Rapor No:0011/2/2011
Sayfa: 1
Tarih / Date: 26.09.2011

| BORING NO	DEPTH (m)	SAMPLE NO	Wn (%)	γn (t/m³)	Gs	LL	PL	PI	#4 (%)	#10 (%)	#40 (%)	#200 (%)	USCS	Triaxial c (kPa)	ø (Deg)	type
SK-1	1,50-1,95	SPT-1	5,1			35,3	18,7	17,1	63,6	44,8	30,6	21,4	SC			
SK-1	6,00-6,45	SPT-4	7,7			32,9	18,5	14,4	77,2	56,6	38,6	27,8	SC			
SK-1	10,50-10,95	SPT-7	13,2			35,7	17,6	18,1	77,0	67,2	52,0	40,8	SC			
SK-1	13,50-13,80	UD-1	6,9	20,80		25,7	14,4	11,3	74,2	52,8	34,6	22,6	SC	20	9	UU
SK-1	18,00-18,45	SPT-12	7,7			21,9	13,1	8,8	89,2	73,4	45,4	26,8	SC			
SK-2	7,50-7,95	SPT-5	5,0			27,6	18,2	9,4	62,6	47,0	31,2	22,4	SC			
SK-2	13,50-13,95	SPT-9	8,1			29,1	15,7	13,4	96,2	87,4	66,6	50,4	CL			
SK-2	18,00-18,20	UD-2	7,1	21,86		27,3	14,1	13,4	84,0	75,4	59,6	46,6	SC	44	7	UU
SK-2	21,00-21,45	SPT-14	6,9			23,0	12,9	10,1	75,6	57,2	38,2	25,0	SC			
SK-4	6,00-6,45	SPT-4	6,6			23,4	13,8	10,0	64,2	44,0	26,8	19,0	CL			
SK-4	10,50-10,95	SPT-7	8,5			29,5	13,5	16,0	82,6	73,8	61,4	51,2	CL			
SK-4	18,00-18,08	SPT-12	4,4			28,8	14,5	14,3	75,4	68,8	56,4	46,2	SC			
SK-5	1,50-1,95	SPT-1	3,1			28,6	15,7	12,9	62,8	44,0	29,8	21,0	SC			
SK-6	10,50-10,95	SPT-7	5,9			28,9	13,8	15,1	94,8	82,8	68,4	55,6	CL			
SK-6	15,00-15,45	SPT-10	7,7			30,5	14,8	15,7	96,8	89,6	74,8	60,6	CL			
SK-7	6,50-6,95	SPT-4	6,8			29,5	17,1	12,4	54,4	41,8	28,6	21,6	SC			
SK-7	10,50-10,95	SPT-7	11,3			30,8	17,6	13,2	95,8	85,8	61,6	44,2	SC			
SK-7	13,50-13,95	SPT-9	8,8			32,7	16,6	16,1	95,8	80,8	72,0	57,0	CL			
SK-8	1,50-1,95	SPT-1	16,3			33,4	13,2	20,8	78,2	58,8	39,2	27,0	SC			

1- Deney sonuçları yukarıda tanımlanan numuneye aittir.
2- Laboratuvarımız Bayındırlık Bakanlığı Laboratuvar Yeterlilik Belgesine sahiptir.
3- Bu rapor Deney laboratuvarının izni olmadan çoğaltılamaz.

TESTİ YAPAN/TESTED BY
Dr.T.Kemal TÜRELİ
Jeoloji Yük. Mühendisi

Lab. Deneticisi Müh.
Jeoloji Mühendisi Gürsel KARAKUŞ
Belge No:4559

FR.13/ REV.NO/TARİHİ:00l—

144

Table B.2- *Akademi Zemin Laboratory Test Results (Kiper Report)*

AKADEMİ ZEMİN ve KAYA MEKANİĞİ LABORATUVARI

Almteri Bulvarı, 1151.Sokak, Gül 86 Sitesi, No: 1/80 Osttim / ANKARA

Tel: 0 312 385 67 67, Faks: 0 312 385 59 52

SUMMARY OF THE LABORATORY TEST RESULTS

FIRM : PETRA MÜHENDİSLİK

PROJECT : KONYA`WAY LANDSLIDE, DİKMEN-ÇANKAYA/ANKARA

PROJECT TYPE : Geological-Geotechnical Site Investigation

Date of Sample Arrival 23,09,2011

Report Date 27,09,2011

Lab. Record No AKD-11 / 09-232

Bay. Record No 1895327

BH No.	Sample No	Depth (m)	Specific Weight (Gs)	Water Content (%)	Natural Unit Weight (kN/m^3)	Dry Unit Weight (kN/m^3)	Sieve Analysis No.4 Retained (%)	Sieve Analysis 200 Passed (%)	Atterberg LL (%)	Atterberg PL (%)	Atterberg PI (%)	Soil Class	Uniaxial Compression Test q_u (kgf/cm^2)	Direct Shear Exp. (CD-Peak) c (kgf/cm^2)	Direct Shear Exp. (CD-Peak) Φ (°)	Direct Shear Exp. (CD-Residual) c' (kgf/cm^2)	Direct Shear Exp. (CD-Residual) Φ' (°)	Consolidation Exp. Swelling (%)	Consolidation Exp. Swelling Pressure (kgf/cm^2)
SK-2	UD-1	3,00-3,50		11,4	18,31	16,44	11,5	41,3	34,6	17,7	16,9	SC		0,176	26	0,096	20		
SK-6	UD-1	3,00-3,50		8,2	17,95	16,59	2,4	55,8	35,3	19,6	15,7	CL		0,118	22	0,062	17		

NP=Non-plastic

Deney Sorumlusu
Jeoloji Müh. Sertan DEMİR

Lab. Denetçi Müh. Yılmaz TUNA
Jeo.Yük.Müh.

145

Table B.3- *Erbey Mühendislik Test Results (Kilci Report)*

LABORATORY TEST REPORT

Date : 09.07.2012
Firm : KILCI MÜHENDİSLİK & MÜŞAVİRLİK İNŞAAT TAAHHÜT SAN. VE TİC. LTD. ŞTİ.
Project : ANKARA CITY/ÇANKAYA COUNTY/AKPINAR DISTRICT 29026 LAND PARCEL - LANDSLIDE GEOTECHNICAL SITE INVESTIGATION
LAB NO : 12.07.2262

No	BH No	Sample No	Depth (m)	Particle Distribution 4 passed %	10 passed %	40 passed %	200 passed %	Atterberg Limits TS 1900-1/MART 2006 LL %	PL %	PI %	Class USCS	Unit Weight Gs t/m3	Natural Unit Weight γn t/m³	Water Content W(n) %	Unconfined Comp. Test qu kg/cm²	c kg/cm²	Direct Shear (CD) c kg/cm²	φ derece	Point Load Test Is(50) (Mpa)	Is(50) (Kg/cm²)	Compressibility Index Cc	Consolidat.	Swelling Percent %	Swelling Pressure kg/cm²
1	SK-1	K-1	9,00										2,60						4,51	46,96				
2	SK-1	K-2	17,00										2,66		366,29				5,14	52,37				
3	SK-1	K-3	26,00										2,64		435,24									
4	SK-2	K-1	10,00										2,68		342,57									
5	SK-2	K-2	15,00										2,53						2,17	22,08				
6	SK-2	K-3	24,00										2,26						2,75	28,00				
7	SK-2	K-4	38,00										2,67		592,32									
8	SK-2	K-5	48,00										2,42						2,43	24,79				
9	SK-3	K-1	19,00										2,40						2,89	29,50				
10	SK-3	K-2	32,00										2,42						2,85	29,03				
11	SK-4	K-1	12,00														0,06	26						
12	SK-4	K-2	25,00										2,65		637,54									
13	SK-4	K-3	32,00										2,63						1,97	20,05				
14	SK-4	K-4	35,00										2,66		627,41									
15	SK-4	K-5	45,00										2,60		103,00									
16	SK-5	K-1	7,00										2,36						1,46	14,90				
17	SK-5	K-2	18,00										2,68		561,45									
18	SK-5	K-3	28,00										2,68				0,08	23						
19	SK-6	K-1	17,00																4,78	48,73				
20	SK-6	K-2	20,00										2,56											

Kontrol Eden :
S. PİŞMİŞ
Jeoloji Mühendisi
ODA NO: 11745

Denetçi Mühendis:
H.KEZER
Belge No: 3912

146

C. Acceleration and Displacement Data of Query Points

Table C.1-*Amplification Factors*

Query Point Number	Material Behavior	PGA (g)	Peak Acceleration at the Query Point (g)	Amplification Factor
1	Drained	0.00100	0.00491	4.91
2	Drained	0.00100	0.00293	2.93
3	Drained	0.00100	0.00171	1.71
4	Drained	0.00100	0.00256	2.56
5	Drained	0.00100	0.00756	7.56
6	Drained	0.00100	0.00280	2.8
7	Drained	0.00100	0.00189	1.89
8	Drained	0.00100	0.00184	1.84
9	Drained	0.00100	0.00687	6.87
10	Drained	0.00100	0.00384	3.84
11	Drained	0.00100	0.00475	4.75
12	Drained	0.00100	0.00376	3.76
1	Drained	0.05000	0.16900	3.38
2	Drained	0.05000	0.08100	1.62
3	Drained	0.05000	0.05300	1.06
4	Drained	0.05000	0.06900	1.38
5	Drained	0.05000	0.28100	5.62
6	Drained	0.05000	0.09100	1.82
7	Drained	0.05000	0.07800	1.56
8	Drained	0.05000	0.08000	1.6
9	Drained	0.05000	0.28000	5.6
10	Drained	0.05000	0.13100	2.62
11	Drained	0.05000	0.18200	3.64
12	Drained	0.05000	0.12300	2.46
1	Drained	0.07500	0.25400	3.39
2	Drained	0.07500	0.09800	1.31
3	Drained	0.07500	0.08400	1.12
4	Drained	0.07500	0.09200	1.23
5	Drained	0.07500	0.36300	4.84
6	Drained	0.07500	0.13400	1.79

Query Point Number	Material Behavior	PGA (g)	Peak Acceleration at the Query Point (g)	Amplification Factor
7	Drained	0.07500	0.12500	1.67
8	Drained	0.07500	0.12800	1.71
9	Drained	0.07500	0.35000	4.67
10	Drained	0.07500	0.18400	2.45
11	Drained	0.07500	0.23000	3.07
12	Drained	0.07500	0.18400	2.45
1	Drained	0.10000	0.29500	2.95
2	Drained	0.10000	0.11500	1.15
3	Drained	0.10000	0.08600	0.86
4	Drained	0.10000	0.10600	1.06
5	Drained	0.10000	0.54600	5.46
6	Drained	0.10000	0.15900	1.59
7	Drained	0.10000	0.17200	1.72
8	Drained	0.10000	0.17900	1.79
9	Drained	0.10000	0.42200	4.22
10	Drained	0.10000	0.21800	2.18
11	Drained	0.10000	0.23200	2.32
12	Drained	0.10000	0.22600	2.26
1	Undrained	0.00100	0.01450	14.5
2	Undrained	0.00100	0.00702	7.02
3	Undrained	0.00100	0.00282	2.82
4	Undrained	0.00100	0.00276	2.76
5	Undrained	0.00100	0.02680	26.8
6	Undrained	0.00100	0.00966	9.66
7	Undrained	0.00100	0.00582	5.82
8	Undrained	0.00100	0.01152	11.52
9	Undrained	0.00100	0.02374	23.74
10	Undrained	0.00100	0.01256	12.56
11	Undrained	0.00100	0.01337	13.37
12	Undrained	0.00100	0.01821	18.21
1	Undrained	0.05000	0.19700	3.94
2	Undrained	0.05000	0.08500	1.7
3	Undrained	0.05000	0.06800	1.36
4	Undrained	0.05000	0.10400	2.08
5	Undrained	0.05000	0.32200	6.44

Query Point Number	Material Behavior	PGA (g)	Peak Acceleration at the Query Point (g)	Amplification Factor
6	Undrained	0.05000	0.09800	1.96
7	Undrained	0.05000	0.09000	1.8
8	Undrained	0.05000	0.07900	1.58
9	Undrained	0.05000	0.28300	5.66
10	Undrained	0.05000	0.14700	2.94
11	Undrained	0.05000	0.17000	3.4
12	Undrained	0.05000	0.12800	2.56
1	Undrained	0.07500	0.27500	3.67
2	Undrained	0.07500	0.13000	1.73
3	Undrained	0.07500	0.10200	1.36
4	Undrained	0.07500	0.15200	2.03
5	Undrained	0.07500	0.41200	5.49
6	Undrained	0.07500	0.14300	1.91
7	Undrained	0.07500	0.14000	1.87
8	Undrained	0.07500	0.11800	1.57
9	Undrained	0.07500	0.36700	4.89
10	Undrained	0.07500	0.19300	2.57
11	Undrained	0.07500	0.23000	3.07
12	Undrained	0.07500	0.16400	2.19
1	Undrained	0.10000	0.32500	3.25
2	Undrained	0.10000	0.16500	1.65
3	Undrained	0.10000	0.16300	1.63
4	Undrained	0.10000	0.19800	1.98
5	Undrained	0.10000	0.55300	5.53
6	Undrained	0.10000	0.18200	1.82
7	Undrained	0.10000	0.17900	1.79
8	Undrained	0.10000	0.15800	1.58
9	Undrained	0.10000	0.39500	3.95
10	Undrained	0.10000	0.23400	2.34
11	Undrained	0.10000	0.28300	2.83
12	Undrained	0.10000	0.19600	1.96

Table C.2-*Plastic Displacements*

Query Point Number	Material Behavior	PGA (g)	Initial (Static, Elastic) Displacement (m)	Peak (Elastic + Plastic) Displacement (m)	End of Earthquake Plastic Displacement (m)
1	Drained	0.001	0.0182	0.0192	0.0010
2	Drained	0.001	0.0163	0.0166	0.0004
3	Drained	0.001	0.0117	0.0120	0.0003
4	Drained	0.001	0.0060	0.0062	0.0002
5	Drained	0.001	0.0312	0.0317	0.0005
6	Drained	0.001	0.0255	0.0258	0.0003
7	Drained	0.001	0.0204	0.0207	0.0003
8	Drained	0.001	0.0111	0.0113	0.0002
9	Drained	0.001	0.0293	0.0297	0.0003
10	Drained	0.001	0.0250	0.0253	0.0003
11	Drained	0.001	0.0188	0.0190	0.0003
12	Drained	0.001	0.0112	0.0114	0.0002
1	Drained	0.050	0.0180	0.0810	0.0630
2	Drained	0.050	0.0160	0.0380	0.0220
3	Drained	0.050	0.0120	0.0260	0.0140
4	Drained	0.050	0.0060	0.0170	0.0110
5	Drained	0.050	0.0310	0.1180	0.0870
6	Drained	0.050	0.0250	0.0460	0.0210
7	Drained	0.050	0.0200	0.0350	0.0150
8	Drained	0.050	0.0110	0.0220	0.0110
9	Drained	0.050	0.0290	0.0600	0.0310
10	Drained	0.050	0.0250	0.0430	0.0180
11	Drained	0.050	0.0190	0.0330	0.0140
12	Drained	0.050	0.0110	0.0230	0.0120
1	Drained	0.075	0.0181	0.1417	0.1236
2	Drained	0.075	0.0163	0.0721	0.0559
3	Drained	0.075	0.0117	0.0425	0.0308
4	Drained	0.075	0.0060	0.0282	0.0222
5	Drained	0.075	0.0312	0.2266	0.1954
6	Drained	0.075	0.0255	0.0880	0.0625
7	Drained	0.075	0.0204	0.0588	0.0384
8	Drained	0.075	0.0111	0.0310	0.0199
9	Drained	0.075	0.0293	0.1224	0.0931
10	Drained	0.075	0.0250	0.0826	0.0576

Query Point Number	Material Behavior	PGA (g)	Initial (Static, Elastic) Displacement (m)	Peak (Elastic + Plastic) Displacement (m)	End of Earthquake Plastic Displacement (m)
11	Drained	0.075	0.0188	0.0638	0.0450
12	Drained	0.075	0.0112	0.0330	0.0219
1	Drained	0.100	0.0180	0.2140	0.1960
2	Drained	0.100	0.0160	0.1170	0.1010
3	Drained	0.100	0.0120	0.0600	0.0480
4	Drained	0.100	0.0060	0.0380	0.0320
5	Drained	0.100	0.0310	0.3570	0.3260
6	Drained	0.100	0.0250	0.1460	0.1210
7	Drained	0.100	0.0200	0.0970	0.0770
8	Drained	0.100	0.0110	0.0430	0.0320
9	Drained	0.100	0.0290	0.2010	0.1720
10	Drained	0.100	0.0250	0.1400	0.1150
11	Drained	0.100	0.0190	0.1120	0.0930
12	Drained	0.100	0.0110	0.0470	0.0360
1	Undrained	0.001	0.0100	0.0110	0.0010
2	Undrained	0.001	0.0110	0.0120	0.0010
3	Undrained	0.001	0.0090	0.0090	0.0000
4	Undrained	0.001	0.0060	0.0060	0.0000
5	Undrained	0.001	0.0290	0.0310	0.0020
6	Undrained	0.001	0.0230	0.0240	0.0010
7	Undrained	0.001	0.0200	0.0200	0.0000
8	Undrained	0.001	0.0130	0.0130	0.0000
9	Undrained	0.001	0.0270	0.0280	0.0010
10	Undrained	0.001	0.0240	0.0240	0.0000
11	Undrained	0.001	0.0190	0.0200	0.0010
12	Undrained	0.001	0.0140	0.0150	0.0010
1	Undrained	0.050	0.0100	0.0270	0.0170
2	Undrained	0.050	0.0110	0.0320	0.0210
3	Undrained	0.050	0.0090	0.0230	0.0140
4	Undrained	0.050	0.0060	0.0160	0.0100
5	Undrained	0.050	0.0290	0.0840	0.0550
6	Undrained	0.050	0.0230	0.0420	0.0190
7	Undrained	0.050	0.0200	0.0390	0.0190
8	Undrained	0.050	0.0130	0.0330	0.0200
9	Undrained	0.050	0.0270	0.0460	0.0190

Query Point Number	Material Behavior	PGA (g)	Initial (Static, Elastic) Displacement (m)	Peak (Elastic + Plastic) Displacement (m)	End of Earthquake Plastic Displacement (m)
10	Undrained	0.050	0.0240	0.0430	0.0190
11	Undrained	0.050	0.0190	0.0390	0.0200
12	Undrained	0.050	0.0140	0.0340	0.0200
1	Undrained	0.075	0.0100	0.0440	0.0340
2	Undrained	0.075	0.0110	0.0520	0.0410
3	Undrained	0.075	0.0090	0.0370	0.0280
4	Undrained	0.075	0.0060	0.0210	0.0150
5	Undrained	0.075	0.0290	0.1490	0.1200
6	Undrained	0.075	0.0230	0.0640	0.0410
7	Undrained	0.075	0.0200	0.0640	0.0440
8	Undrained	0.075	0.0130	0.0550	0.0420
9	Undrained	0.075	0.0270	0.0700	0.0430
10	Undrained	0.075	0.0240	0.0670	0.0430
11	Undrained	0.075	0.0190	0.0650	0.0460
12	Undrained	0.075	0.0140	0.0590	0.0450
1	Undrained	0.100	0.0100	0.0690	0.0590
2	Undrained	0.100	0.0110	0.0840	0.0730
3	Undrained	0.100	0.0090	0.0580	0.0490
4	Undrained	0.100	0.0060	0.0270	0.0210
5	Undrained	0.100	0.0290	0.2280	0.1990
6	Undrained	0.100	0.0230	0.1010	0.0780
7	Undrained	0.100	0.0200	0.1050	0.0850
8	Undrained	0.100	0.0130	0.0910	0.0780
9	Undrained	0.100	0.0270	0.1090	0.0820
10	Undrained	0.100	0.0240	0.1060	0.0820
11	Undrained	0.100	0.0190	0.1060	0.0870
12	Undrained	0.100	0.0140	0.0980	0.0840